



HAL
open science

Functionalization of titanium surface for dental implants design

Sabin Issa

► **To cite this version:**

Sabin Issa. Functionalization of titanium surface for dental implants design. Chemical Sciences. Université Paris-Est, 2014. English. NNT : 2014PEST1075 . tel-01124334

HAL Id: tel-01124334

<https://theses.hal.science/tel-01124334>

Submitted on 6 Mar 2015

HAL is a multi-disciplinary open access archive for the deposit and dissemination of scientific research documents, whether they are published or not. The documents may come from teaching and research institutions in France or abroad, or from public or private research centers.

L'archive ouverte pluridisciplinaire **HAL**, est destinée au dépôt et à la diffusion de documents scientifiques de niveau recherche, publiés ou non, émanant des établissements d'enseignement et de recherche français ou étrangers, des laboratoires publics ou privés.

Ecole doctorale n°531: Sciences, Ingénierie et Environnement (SIE)

Doctorat de l'Université Paris-Est Créteil (UPEC)

THESE

Pour obtenir le grade de docteur délivré par

L'Université Paris-Est Créteil

Spécialité Science de matériaux

Présentée par

Sabin ISSA

Sous la direction de P. Cenedese et P. Dubot

**Fonctionnalisation de la surface du titane pour les
implants dentaires**

INSTITUT DE CHIMIE ET DES MATERIAUX PARIS-EST- UMR 7182

Jury

Mr le Pr Ivan Guillot
Mme le Pr. Laurence Jordan
Mme Isabelle Frateur
Mr Christophe Azevedo
Mr Davy Louis Versace
Mr Pierre Dubot

Président
Rapporteur
Rapporteur
Examineur
Examineur
Examineur

UNIVERSITÉ —
— **PARIS-EST**



To the love of my life, Mahmoud, yes we did it and soon we'll be together!

To my beloved parents, you have been waiting a life for this moment. This is for you

To my sisters, the colors of my life

To Wahib, you'll be in our hearts.. always

To my family and friends

To Syria.. Peace

روح اسألن عاللي وليفه مش معه، مجروح بجروح الهوى شو بينفعه، موجوع ما بيتقول عاللي بيوجعه
وتعن عا باله ليالي الولدنة..

لعيلتي اللي بجبا كتير.. نحن مهمما بعدنا وضعنا.. بلحظة بتلاقينا رجعنا.. وحده الحب بيتقى معنا
وطن وغربة..

لأمل البلد.. أنتو الأحبة وإلكم الصدارة.. بكم نبي الغد الأحلى.. بكم نمضي وننتصر

If your dreams do not scare you, they are not big enough.

Chase your dream and be strong, don't let anyone or anything stop you

REMERCIEMENTS

Je tiens à remercier vivement monsieur Ivan GUILLOT pour avoir eu l'aimable gentillesse de présider mon jury de thèse. Permettez-moi de vous exprimer mon profond respect et ma gratitude pour votre disponibilité. C'est un véritable honneur.

Je désire également remercier madame Laurence JORDAN. Je ne trouve pas vraiment de mots assez suffisamment précis pour qualifier la gratitude et l'admiration que j'éprouve pour m'avoir orienté dans le domaine des biomatériaux. Merci d'avoir accepté d'être rapporteur de ce travail et pour tous vos remarques et conseils pertinents.

Tous mes remerciements à madame Isabelle FRATEUR pour avoir accepté d'être un rapporteur de ce travail et pour le temps que vous avez accordé à la lecture de cette thèse et à l'élaboration de votre rapport. Mes remerciements vont également à monsieur Davy Louis VERSACE qui a eu la gentillesse de bien vouloir assister à cette soutenance de thèse. Que vous soyez assuré de mon entière reconnaissance.

Mes plus sincères remerciements vont maintenant à Pierre DUBOT et Pierre CENEDESE. Je vous remercie très sincèrement d'être les merveilleux professeurs que vous êtes. Je suis heureuse de progresser sous votre direction

Pierre DUBOT, j'estime avoir été extrêmement chanceuse de vous avoir eu comme directeur de thèse. Je vous remercie pour le temps et la patience que vous m'avez accordés tout au long de ces années. Je garderai dans mon cœur votre générosité, votre compréhension et votre efficacité. Pour tout ce que vous m'avez apporté, MERCI.

Pierre CENEDESE, merci d'avoir accepté d'encadrer ce travail. Merci de votre disponibilité, votre patience à prodiguer des conseils pertinents, votre savoir et la générosité pour le transmettre. J'ai beaucoup apprécié travailler à vos côtés tant sur le plan scientifique que sur le plan humain.

Je désire également exprimer mes remerciements à Christophe AZEVEDO. Merci de votre gentillesse, vos remarques et vos conseils lors de la finalisation de ce travail. Je déclare mon admiration de votre maîtrise remarquable de domaine dentaire.

J'adresse également de sincères remerciements à tous les membres de l'équipe (MCMC, ICMPE) de l'amitié, les aides scientifiques et techniques. J'en garderai un souvenir ému et profond. Je remercie toute l'équipe de direction d'ICMPE et l'école doctorale SIE de l'Université Paris-Est en particulier Mr le Professeur Denis DUHAMEL et Mme Brigitte DAVIDE, Merci de votre générosité et gentillesse.

Je désire également exprimer mes remerciements à l'Université de Tichrine et le ministère de l'enseignement supérieur en Syrie pour le financement de ce travail.

A titre personnel, merci à tous ceux qui d'une manière ou d'une autre ont contribué à rendre mon séjour en France très vivant et riche. Alia, ma sœur de cœur, je n'oublierai jamais ce que tu as fait pour moi. Wesam, ton amitié sera toujours le meilleur prix que j'ai gagné pendant ces ans. Je voudrais remercier aussi tous mes amis, Micheline, Rasha, Hatem, Ali, Hala, Ranim, Randa, Issam, Odette, Aline et Fabienne pour leur aide et leur soutien avec mes sincères vœux de réussite.

A titre plus personnel, aux gens qui sont toute ma vie : mes parents (Nazih et Faten) ; je suis la plus chanceuse fille au monde de vous avoir comme mes parents, sans vous l'enfant que j'étais ne serait pas devenue la fille que je suis. C'est avec émotion qu'à mon tour je vous dévoile le fruit de mes efforts. J'espère être à la hauteur de votre fierté inconditionnelle. Mes sœurs (Yara, Amar, Laure, Ezis, Ninar), vous êtes un merveilleux cadeau que je porte toujours dans mon cœur et je vous souhaite réussite et surtout bonheur. Iyad, Ashraf, Ghonwa et sa famille et l'inoubliable Wahib.

Mes derniers remerciements et non les moindres, s'adressent à toi mon homme, pour ton soutien, ta tendresse, ton humour, ta joie, ton originalité, ton amour et la compréhension dont tu as toujours fait preuve à mon égard. Mahmoud, merci pour la confiance que tu me portes mon chéri, je t'aime infiniment.

La seule peine et tristesse que je ne peux pas oublier ; la Syrie, prions pour la paix et la fin de toute violence et terrorisme.

TABLE OF CONTENTS

INTRODUCTION AND OBJECTIVES	11
CHAPTER I	15
Bibliographic Review.....	15
1. Dental implants: Biological review	15
1.1. Bone tissue	17
1.2. Biomaterials used in implantology: Titanium	18
1.3. Osseointegration of dental implants	21
2. Challenges and advancing in dental implantology	25
3. Surface modification.....	26
3.1. Surface roughness of dental implants /Topographical modifications	28
3.2. Nanotechnology and dental implants	29
3.3. Calcium Phosphate-based osteoconductive materials	31
3.4. Surface modification methods.....	33
CHAPTER II.....	45
Analysis techniques for the physicochemical characterization of TiO₂ functionalized surfaces.	45
1. Scanning Electron Microscopy (SEM).....	45
2. X-ray Photoelectron Spectroscopy (XPS)	46
3. Infrared Reflection-Absorption Spectroscopy (IRRAS)	51
CHAPTER III	61
Functionalization of TiO₂ surfaces.....	61
1. Nanostructuring of TiO ₂ surface.....	61
1.1. Fabrication of TiO ₂ nanotube arrays by anodisation.....	61
1.2. Mechanism of nanotubes formation	63
1.3. Experiments of the present thesis for TiO ₂ nanotubes fabrication.....	67
2. Analysis of nanostructured TiO ₂ reactivity toward phosphate	71
2.1. Experimental results	75
3. Alkaline treatment of nanostructured TiO ₂ surface.....	78
3.1. SEM and XPS experimental results for alkaline treatment.....	79

3.2. NaOH pretreatment effect on phosphate adsorption onto TiO ₂ nanotubes	82
4. Functionalization of nanostructured TiO ₂ surface with calcium phosphate and Strontium-doped Calcium phosphate.....	84
4.1. Calcium Phosphate compounds.....	85
4.2. Strontium Substituted Calcium Phosphate.....	87
4.3. Pulsed Electrodeposition.....	90
4.4. Experimental Results.....	92
CHAPTER IV	105
Protein adsorption onto functionalized TiO ₂ surfaces	105
1. Protein adsorption onto implant surface (biological effect)	105
2. Protein analysis by IR spectroscopy	120
3. Experimental results of BSA adsorption onto functionalized TiO ₂ surfaces .	125
CONCLUSION	139
REFERENCES	143

List of abbreviations

ACP	Amorphous Calcium Phosphate
ALP	Alkaline Phosphatase
BIC	Bone–Implant Contact
BMP	Bone Morphogenetic Proteins
BSA	Bovine Serum Albumin
BSE	Backscattered Electrons
CaP	Calcium Phosphate
Cbfa1	Core-binding factor 1
DCPD	Dicalcium Phosphate Dihydrate
DI	Deionized Water
E _B	Binding Energy
E _K	Kinetic Energy
ECM	Extracellular Matrix
ESCA	Electron Spectroscopy for Chemical Analysis
IRRAS	Infrared Reflection Adsorption Spectroscopy
FWHM	Full Width at Half Maximum
HAp	Hydroxyapatite
HF	Hydrofluoric acid
hν	Energy of the incident X-ray beam
HAS	Human Serum Albumin
IR	Infrared
MBL	Marginal Bone Loss
MRI	Magnetic Resonance Imaging
nT-TiO ₂	Nanostructured Titanium oxide
OCP	Octacalcium Phosphate
PLD	Pulsed Laser Deposition
PP	Potential Pulses
PS	Plasma-spraying

PZC	Point of Zero Charge/ Isoelectric Zero Point
RGD	Arginine-glycine-aspartic Acid
SBF	Simulated Body Fluids
SEM	Scanning Electron Microscopy
SLA	Sandblasting and Acid-etching
TCP	Tricalcium Phosphate
TPS	Titanium Plasma-Spraying
TTCP	Tetracalcium Phosphate
XPS	X-ray Photoelectron Spectroscopy

RESUME

Les implants dentaires sont des dispositifs médicaux invasifs à visée prothétique et pour ce faire doivent s'intégrer à l'os par un processus appelé ostéointégration. Le terme «ostéointégration» est synonyme d'un contact au sens physique et biologique entre la surface d'un implant et l'os vivant environnant, ces interactions doivent perdurer dans un contexte mécanique et bactériologique défavorable au cours du temps.

Historiquement, le Titane (Ti) et ses alliages sont considérés comme des matériaux de choix pour la majorité des implants orthopédiques et dentaires à cause de leur biocompatibilité et de leurs bonnes propriétés mécaniques. L'ostéointégration clinique n'est pas synonyme d'une interactivité os-implant totale. Aussi existe-t-il des échecs immédiats et ultérieurs dans l'implantologie actuelle. Des travaux expérimentaux biologiques et physico-mécaniques se poursuivent dans le but de mieux appréhender ces phénomènes d'interactivité et si possible d'augmenter la qualité de cette dernière.

Les effets des propriétés de surface sur l'ostéointégration de l'implant ont été pointés dans un certain nombre d'études. En outre, il a été rapporté que la prolifération et la différenciation des ostéoblastes et l'interaction des protéines sont influencées tant par la morphologie de la surface de l'implant que de sa chimie, aussi les nouvelles approches visent à modifier les propriétés topographiques et chimiques des surfaces d'implants dentaires. Ces tentatives peuvent également répondre à des situations cliniques difficiles comme pallier à une mauvaise qualité ou une faible quantité osseuse. L'optimisation du processus d'ostéointégration des implants dentaires peut améliorer en parallèle les procédures et les techniques chirurgicales telles que des mises en fonction plus rapides.

La nanostructuration est une technique prometteuse pour produire des surfaces dont la topographie et la chimie sont contrôlées. Les morphologies obtenues permettent de moduler le comportement des cellules et de modifier les interactions entre protéines et surface. Elles fournissent une plus grande surface pour l'adhérence des cellules, donc améliorent l'ostéointégration et accélèrent la cicatrisation après la pose de l'implant.

En plus de la topographie de la surface, la composition chimique est également essentielle pour l'adsorption des protéines et l'adhésion des cellules. Récemment, des compositions de phosphate de calcium (CaP) ont été largement utilisées comme revêtements pour les surfaces de titane afin d'accroître leurs propriétés biologiques et leur bioactivité. Suite à l'implantation, la libération de phosphate de calcium dans la région péri-implantaire augmente la saturation des fluides corporels et en conséquence augmente la précipitation de l'apatite biologique sur la surface de l'implant.

Bien que le revêtement de CaP puisse être incorporé tel quel, il peut également être dopé avec des ions et/ou des molécules thérapeutiques comme des facteurs de croissance, des protéines ou bien des antibiotiques afin de combiner, en les contrôlant, plusieurs agents à visée thérapeutique ciblée.

L'objectif de cette thèse est de créer de nouvelles surfaces de titane nanostructurées et fonctionnalisées avec des revêtements bioactifs et d'étudier leurs propriétés physico-chimiques pour développer de meilleurs modèles d'implants dentaires afin d'optimiser la formation osseuse interfaciale et favoriser ainsi le processus d'ostéointégration.

Dans le chapitre I, nous présentons les études déjà réalisées dans ce domaine en expliquant les principes biologiques de base des implants dentaires et l'effet des priorités de surface sur le processus d'ostéointégration. Les méthodes de modification de surface sont brièvement discutées.

Dans le chapitre II, nous présentons les techniques d'analyse utilisées dans ce travail pour réaliser la caractérisation physico-chimique de la surface de TiO₂. Dans ce travail, la Spectrométrie de Photoélectrons X (XPS) et la Spectroscopie Infrarouge (Infrared Reflection-Absorption Spectroscopy, IRRAS) sont utilisées pour étudier la chimie interfaciale et caractériser les espèces adsorbées. La microscopie électronique à balayage (MEB) est également utilisée pour caractériser la topographie des surfaces.

Le chapitre III concerne la double fonctionnalisation de la surface du titane par modifications topographiques (formation de nanotubes) et chimiques (dépôt de revêtements fonctionnels).

Nous avons commencé par la nanostructuration de surface de TiO_2 en appliquant la méthode d'anodisation afin de créer des nanotubes de TiO_2 alignés perpendiculairement à la surface. Les propriétés à l'échelle nanométrique peuvent être maîtrisées par l'ajustement des paramètres d'anodisation tels que le potentiel, le temps et la température. L'anodisation des échantillons de titane a été réalisée en utilisant une cellule électrochimique composée d'une électrode de référence, une électrode de platine et de l'électrode de travail (titane). Les échantillons ont été anodisés à 8,5V à la température ambiante pendant 600s dans un électrolyte d'acide acétique et HF 0,5%.

La surface de titane anodisée présente des nanotubes de TiO_2 amorphes alignés en structure compacte perpendiculairement à la surface avec un diamètre moyen d'environ 35 nm. La formation d'un film mince d'oxyde de titane nanostructuré a été visualisée par MEB et confirmée par XPS et spectroscopie infrarouge qui révèle une large bande d'adsorption ($700\text{-}1000\text{cm}^{-1}$) attribuables aux modes de vibrations des liaisons chimiques Ti-OH et Ti-O.

Dans la deuxième partie de ce chapitre, nous avons évalué l'aptitude d'une telle nanostructure à adsorber de petites molécules telles que les ions phosphate et observer les espèces adsorbées. Nous avons également évalué l'influence d'un prétraitement alcalin sur l'adsorption de phosphate. Deux méthodes de déposition ont été utilisées ; la première consiste simplement en l'immersion des échantillons dans les solutions de phosphate et la seconde consiste à l'électrodéposition standard en utilisant une cellule électrochimique classique de trois électrodes avec des solutions aqueuses des molécules étudiées à température ambiante et potentiel constant.

A partir de l'analyse des spectres IRRAS des échantillons étudiés, nous avons constaté que phosphate est adsorbé par les nanotubes (nT- TiO_2) sous forme de deux types de complexes. Un prétraitement des nanotubes de TiO_2 par NaOH conduit à la croissance d'une couche de titanate de sodium sur la surface (nT- TiO_2) au bord des nanotubes. Les spectres IRRAS des échantillons prétraités par NaOH, après adsorption de phosphate, présente un pic dominant à environ 870 cm^{-1} que nous associons à un complexe tri-coordonné, qui confirme que le prétraitement alcalin induit une adsorption moléculaire plus forte.

La troisième partie de ce chapitre étudie la nucléation et la croissance des CaP et CaP dopé par Sr (CaPSr) *in vitro* par électrodéposition pulsée à la température ambiante. Le strontium Sr est utilisé comme un substituant ionique pour optimiser la formation osseuse car conformément à des études antérieures, la présence de Sr à l'interface entre l'implant et l'os favorise l'ostéointégration et augmente les chances de succès de l'implant.

La topographie et la chimie du revêtement sont évaluées en fonction du temps de dépôt par MEB, XPS et IRRAS.

Les images MEB des échantillons revêtus avec CaP et CaPSr ont montré que les dépôts se développent sur les bords extérieurs des nanotubes de TiO₂ traduisant que ces bords sont les sites les plus réactifs de la surface des nanotubes. Ces sites agissent comme des points d'ancrage du revêtement. Le taux de recouvrement de surface par les dépôts croît en fonction de temps et les nanoparticules de CaP ancrées sur les bords des nanotubes finissent par s'agréger et recouvrir toute la surface du matériau.

À partir des spectres XPS, nous déduisons que pour le CaP non-dopé, le rapport de concentration entre calcium et phosphore est de l'ordre de $[Ca]/[P] = 1,30$. La déconvolution des pics de O_{1s} et P_{2p} nous indique un composé riche en OH. Dans le cas d'un composé désordonné amorphe (Amorphous-Calcium-Phosphate) développé dans un milieu alcalin avec une déficience en calcium, une gamme de composition d'ACP peut être représentée par les formules suivantes: Ca_{9-y}(PO₄)_{6-x}(HPO₄)_x(OH)_{x-2}. La quantification par photoémission suggère un composé de type Ca₄(HPO₄)₃(OH)₂.

Dans les mêmes conditions d'élaboration électrochimique du dépôt de CaPSr, le rapport $[Ca]/[P]$ est de l'ordre de 1,0. Dans ce cas nous devons avoir un composé tel que Ca_{1-x}Sr_xHPO₄. Il a été remarqué aussi que le rapport $[O]/[P]$ est $> 4,0$ ce qui signifie que les revêtements sont fortement hydratés.

Pour les revêtements de CaP non-dopé, les spectres IRRAS révèlent des vibrations symétriques et asymétriques à 1030-1100 et 900 cm⁻¹ confirmant la nature apatitique des films de CaP formés sur tous les substrats. Les spectres IR et XPS ont clairement montré que l'addition de Sr dans la couche de CaP favorise un composé non-apatitique de Ca_{1-x}Sr_xHPO₄ qui est de type brushitique et similaire au DCPA (Phosphate

dicalcique anhydre) ou au DCPD (Phosphate dicalcique dihydraté), tandis que le revêtement de CaP non-dopé ressemble à un composé d'apatite amorphe (ACP). Il a été rapporté que les composés non-apatitiques sont plus solubles aux milieux biologiques que ceux de type apatitiques. Ainsi, l'addition de strontium présente le double avantage de supporter les mécanismes de la croissance cellulaire et d'obtenir une phase inorganique plus facilement bio-résorbable que les composés apatitiques lorsqu'ils sont utilisés pour les implants dentaires.

Dans le chapitre IV, nous avons étudié les propriétés d'adsorption des surfaces fonctionnalisées par interaction avec une protéine, la BSA (sérum albumine bovine). Nous avons réalisé l'adsorption de BSA sur nanotubes vierges (nT-TiO₂), nanotubes revêtues par CaP (CaP.nT-TiO₂) et nanotubes revêtues par CaP dopé par Sr (Sr.CaP.nT-TiO₂) afin d'évaluer l'influence de la nature chimique de la surface sur l'adsorption de la protéine. De plus, nous avons étudié l'influence du pH de la solution sur l'adsorption de la protéine. L'interaction BSA-surface a été réalisée par immersion des échantillons dans des solutions des BSA à 0.1gL⁻¹ et trois valeurs de pH; acide~4.5, neutre~7.0, et basique~10.0 ont été étudiées.

Afin d'étudier qualitativement l'adsorption de BSA sur les différentes surfaces, nous avons déconvolué les spectres infrarouges obtenus en fonction de la quantité de BSA adsorbée sur la surface. On a regardé l'intensité de la bande amide I situé dans une région spectrale 1600-1700 cm⁻¹. Nous avons également étudié le rapport des bandes d'absorption Amide I et Amide II qui peut être relié à la modification de structure et/ou des géométries d'adsorption. Nous avons constaté que l'adsorption de la BSA dépend fortement des caractéristiques physico-chimiques de la solution et de la surface.

Ces observations peuvent être exploitées pour concevoir une fonctionnalisation de la surface d'implant afin d'améliorer l'adhésion et la colonisation cellulaire. L'évaluation de l'adsorption des protéines et leur conformation et aussi les interactions protéine-protéine peut offrir une très bonne base de données pour comprendre ses interactions avec les cellules adhérentes dans les premiers stades de la colonisation cellulaire.

INTRODUCTION AND OBJECTIVES

Titanium has been a material of choice for many orthopaedic and dental implants due to its biocompatibility and good mechanical properties. Despite all these excellent properties, a true adhesion between the bone and the metal surface has not yet been observed because of insufficient bone-implant contact (BIC) and fibrous encapsulation which may not always ensure proper biomechanical fixation and lead to the failure of medical implants. The need for improved healing response and increased speed of osseointegration of the biomaterial with the host tissue is still a relevant topic. In order to improve both the short and long-term osseointegration of titanium dental implants, a few strategies should be considered. These trends concern the modification of the topographical and chemical proprieties of dental implant surfaces as surface priorities have great influence on the success of the osseointegration of the implant

These attempts may also respond to difficult clinical situations with poor bone quality and quantity and enhance the osseointegration process of dental implants and consequently improve surgical procedures (e.g. immediate loading) and further results of the prostheses and long-term success.

Nanostructuration may produce surfaces with controlled topography and chemistry that could help developing novel implant surfaces with predictable tissue-integrative properties. Such topography was reported to modulate cell behavior, alter protein interactions with the surface and provide a very high surface-to-volume ratio for more cells adhesion, thus enhance the osseointegration and accelerate the wound healing following implant placement.

Beside surface topographical features, surface chemical composition and local atomic charges are critical for protein adsorption and cell attachment. Recently, Calcium phosphate compositions CaPs have been widely used as a coating for metallic prostheses to improve their biological properties. Such coatings enhance the bioactivity of titanium surface and favor their biocompatibility, thus promote cellular adhesion to the implant surface.

Furthermore, such CaP coating could be incorporated or doped with several therapeutic ions and molecules or even growth factors, proteins and antibiotic in order

to combine many controlled positive agents on the implant surface and get better results.

The objective of the present thesis is to create new functionalized nanostructured surfaces with bioactive coatings and to study the physicochemical priorities of these surfaces to develop better dental implants designs in order to optimize their interfacial bone formation and thus promote their osseointegration process.

In Chapter I, bibliographic reports will be reviewed, explaining the basic biological principles of dental implants and the effect of surface priorities on the osseointegration process. Also in this chapter, surface modification methods will be briefly discussed.

In Chapter II, we will present the analysis techniques for the physicochemical characterization of TiO₂ surface. In this work both X-ray photoelectron spectroscopy (XPS) and infrared spectroscopy (IR) are used as sensitive powerful tools to investigate interfacial chemistry and chemical bonds of adsorbed species. Also scanning electron microscopy (SEM) is used to characterize surface topographical priorities.

Chapter III will discuss the functionalization of TiO₂ surface by specific physicochemical modifications targeting the topographical and chemical features of TiO₂ surfaces. Starting with TiO₂ surface nanostructuring by anodization method in order to create controlled TiO₂ nanotubes which have nucleation reactive sites that cannot be existed on traditional bulk TiO₂ thin films.

The second part of this chapter will be an evaluation of the adsorption of small molecules such as phosphate to test nanostructured TiO₂ surface reactivity and to observe the bonding behavior between phosphates and TiO₂ nanotubes. The influence of alkaline pretreatment on the reactivity of TiO₂ nanotubes and phosphate adsorption will be presented too.

The third part of this chapter will discuss the development of CaP calcium phosphate coatings on the TiO₂ nanotubes by pulsed electrodeposition. In this part we will study the surface treatment and coating with calcium phosphate and (Sr) strontium doped calcium phosphate. Strontium is used as an ion substitution that optimizes bone formation as it is believed that its presence in the interface between the implant and the bone via a calcium phosphate coating will enhance osseointegration, and thus ensure the success of the implant. The coating morphology and chemistry will be

evaluated at different levels of deposition discussing the effect of Sr on CaP coating structure, adsorption and growth onto TiO₂ nanotubes.

In Chapter IV, we will study the adsorption properties of these doubly functionalized surfaces by investigating the adsorption of proteins such as BSA (bovine serum albumin). In this chapter, BSA-nT-TiO₂, BSA-CaP and BSA-CaPSr interfaces were investigated in order to compare the differences in adsorption capability between different functionalized surfaces. Actually, we'll discuss the influence of pH solution on adsorption processes by changing the charge state of the protein and the oxide surface.

So in general this work will be a physicochemical functionalization of TiO₂ surfaces that may offer a good idea to develop dental implant design and enhance this performance in the living body.

CHAPTER I

Bibliographic Review

1. Dental implants: Biological review

Oral implants are inert alloplastic materials which integrated into the bone of the maxilla and/or mandible, serving as abutments for prosthetic restorations instead of missing teeth or for the restoration of damaged/lost oro-facial structures, as a result of trauma, neoplastic or congenital defects in the bone [1].

The most commercially and clinically accepted and used dental implants are the Ti screw-shaped endosseous ones because of their high stability at insertion and their bio-mimesis.

A typical implant is formed by 3 main bodies: (Fig.1.1) (a) The implant body (b) The abutment (c) The dental crown.



Fig.1.1. (a) The dental implant parts, (b) Structure of a dental implant in comparison with a natural tooth (<http://www.theguelphdentist.com/dental-implants.html>)

Brånemark was the first who discovered this system in 1959 [2], since then, many improvements and progresses in the titanium implants design were developed and they have all based on the development of the Brånemark [3, 4] osseointegrated titanium implants in the treatment of the edentulous.

Clinically, Brånemark's protocol of the implantation procedure [4] involves two stages (Fig 1.2, Fig 1.3). The first is installing the implant in a surgical cavity in the bone followed by a healing period to allow tissue rebuilding. The waiting time for bone healing depends on bone quality and the region in which the implant was placed and was estimated by Brånemark as between 3-6 months. The second stage is the prosthesis connecting when a precise impression of the site is taken before the construction and attachment of the abutment preparation which, can range from a single crown or a prosthetic restoration containing multiple teeth to restoration of an entire denture of edentulous arch.



Fig.1.2. Two stages implant placing for single missing tooth

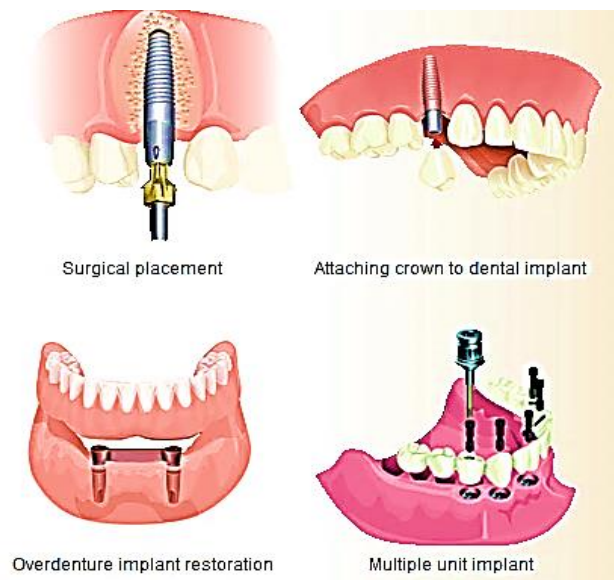


Fig.1.3. Different prosthetic restorations
(http://www.cairnsperiodontics.com.au/dental_implants.html)

With the permanent progressing of dental implant systems, it was required to shorten the long healing periods between procedures stages which can be one of the disadvantages of implantation.

According to Brånemark's theory it was suggested that early loading would lead to encapsulation of the implant leading to failure. But recent studies have reported otherwise [5, 6] suggesting that insertion of the implant and prosthesis placement can be made in a single step. In this case, the protocol is called **immediate loading**. Dentists are interested in reducing the healing time after first stage but it should be taken in consideration that the body has a minimum time to perform the reactions that lead to osseointegration. Thus to shorten the healing time, they were more oriented toward controlling the biocompatibility of titanium implant surfaces, modifying the surgical technic and changing the implant design. [7]

1.1. Bone tissue

Bone is a connective tissue formed of cells and a mineralized extracellular matrix. It contains about, 25% organic matrix, 10% water and the rests are crystallized mineral salts [8]. The main composing mineral is calcium phosphate ($\text{Ca}_3(\text{PO}_4)_2$), which combines with calcium hydroxide ($\text{Ca}(\text{OH})_2$) to form calcium hydroxyapatite crystals which in turn combine with other mineral salts like calcium carbonate (CaCO_3) and ions such as Mg^{+2} . These minerals are deposited in the collagen fibers structure of the extracellular matrix; get crystallized and thus hardening the tissues. This calcification is initiated by bone forming cells which called osteoblasts. [9]

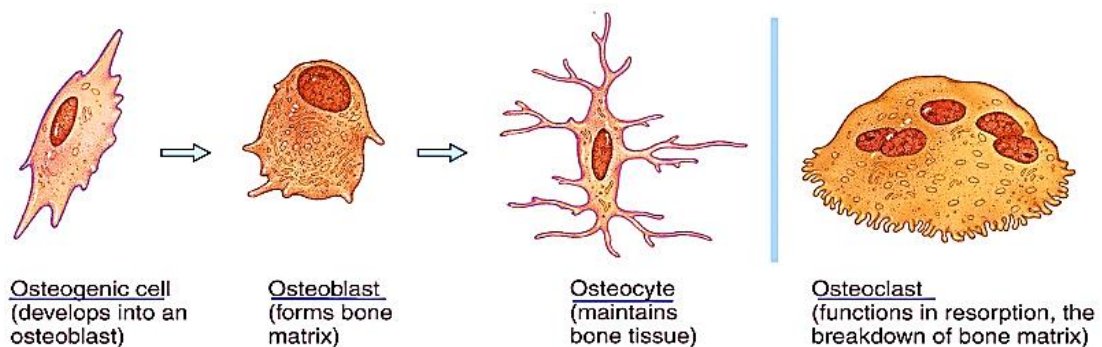


Fig.1.4. Bone cells [11]

Four types of cells exist and maintain bone formation, resorption and maintenance; osteogenic cells, osteoblast cells, osteocytes, and osteoclasts. (Fig.1.4)

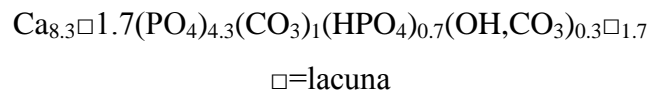
Osteoblast cells are bone building cells. They secrete collagen type-1 fibers and save extracellular matrix containing calcium hydroxyapatite and get intercepted to become osteocytes. Osteocytes help in exchanging the nutrients and wastes with blood stream. They do not undergo any further cell division. Osteoclasts are multinucleated cells which release lyzosomal enzymes and acids and thus help in resorbing fractured or damaged bone. [9, 10]

Mechanical properties of the bone

Bone is a relatively hard and lightweight material. It has relatively high compressive strength of about 170 MPa (1800 kgf/cm²) but poor tensile strength of 104–121 MPa and very low shear stress strength (51.6 MPa), [12] meaning it resists well pushing forces, but not pulling or torsional forces. Modulus of elasticity of bone samples are estimated about 420 to 700 kg/cm². [12]

Bone mineral structure ;

Bone miner has a structure represented by the formula [13]



Bone mineral apatite has non-apatitic carbonate and phosphate groups, which are unstable and very reactive compounds that provide certain physicochemical, biological and functional features for the crystals formation and dissolution in biological tissues . Bone contains also minor or trace elements, which are not indicated in the above formula [13].

1.2.Biomaterials used in implantology: Titanium

The most important property of materials used for implants is biocompatibility [14]. Common metallic biomaterials are stainless steels, cobalt alloy (Co-Cr alloys), titanium and its alloys.

Among bio-metals, titanium alloys have high biocompatibility, strength, low density and good corrosion resistance, attributing the best requirements for biomedical applications [14].

Titanium is element number 22 in the periodic table; it was discovered by William Gregor in 1795. [15] It has high strength-to-weight ratio with a density of 4.5 g/cm^3 (0.16 lb/in.^3) and still functional at high temperatures (370 to 590 °C) with a corrosion resistance that is superior to both steel and aluminum alloys. [15]

Furthermore, Titanium is considered as the most biocompatible of all metals due to its ability to resist body fluids attack, stay inert in the human body and bear functional pressures and loads during use. [16] These features are due to the protective oxide film that forms naturally in the presence of oxygen. [16] This oxide film is highly adherent, insoluble, and chemically non transportable, preventing reactions from occurring. It has the inherent ability to osseointegrate, enabling its use for dental implants that can remain in place for longtime. Compatibility with MRI (Magnetic Resonance Imaging) and CT (Computed Technology) also contribute to the selection of titanium as the material of choice in orthopedic applications.

Titanium is often alloyed with about 4% aluminum [17] or 6% Al and 4% vanadium. (Which is Grade 5 of Titanium alloys and also known as Ti6Al4V, Ti-6Al-4V or Ti 6-4) which had far superior mechanical strength. [17, 18]

Biomedical applications

Titanium is the standard material of choice for orthopedic devices such as artificial hip joints (total and partial hip replacement), bone screws, knee joints replacement, spinal fusion cages, shoulder and elbow joints, and bone plates. [19] (Fig. 1.5).

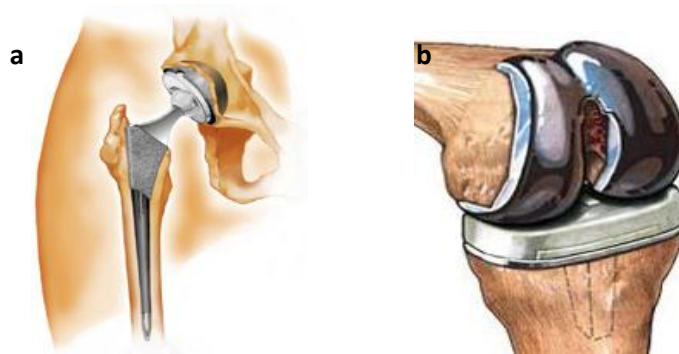


Fig.1.5. Orthopedic applications of Titanium (a) titanium hip joint (b) knee joint replacement

Also, one of the most common applications of Titanium is in the dental implants domain. Dental implants can be classified as subperiosteal, transosteal, and endosseous according to their position and shape. (Fig.1.6)

Subperiosteal implants [20] consist of a custom-cast framework which stays on the bone surface beneath the muco-periosteum. Transosteal implants can only be placed in the frontal lower jaw while endosseous implants can be placed in both the upper and lower jaws via a muco-periosteal incision.

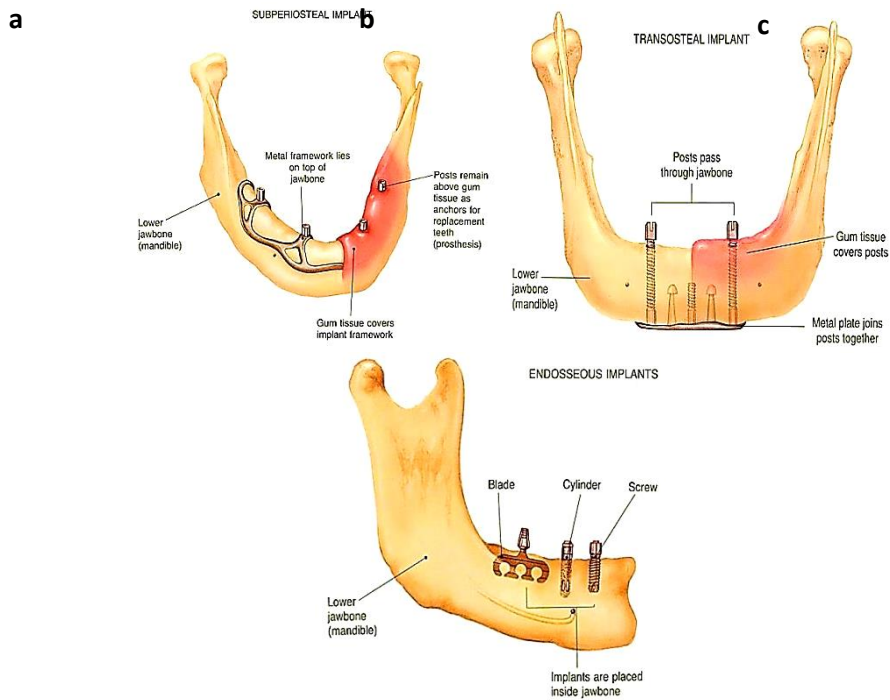


Fig.1.6. Implants according to their position (a) subperiosteal “on top of the bone”, (b) transosteal “through the bone” (c) endosseous “within the bone” (<http://dentalimplants.uchc.edu/about/types.html>)

The endosseous implants are the most commonly used implant types and can be used in almost all situations such as single implants to replace one missing tooth and also in cases of partial and total edentulism. Many shapes have been designed to maximize the osseointegration area and provide good stability such as hollow-cylinders, solid cylinders, hollow screws or solid screws. (Fig.1.7)

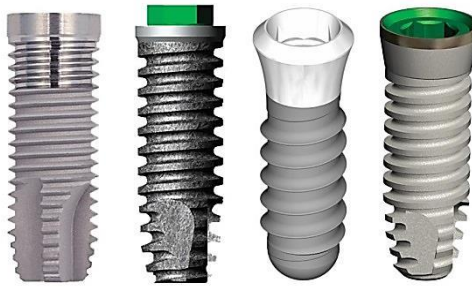


Fig.1.7. Different shapes of endosseous screws.

Other Titanium alloys applications are prosthetic heart valves, protective cases in pacemakers artificial hearts, stents and circulatory devices [19]. (Fig.1.8)

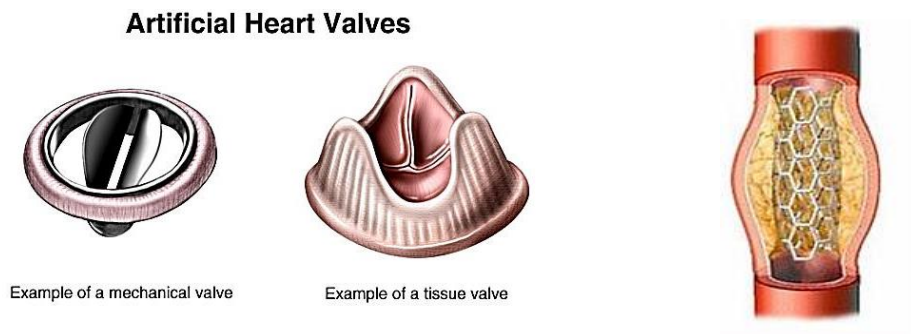


Fig.1.8. Artificial heart valve and artificial vascular stents

Titanium alloys are also used in osteosynthesis implants [24] including bone screws, bone plates, maxillofacial implants, etc. Bone screws are used as single screws for direct bone fixation for the fixation of plates or other devices to the bones. Titanium is also used for the surgical instruments used in image-guided surgery and all products or instruments which require both high strength and low weight.

1.3.Osseointegration of dental implants

A Swedish orthopedic surgeon Dr. Per-Ingvar Brånemark in the late 1950's found out by chance the conception of osseointegration [2, 21] but it was only until 1965 when his concept of osseointegration was applied clinically for the very first time [3]

The term “**osseointegration**” was defined as a functional and structural contact between the surface of an implant and the surrounding living bone that last under functional loading without any symptoms [4]. Later, osseointegration was defined as”

The process whereby clinically asymptomatic rigid fixation of alloplastic materials is achieved, and maintained, in bone during functional loading” [22]

An implant is considered to be osseointegrated when there is an absence of movement between the implant and bone under normal loading conditions following a defined healing period. This is a result of direct bone integration with implant surface without formation of a poorly vascularized collagenous capsule, called fibrous encapsulation.

Different factors determine the progress of osseointegration, including the implant's material properties, form and surface characteristics, mechanical load, surgical technic, location and local quality of the host bone [23].

The mechanisms of implants osseointegration are as follows; An initial surgical injury is caused through creation of the implant cavity, then, the necrotic tissue is resorbed and new matrix is formed to close the gap between bone and implant [23]. For good anchorage of the implant, primary bone healing is required to insure immediate stability, this is characterized through direct precipitation of new bone at the interface with a minimal distance ($< 1\mu\text{m}$) between implant and bone [24].

Bioactive coated materials bond to bone tissue through chemical bridges that are mediated by calcium and phosphorus ions, while the non-coated titanium implants bond to bone through weak Van Der Waals and hydrogen bonds [25]. Thus, chemical compositions of oxide and surface state have great influence on the occurrence of strong bonds [7].

Histologically, osseointegration is identified by the presence of regenerated bone at the implant-bone interface [25, 26]. Microanalysis and tracing of chemical elements in the region around the implant indicated the presence of titanium, calcium and phosphorus, confirming the bone mineralization [26].

The implant healing starts by an initial formation of a blood clot followed by a cellular activation and osteoblast differentiation and finally bone mineralization [27]. (Fig.1.9)

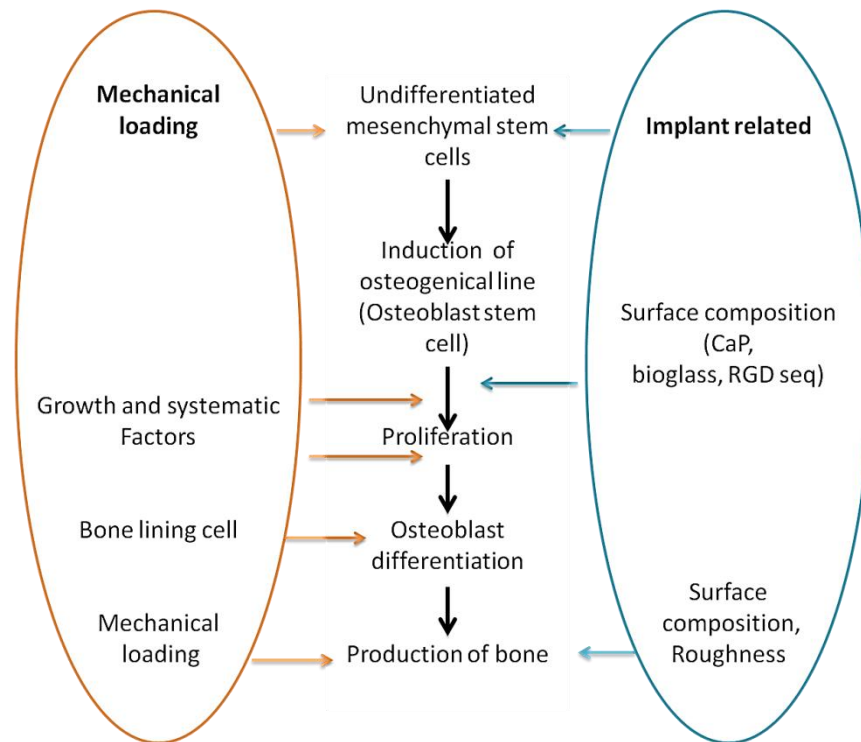


Fig.1.9. The implant healing process

During surgery, plasma proteins (e.g. fibrin) get adsorbed on the implant surface. Fibrinogen is converted to fibrin and also kinin and other systems become activated. [29]. Activation of platelets (a rich source of growth factors) occurs as a result of their interaction with the implant surface and the fibrin scaffold which leads to blood clotting [29]. Protein adsorption by implants surface depends on the surface properties of the material. Thus, dental implants were developed with high hydrophilic and rough surfaces to obtain better protein adsorption. [30]

The micro-mechanism of the bone-implant connection (BIC) depends on specific surface chemical properties. According to Albrektsson et al. [31], commercially pure titanium implants (cp.Ti) were shown to form very close contacts with bone. (Fig.1.10). Many other studies confirmed those reports, indicating that cp.titanium is perfectly compatible with tissues. [19, 29]

Surface characteristics influence the binding capacity of fibrin and the growth factors release, thereby affecting the mesenchymal cells migration [23]. Titanium materials have perfect fibrin retention on their surface. Through this fibrin matrix, osteogenic cells migrate to the implant surface and create bone directly on the surface. Davis [32] termed this phenomenon as *de novo* bone formation through contact osteogenesis.

Upon arrival to the surface, the differentiated osteogenic cells secrete the collagen-free matrix for the mineralization by calcium and phosphate precipitation. This matrix consists of non-collagenous proteins (mostly osteopontin and bone sialoprotein) and proteoglycans. [32]

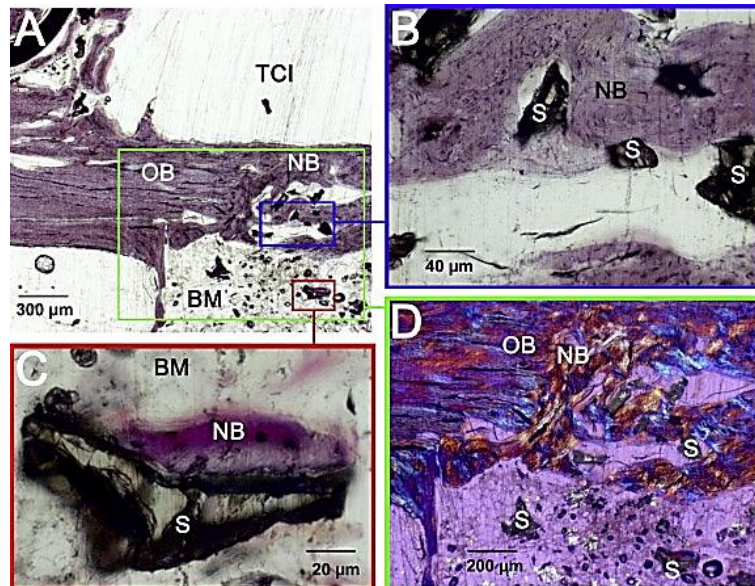


Fig.1.10 Histo-microphotographs of section from defect site implanted with TiO_2 scaffold. Section surface-stained with van Gieson. (A) Overview microphotograph. (B) Newly formed cortical bone inside scaffold. (C) New bone on scaffold surface within the bone marrow, distant from the cortical bone. (D) Old cortical bone next to new cortical bone. This bony border illustrates the vertical dimension of the original defect (polarized light). BM = bone marrow, TCI = titanium coin implant, OB = old bone, NB = new bone, S = scaffold. [28].

After the calcium phosphate precipitation, the formation and mineralization of collagen fibers start by establishing a non-collagenous tissue between the implant surface and the calcified collagen through osteogenesis. This intermediary tissue is very important to understand the bonding mechanism between bone and a bioinert titanium implant.

After that, woven bone formation and organization of trabecular bone start to take place for the reconstitution of the damaged bone at the peri-implant area [33]. At three months of healing the implant is mostly surrounded by a mixture of woven and lamellar bone [33].

2. Challenges and advancing in dental implantology

Implantology is always progressing and over the years, many different implant systems have been introduced in many designs and for different indications.

Although the high success rates reported for many implant systems [34], failures leading to implant removal still occur. The failure rates in the edentulous maxilla and mandible are reported about 10% and 3%, respectively [35]. Failure rates were higher in the posterior maxilla (19.1%) and anterior maxilla (16.82%), while mandibular failure rates were between 4% and 5%. Studies reported that success rate of standard implants ($D > 3\text{mm}$), after a 5 years survey, varies between 87,9% and 91,2%. [36].

Implants fail for many reasons; biological factors, biomechanical and biomaterial factors, implant surface treatments (e.g., etching, coating), insufficient quality and/or quantity of bone to support the implant fixture, the surgical technique, implant location, systemic health of the patient; etc. [37, 38]

Implant failure is defined as the insufficiency of the host tissue to establish or to maintain osseointegration [35]. Failing implants are characterized by loss of supporting bone, mobility and peri-implant radiolucency. Patients feel spontaneous pain as well as pain on clenching, percussion or palpation. Deep pockets may present also.



Fig.1.11 X-ray photo shows the difference between a successful and a failed dental implant

Peri-implantitis is the destructive inflammatory process affecting the soft and hard tissues surrounding dental implants causing their failure. The higher rates of many

systems implant failure due to peri-implantitis has been attributed to differences in implant design and surface characteristics [35]

In 1986, Albrektsson et al, [39] suggested success criteria for Marginal bone loss (MBL). During the first year after abutment connection, 1 mm of MBL is allowed followed by 0.2 mm per year. Today, these criteria are still referred to as the “gold standard” for implant success. According to Albrektsson [39], factors that determine the achievement of osseointegration include; biocompatibility of the implant material, implant design, implant surface conditions, the host bed and the surgical technique. Since then, many studies were developed to achieve the requirements for successful implant systems (i.e., mechanical compatibility, biological compatibility, and morphological compatibility) [40] by altering surface characteristics to get over the implantation difficulties, obtain better osseointegration and reduce the tissue healing time for immediate loading of implants essentially in aesthetic cases.

3. Surface modification

The implant design has a key role in the primary stability and following functions. Many techniques were applied to improve commercial implants systems and to enhance their biological and functional priorities.

Implant surface characteristics play a key role in the success of osseointegration. Therefore, many researchers were interested in optimizing the biological response using surface modification approaches [40, 41]. Implants surface characteristics, such as nano/micro-topography, and chemical composition, have a great influence on the osseointegration outcomes [42].

Although titanium is preferable compared to other implant metals, still, its osteoconductivity is lower than calcium phosphate (CaP) based bio-ceramics. [41, 42] For this reason, studies have focused on improving titanium bioactivity and providing a higher osteoconductivity to the bulk material by altering the surface properties to increase the local quantity and quality of osseous tissue at the interface, especially in regions of the jaw such as the edentulous posterior maxillae where the cortical thickness is frequently insufficient for the primary stability.

Surface morphology and roughness have been shown to alter the cellular response to dental implants by affecting their biomechanical properties and providing a greater amount of bone connected to implant surface. [43]. (Fig.1.12)

Moreover, surface chemistry is another key factor for bone-implant apposition, since it influences biological and the chemical reactions with the physiologic environment. Wettability and surface energy also influence the adsorption of proteins, and increase adhesion of osteoblasts on the implant surface.

The expressions of specific growth factors for osteoblasts are higher on hydrophilic surfaces than hydrophobic ones; consequently, dental implants manufacturers have developed high hydrophilic and rough implant surfaces which in turn exhibited better osseointegration than implants with smooth surfaces. [43].

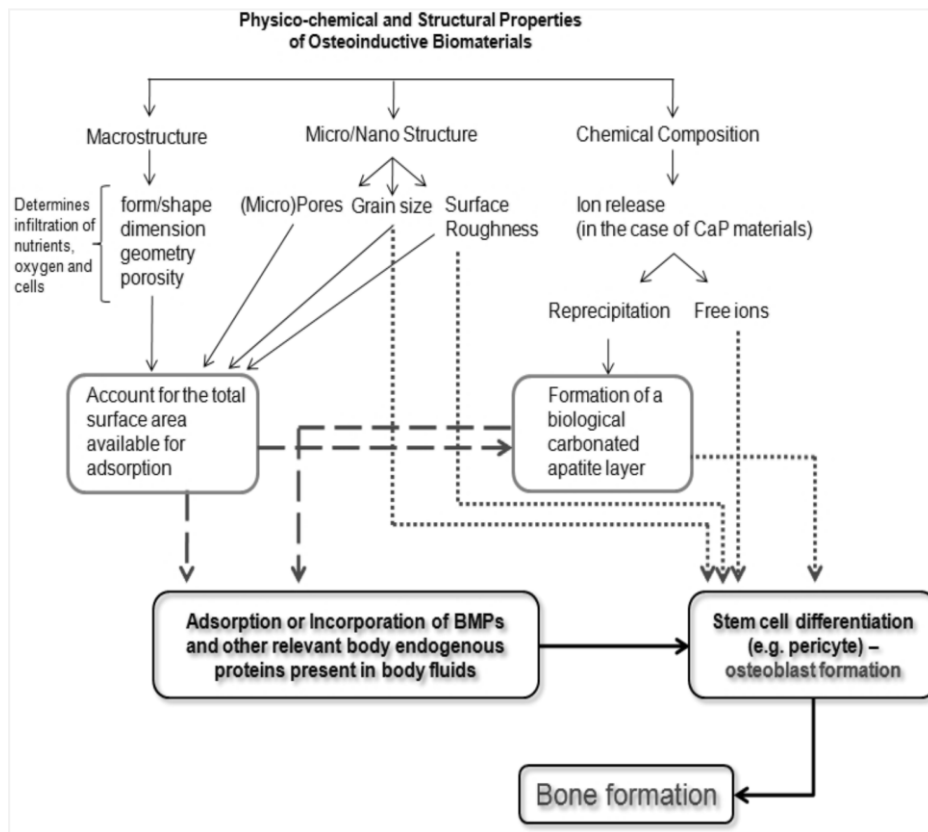


Fig.1.12. Schematic summarizing hypothesized mechanisms behind osteoinduction by biomaterials.[44]

3.1. Surface roughness of dental implants / Topographical modifications

Several implant-related factors such as surface topography, chemical composition and surface roughness that influence osseointegration have been studied. It has been shown that titanium implants with adequate roughness may influence the initial stability of implants, enhance BIC (bone-to-implant contact), and may increase removal torque force. [45]

The first generation of dental implants, termed the **turned implants (machined dental implants)**, had a relatively smooth surface. Thus, osteoblastic cells can't grow along the grooves existing on the surface due to manufacturing tools. This characteristic requires a longer waiting time between surgery and implant loading. The use of these implants follows the protocol suggested by Brånemark i.e., 3-6-month healing or waiting time prior to loading.[4]

Due to morphological characteristics, lower resistance to removal torque and relative lesser success ratios, machined dental implants are becoming commercially unavailable.

Progressively, experiments with bioactive physicochemical surface modification to develop new implant surfaces encouraged new considerations of improvements in bone formation at the implant surface. [46]

The main clinical indication for using a rough surface implant is the poor quality or volume of the host bone. In these situations, early and high bone-to-implant contact would be beneficial for allowing stability and tolerance. In such cases, short designed implants with a rough surface have demonstrated superior clinical outcomes than smooth turned surfaces [47]. Several *in vivo* and clinical studies have suggested a positive correlation between surface roughness and BIC [48].

The surface roughness of the titanium implants can significantly alter the osseointegration process due to the fact that cells react differently to smooth and rough surfaces. Fibroblasts and epithelial cells adhere stronger to smooth surfaces, whereas osteoblastic proliferation and collagen synthesis are increased on rough surfaces [49]. Therefore, such selective cell adhesion property offers an advantage of a roughened surface with respect to its potential to induce true direct bone contact but not unfavorable integration such as fibro-osseous integration. [49].

However, it is possible that implant materials with a rough surface topography induce a three-dimensional growth of cells, promoting osteoblast and mesenchymal cells differentiation by activation of several osteogenic-associated genes, e.g. core-binding factor 1 (Cbfa1), collagen, alkaline phosphatase, osteonectin, osteopontin and bone sialoprotein. [50].

Implant surface with various roughness have been used to increase the total area available for osseointegration, and to have a larger surface to get a better mechanical interaction. Implant surface roughness is divided, depending on the dimension of the measured surface features into macro, micro, and nano-roughness [51, 52]. (Fig.1.13)

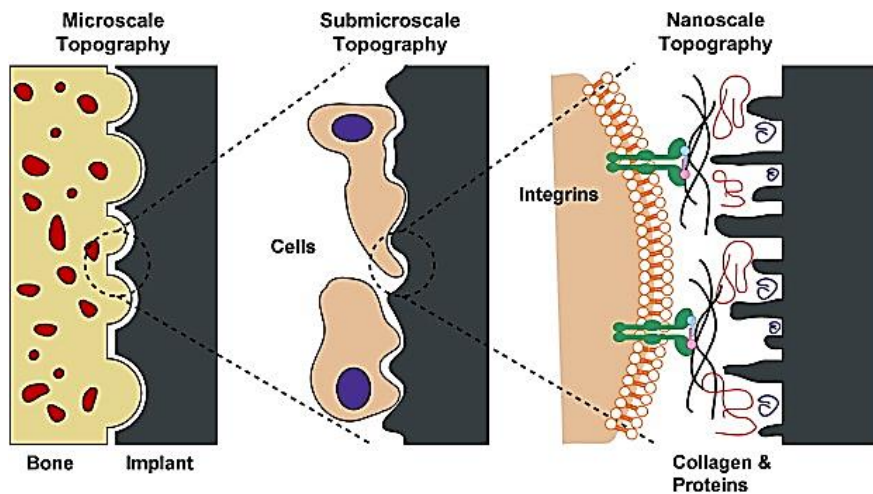


Fig.1.13. Schematic of the interactions between bone and the implant surface at different topographical scales.

Macro roughness comprises features in the range of millimeters to tens of microns while micro roughness is determined at the range of 1–10 μm . However, with this scale, peri-implantitis may increase with an increase in ionic leakage. A moderate roughness of 1–2 μm may limit these two parameters [53]. Nanotechnology involves materials that have a nano-sized topography with a size range between 1 and 100 nm. Nanometer roughness plays an important role in the adsorption of proteins, adhesion of osteoblastic cells and thus the rate of osseointegration [54].

3.2. Nanotechnology and dental implants

The nanometer-sized roughness influences the surfaces interactions with proteins and cells. At nanoscale, surface topography increases the surface energy which in turn

increases the wettability of the surface to blood, adhesion of cells to the surface by inducing a three-dimensional cell growth, and facilitates binding of fibrin, matrix proteins and growth factors. Nanotopography alters cellular responses; by direct (cell–surface interactions) and indirect (affecting protein–surface interactions) mechanisms [55].

Kubo et al. [56] observed a substantial increase by 3.1 times in bone-titanium interfacial strength by Ti nanotube (300nm) at 2 weeks of implantation in femur rats.

It is possible that nano-roughness topology could modify the protein adsorption and conformation of integrin-binding molecules and thus modulating intracellular integrin pathway [55]. Recent studies have shown strong cell responses with increased levels of two important bone matrix proteins, osteocalcin and osteopontin. [57]

Moreover, Oh et al. [58] have shown that the optimal dimension (approximately 30–100 nm diameter) of nanotube titanium oxide surface structures notably induce human mesenchymal stem cells differentiation into osteoblasts without supplemented use of osteogenic-inducing factors *in vitro*. The reason for this is not yet well determined, but it is possible that such pore size may allow stem cell elongation that in turn influences cytoskeletal stress, thus promoting stem cell differentiation into osteoblastic cells.

Material topography also plays a significant role in the bacterial attachment to the surface, probably when the surface roughness is comparable to the bacterial size and thus can protect the surface from unfavorable environment. Generally, most common bacteria range 0.5 -5 μm , thus, it is possible that surface roughness on a scale much smaller than the bacterial one would not be expected to influence the initial attachment. It is notable that while osteoblastic cells are selectively adhered onto nanoscale surface, bacterial adhesion and growth on such surface is reduced [59]. Such nanometer-roughness may provide favorable condition for successful osseointegration by preventing post-operative bacterial infection. Moreover, nanotubular layer provides a very high surface-to-volume ratio for more cells adhesion.

Davis [60] indicated that nanoscale modification of the implant surface may modify the endosseous implants surface reactivity and change the chemical reactivity of bulk materials [60]. Existing reports suggest that little bone bonding occurs at endosseous titanium implants, particularly in the early phases of bone formation [60]. Nanoscale

modification of the titanium endosseous implant surface may affect both the topography and the chemistry of the surface.

3.3. Calcium Phosphate-based osteoconductive materials

Calcium Phosphates are the main mineral constituent of teeth and bones. CaPs have excellent bioactivity with a great ability to form a direct bond with bone. In addition, they can be resorbable, with a resorption rate that depends on their composition and microstructural features. [61]. Bone inorganic constituent is made up of biological apatites. These apatites, along with other CaPs such as fluorapatite (FAP, $\text{Ca}_5(\text{PO}_4)_3$), monetite (M, CaHPO_4), tricalcium phosphate (TCP, $\text{Ca}_3(\text{PO}_4)_2$), tetracalcium phosphate (TTCP, $\text{Ca}_4(\text{PO}_4)_2$), and octacalcium phosphate (OCP, $\text{Ca}_8\text{H}_2(\text{PO}_4)_6 \cdot 5\text{H}_2\text{O}$) belong to a family of calcium phosphates minerals [62]. The atomic ratio of Ca/P in calcium phosphates can be varied between 1.5 and 2 to produce compounds ranged from TTCP, HAp to TCP. (Table.1.1). summarizes the mineral and chemical names and composition of various phases of calcium phosphates. These materials demonstrate similar structural formula as $\text{X}_3\text{Y}_2(\text{TO}_4)\text{Z}$. In nature, apatite compositions include X and Y = (Ca, Sr, Ba, Re, Pb, U or Mn) ; T = (P, As, V, Si, S, or C); and Z = (F, Cl, OH, or O).

In biomedical application, apatites have X = Y = Ca, T = P, and Z = F or OH. For example, the apatite is called hydroxyapatite (HAp) when T = P and Z = OH. [62, 63] Mineral HAp ($\text{Ca}_{10}(\text{PO}_4)_6\text{OH}_2$) and brushite ($\text{CaHPO}_4 \cdot 2\text{H}_2\text{O}$) are the closest to biological CaP materials. Only these two forms of calcium phosphates are stable at the body temperature and in body fluid. At $\text{pH} < 4.2$ the stable calcium phosphate phase is brushite. At $\text{pH} > 4.2$ the stable phase is HAp. [62] (Fig.1.14) Their solubility and hydrolysis speed increase with decreasing Ca/P ratio, for this reason not all CaPs compounds are useful for implantation in the body. Driessens et al, [66] indicated that compositions with a Ca/P ratio less than 1:1 are not suitable for biological implantation.

Small dimensions and low crystallinity are notable advantages of biological apatite. Crystalline disorder and the fact that the crystal lattice contains other ions, interpret their biological priorities. For example, the small crystal size means that a large

proportion of the atoms are on the crystal surface, creating a large surface area to deposit ions, proteins and drugs [65]. (Fig.1.14)

Ca/P molar ratio	Compound	Formula	Solubility at 25 °C, $-\log(K_s)$	Solubility at 25 °C, g/L	pH stability range in aqueous solutions at 25 °C
0.5	Monocalcium phosphate monohydrate (MCPM)	$\text{Ca}(\text{H}_2\text{PO}_4)_2 \cdot \text{H}_2\text{O}$	1.14	~ 18	0.0 – 2.0
0.5	Monocalcium phosphate anhydrous (MCPA or MCP)	$\text{Ca}(\text{H}_2\text{PO}_4)_2$	1.14	~ 17	[a]
1.0	Dicalcium phosphate dihydrate (DCPD), mineral brushite	$\text{CaHPO}_4 \cdot 2\text{H}_2\text{O}$	6.59	~ 0.088	2.0 – 6.0
1.0	Dicalcium phosphate anhydrous (DCPA or DCP), mineral monetite	CaHPO_4	6.90	~ 0.048	[a]
1.33	Octacalcium phosphate (OCP)	$\text{Ca}_8(\text{HPO}_4)_2(\text{PO}_4)_4 \cdot 5\text{H}_2\text{O}$	96.6	~ 0.0081	5.5 – 7.0
1.5	α -Tricalcium phosphate (α -TCP)	$\alpha\text{-Ca}_3(\text{PO}_4)_2$	25.5	~ 0.0025	[a]
1.5	β -Tricalcium phosphate (β -TCP)	$\beta\text{-Ca}_3(\text{PO}_4)_2$	28.9	~ 0.0005	[a]
1.2 – 2.2	Amorphous calcium phosphates (ACP)	$\text{Ca}_x\text{H}_y(\text{PO}_4)_z \cdot n\text{H}_2\text{O}$, $n = 3 - 4.5$; $15 - 20\% \text{H}_2\text{O}$	[b]	[b]	~ 5 – 12 [d]
1.5 – 1.67	Calcium-deficient hydroxyapatite (CDHA or Ca-defHA) [d]	$\text{Ca}_{10-x}(\text{HPO}_4)_2(\text{PO}_4)_8(\text{OH})_2$, $(0 < x < 1)$	~ 85	~ 0.0094	6.5 – 9.5
1.67	Hydroxyapatite (HA, HAp or OHAp)	$\text{Ca}_{10}(\text{PO}_4)_6(\text{OH})_2$	116.8	~ 0.0003	9.5 – 12
1.67	Fluorapatite (FA or FAp)	$\text{Ca}_{10}(\text{PO}_4)_6\text{F}_2$	120.0	~ 0.0002	7 – 12
1.67	Oxyapatite (OA, OAp or OXA) [d]	$\text{Ca}_{10}(\text{PO}_4)_6\text{O}$	~ 69	~ 0.087	[a]
2.0	Tetracalcium phosphate (TTCP or TetCP), mineral hilgenstockite	$\text{Ca}_4(\text{PO}_4)_2\text{O}$	38 – 44	~ 0.0007	[a]

Table.1.1 Existing calcium orthophosphates and their major properties [64]

[a] These compounds cannot be precipitated from aqueous solutions

[b] Cannot be measured precisely. However, the following values were found: 25.7 ± 0.1 (pH = 7.40), 29.9 ± 0.1 (pH = 6.00), 32.7 ± 0.1 (pH = 5.28). The comparative extent of dissolution in acidic buffer is: $\text{ACP} \gg \alpha\text{-TCP} \gg \beta\text{-TCP} > \text{CDHA} \gg \text{HAp} > \text{FA}$

[c] Stable at temperatures above 100 °C

[d] Always metastable [e] Occasionally, it is called “precipitated HA (PHA)”

[f] Existence of OA remains questionable

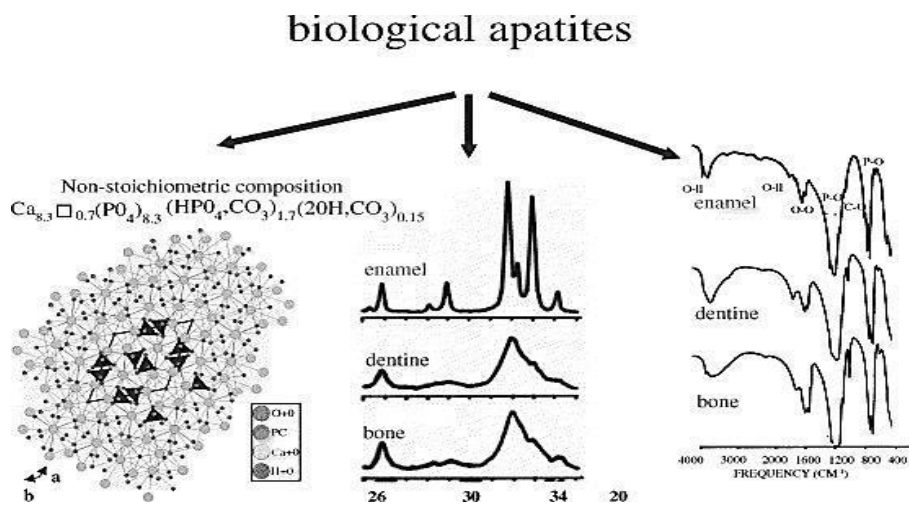


Fig.1.14 Crystal structure of biological apatites. Powder X-ray diffraction patterns and infrared spectra of enamel, dentine and bone [65]

Each of the CaP phases has a different bioactivity and different dissolution rate in aqueous environments. Dissolution rate decrease in the following order:

Amorphous HAp >> TTCP > α -TCP > OHA >> β -TCP >> Crystalline HAp. [65]

As crystalline HAp is the most stable phase in biological environment, it became one of the main CaP phases that have been evaluated and used clinically. However, CaPs can be resorbed by two different mechanisms upon implantation; active resorption by macrophages or osteoclasts, and/or passive resorption by chemical dissolution or hydrolysis in the body fluids. Brushite cements are mainly resorbed by passive mechanism because they are soluble in body fluids [67] while apatites, being less soluble, are mostly resorbed by the active mechanism [67], i.e. macrophages and osteoclasts cause a local decrease of pH values at which apatite becomes soluble. The incorporation of ionic substitutions can control CaPs dissolution. For example, carbonates incorporation increases apatite lattice disorder enhancing crystal dissolution [68, 69]. Besides, external factors like patient age, sex, metabolism, health, social habits, implantation site, blood supply or mechanical loads, can affect resorption.

3.4. Surface modification methods

Many methods have been developed to create a better titanium surface for endosseous implants and improve their osseointegration (Table.1.2).

A summary of the current advanced surface modifications of implants	
Topographical modification (Surface roughening)	<ol style="list-style-type: none"> 1. Physical compaction 2. Molecular self-assembly method 3. Chemical modification: acid/alkaline treatment, peroxidation. 4. Nanoparticle deposition: sol-gel, crystalline deposition
Biomimetic calcium phosphate coatings	<ol style="list-style-type: none"> 1. Electrochemical method 2. Immersion method
Incorporation of biologically active agents	<ol style="list-style-type: none"> 1. Osteogenesis-inducing agents: BMPs, TGTs, VEGFs, PDGFs, IGFs. 2. Bone remodeling-associated agents: Bisphosphonates. 3. Synthetic RGD peptides. 4. Antibiotics.

Table1.2. A summary of the current advanced surface modifications of implants [70]

These methods are mainly classified as surface roughening methods and surface coating with different compositions.

3.4.1. Acid-etching

A very common method to roughen the titanium implant surface is etching with strong acids such as HCl, H₂SO₄, HNO₃ and HF. By acid-etching, it's possible to create homogenous micro-porous roughness and increase surface activity. Moreover, it's possible to produce micro pits with a diameter range (0.5 to 2µm) on titanium surfaces [71]. (Fig.1.15)

Furthermore, titanium implants immersion in a solution of concentrated HCl and H₂SO₄ with a temperature above 100 °C (**dual acid-etching**) for many minutes is used to create a micro-scale surface [71]. It was reported that dual acid-etched surfaces can favor osseointegration through the attachment of fibrin and osteogenic cells, and thus forming bone directly on the surface of the implant [72, 73]. Nevertheless, this technic still has many disadvantages as it may minimize the mechanical properties of titanium by creating micro cracks on its surface that could reduce the fatigue resistance of the implants [73].

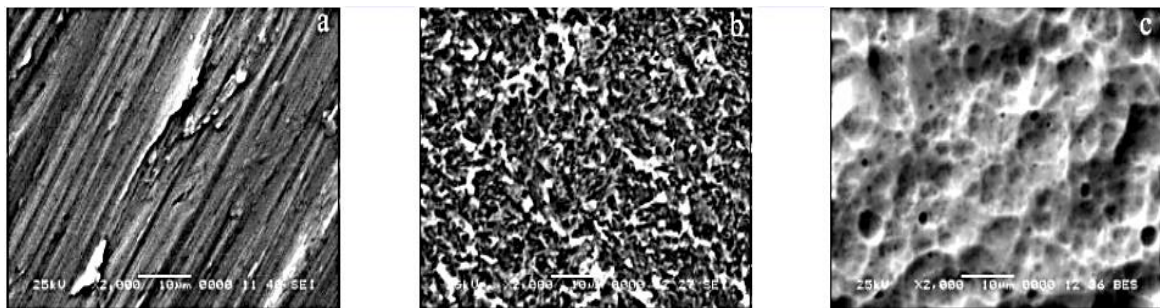


Fig.1.15. SEM images of titanium discs. (a) Disc with machined surface. Regular machining grows apparent on the surface. X2000 mag. (b) Disc with acid etched (HCl) surface with micro-texture without micro pits. (c) Disc with acid etched (HCl and H₂SO₄) surface. Micro-texture with few micro pits and smooth waviness [74]

3.4.2. Sandblasted and acid-etched (SLA) implants

The sandblasting procedure by 250-500µm grits creates surface within the optimal range of 1.0–2.0µm [76]. When followed by the hydrochloric/sulfuric acid etching, it can produce smaller pits at the sub-micron to micron level. The SLA technique

combines the advantages of both sandblasting and acid-etching methods to obtain macro-roughness and micro pits.

The roughness value is dependent upon sandblasting factors such as blasting material, particle size, blasting pressure; etc. The micro morphology formed on the SLA treated surface increases the surface area, and benefits osteoblast proliferation. [77].

It was reported that some residual particles were found on the implant surface after the sandblasting, which is a contamination that must be removed with ultrasonic bath and acid etching. [7]. (Fig.1.16)

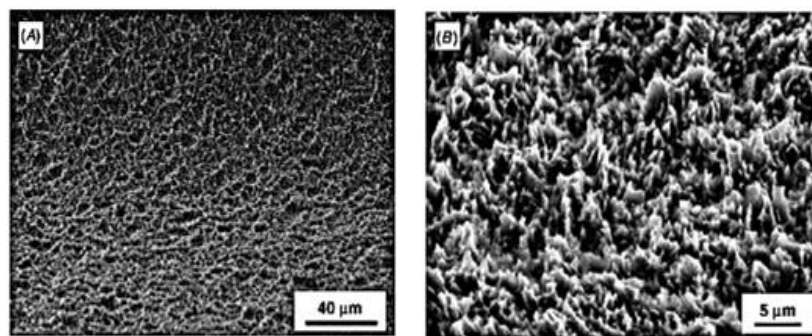


Fig.1.16. SEM images of SLA Ti surface [77].

3.4.3. Grit-blasting

The goal of grit blasting technic is to control surface roughness by using hard ceramic particles and varying the selected particle size. The blasting material should be chemically stable and biocompatible such as silicon oxide, aluminum oxide, titanium oxide and calcium phosphate compounds. The common size of used blasting materials is about (25- 75μm) but the final roughness may be controlled by varying the selected particle size [78]. (Fig 1.17)

Titania blasted surfaces presented higher osseointegration ratios compared to machined implant surfaces but it also has a disadvantage that the chemical heterogeneity of the implant surface may reduce the corrosion resistance of titanium in biological environment [79].

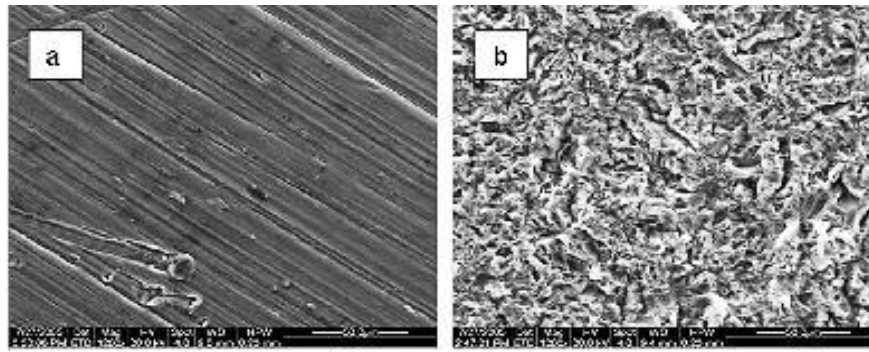


Fig.1.17. SEM images showing the morphology of the surfaces of the Ti6Al4V substrates: machine-polished (a), grit-blasted (b) (<http://dentalis-implants.com/documentation/bas-bio-active/the-optimal-ra-micro-roughness-surface>)

3.4.4. Anodisation

Anodic oxidation/ Anodisation is an electrochemical process that changes the TiO₂ layer characteristic, increases its roughness in a controlled manner [80].

In potentiostatic or galvanostatic anodisation, the implant is immersed in an electrolyte of strong acids (H₂SO₄, H₃PO₄, HNO₃, HF) representing the anode in an electrochemical cell. When a potential is applied to the sample, ionic transport of charge occurs through the cell, and an electrolytic reaction occurs at the anode, by dissolving the oxide layer along current transport paths and thickening in other regions. The oxide layer dissolution regions form micro or nano-pores on the titanium surface [81]. The anodisation process and the oxide layer thickness depend on various parameters such as current density, concentration of acids, composition and electrolyte temperature and they can be controlled by modifying these parameters. Higher clinical success rates were observed for the anodized titanium implants in comparison with turned titanium surfaces of similar shapes [82]. This was explained by the mechanical interlocking through bone growth in pores and the biochemical bonding [81, 82]. The anodized surface implant has a higher polarity compared with acid-treated samples, which promote water and molecules adsorption. [7]. Also those surfaces allow primary stability as they present a larger surface area and allow a stronger mechanical link to the surrounding tissues. [7]. (Fig.1.18) This method will be discussed more in the following chapters.

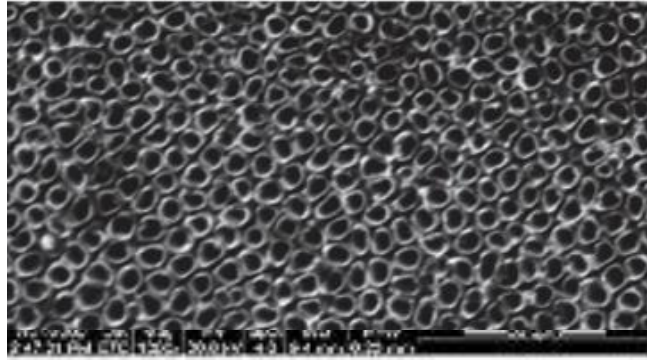


Fig.1.18. SEM image of anodized nanotubular titanium 200 nm

3.4.5. Titanium plasma-spraying (TPS)

This method consists in injecting titanium powders into a plasma torch at high temperature and releasing the titanium particles on the implant surface forming a film of a thickness that must reach 40–50 μm to be uniform. The resulting TPS coating has an average roughness of $\sim 7\mu\text{m}$, which increases the surface area of the implant [83]. (Fig. 1.19)

Although higher bone formation rates were observed when TPS treated surface were used compared to machined ones, particles of titanium have been found in the bone adjacent to these implants [84]. The presence of metallic wear particles from endosseous implants in other places in the body such as, the liver, spleen and even in the para-aortic lymph nodes have also been reported [84]. Metal ions released from implants may be because of dissolution, fretting and wear, and may be a source of concern due to their potentially harmful local and systemic carcinogenic effects [83, 84].

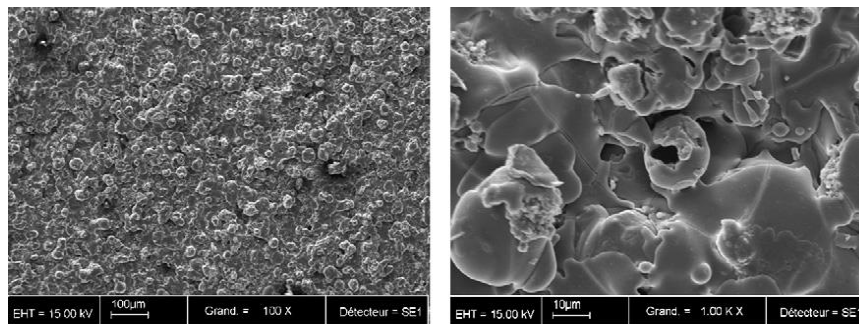


Fig.1.19. SEM images of a titanium plasma-sprayed (TPS) surface (Courtesy of Cam Implants BV, The Netherlands).

3.4.6. Hydroxyapatite coating

The coating with hydroxyapatite ($\text{Ca}_{10}(\text{PO}_4)_6(\text{OH})_2$) has been recently applied considering such technic as bioactive coating of implant surface that enhance biological process and bone healing through the rich CaP calcium phosphate coating reactions with the surrounding environment [85]. Following implantation, the release of calcium phosphate into the peri-implant region increases the body fluids saturation and precipitates a biological apatite on the implant surface [86]. Moreover, this layer of biological apatite may contain several proteins and serve as a matrix for osteogenic cell attachment and growth and thus enhancing the bone healing process [32].

Furthermore, it was reported that CaP coatings have led to better clinical success rates in the long-term than uncoated Ti implants due to a superior primary rate of osseointegration [86].

Several authors have investigated the CaP-coated titanium implants for improving the osseointegration comparing to other methods of surface modification. For example, Elias et al. [87] have studied the osseointegration of four implant surfaces in the femoral epiphyses of rabbits after 2 and 8 weeks of healing. They compared the bone-implant contact and bone growth inside the chambers for four different implant surfaces and shown that biomimetic coating method may enhance the bone formation onto titanium. (Fig.1.20)

Another advantage of these CaP coatings is that CaP crystals have similar proprieties to bone-mineral in terms of size and composition. Furthermore, it is possible to incorporate biologically active drugs such as antibiotics or growth factors during the precipitation of CaP coatings on Ti implants [87, 88]. These molecules could be released in the peri-implant region for either preventing bacterial infections or stimulating bone growth.

Different methods have been developed to coat metal implants: plasma spraying, sputter-deposition, laser deposition, sol-gel coating, electrodeposition or biomimetic precipitation.

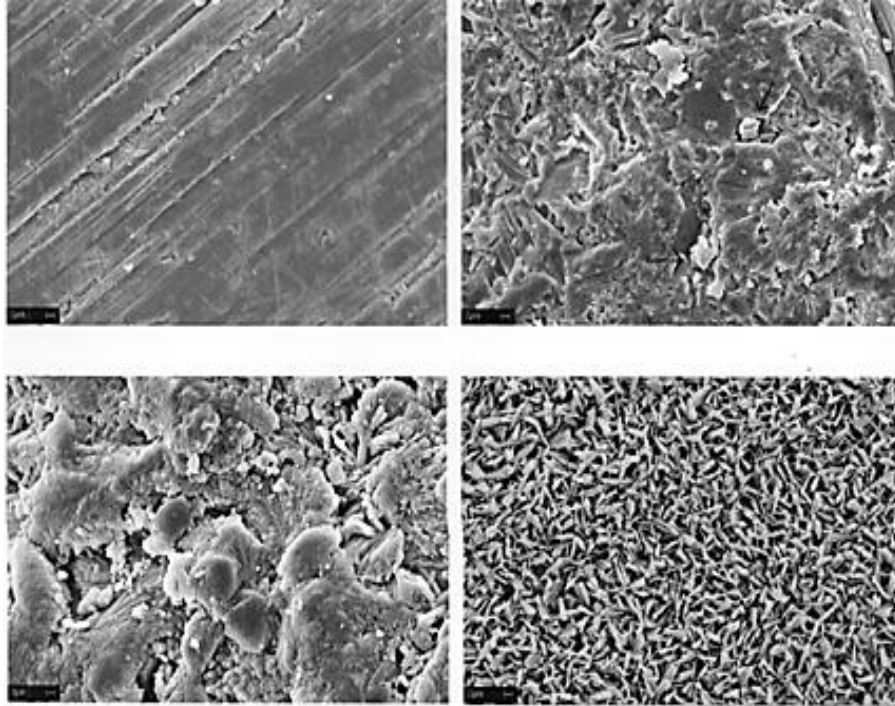


Fig.1.20. SEM images of the implant surface: (x 3.000). a) as-machined; b) Al₂O₃ blasted; c) plasma-sprayed with titanium; d) electrochemically coated with HAp [87].

a. Sol-gel coated implants

The sol-gel process is commonly used to deposit thin (<10 μm) ceramic coatings. It allows controlling the chemical composition and microstructure of the coating and improving a chemical homogeneity of the CaP coating by applying a simple low cost technic [19]. This process permits lower processing temperature during sintering. By sol-gel method, materials such as TiO₂, CaP, TiO₂-CaP composite and silica-based coatings can be deposited on the titanium surface [89].

b. Laser deposition

Pulsed laser deposition (PLD) is a physical vapor deposition technique to deposit thin films of CaP on the implant surface. The PLD process involves the surface irradiation by a concentrated pulsed laser creating compounds such as Ca₄P₂O₉, Ca₃(PO₄)₂, CaO, P₂O₅, and H₂O [90]. This high energy plasma cloud is composed of electrons, atoms, ions, molecules and molecular clusters. This plasma cloud expands with a temperature in the range of 350–600 °C, producing a thin adherent film onto the target [91].

The main advantages of this method are having hard titanium surface microstructures with a greater corrosion resistance, and a high purity degree with a standard roughness and thicker oxide layer [91].

c. Sputter deposition

Sputtering is applied by shooting atoms or molecules of a material in a vacuum chamber by bombardment of high-energy ions. A common disadvantage of this method is that the deposition rate and the process itself are very low [92]. The deposition rate could be enhanced by using a magnetically promoted variant of diode sputtering, known as radiofrequency (RF) magnetron sputtering which is largely used to deposit thin films of CaP coatings on titanium implants [92]. Studies in animals have shown higher BIC percentages with sputter coated implants [93].

d. Plasma-spray coating

Plasma-spraying (PS) is used to coat implant surface with CaP ceramic particles which are the injected materials in the plasma torch, used in conventional plasma spraying method, forming a thin CaP film on the surface of the titanium. The main advantage of plasma sprayed titanium coating is that these coatings create implants with a porous surface that bone can easily penetrate.

It was reported that this three-dimensional topography increased the tensile strength at the implant-bone interface. Therefore, plasma sprayed implants have been often recommended for low bone density regions. Studies have shown that the implant-bone interface formed faster with a plasma sprayed surface than with machined implants [94]. (Fig.1.21)

Nonetheless, the plasma-spraying method has disadvantages, such as the coating porosity and residual stress at the substrate/coating interface and also the strong changes in the CaP composition and crystallinity [96].

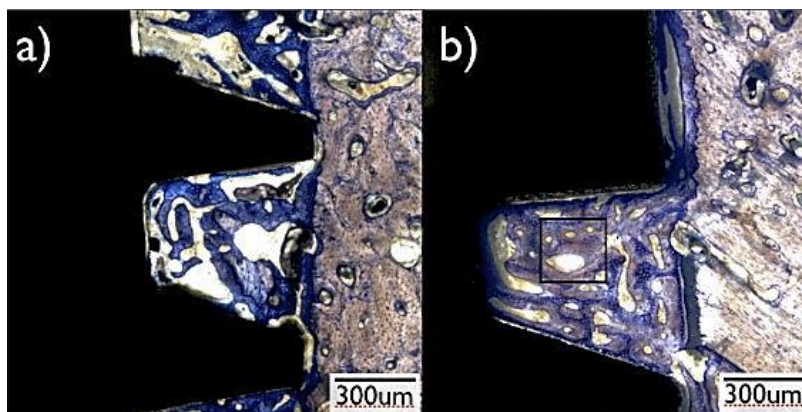


Fig.1.21. Optical micrographs obtained at $\times 40$ original magnification of the plasma-sprayed calcium phosphate-coated surface group at (a) 3 weeks and (b) 5 weeks implantation time. Note the remarkable amount of remodeling evidenced by the lighter staining at 5 weeks (*box*), showing rapid replacement of woven bone (dark blue) by lamellar bone throughout the healing chamber. Toluidine blue stain. [95].

Moreover, the plasma-spraying technique is not very effective for coating small dental implants with a complex shape. One of the major concerns with plasma-sprayed coatings is the possible delamination of the coating from the surface of the titanium implant and failure at the implant-coating interface despite the fact that the coating is well-attached to the bone tissue.

The difference in dissolution between the different phases that compose the coating is the responsible of the delamination, particle release and thus the clinical failure of implants. For all of the above reasons, the clinical use of plasma-sprayed HAP-coated dental implants is limited [97, 98].

e. Biomimetic precipitation of HAP coatings

In order to avoid the drawbacks of other coating methods, scientists tried to develop new coating methods based on biomineralization process by precipitating of calcium phosphate crystals onto the titanium surface from simulated body fluids (SBF) to form a thin coating at room temperature [99]. (Fig. 1.22)

Two methods have been developed in order to optimize and accelerate the deposition of coatings from aqueous solutions. The first method involves the electrodeposition of calcium phosphate by using an electrochemical cell which is conducted in calcium phosphate solutions and leads to the formation of CaP cements [99].

The electrochemical deposition performed in simulated body fluid can produce a carbonated apatite coating directly on the titanium surfaces [100].

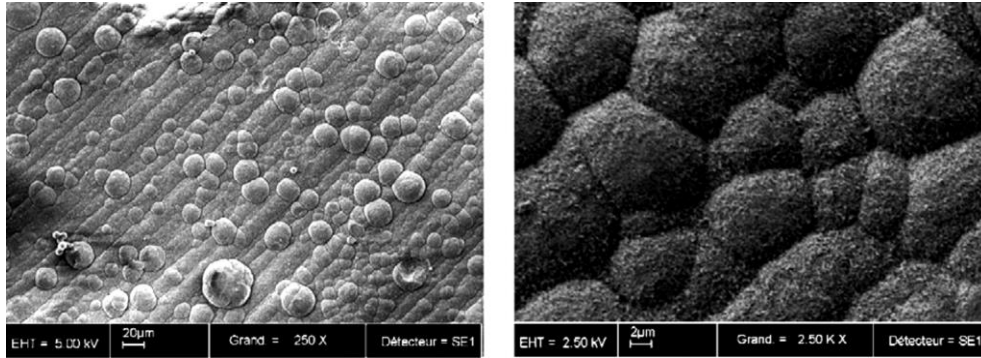


Fig.1.22. SEM images of a biomimetic calcium phosphate coating [99]

With this technic it's easy to control the deposit thickness on all kinds of complicated surfaces. Moreover, this process requires a short time and it is highly reproducible and effective [100,101].

The second method is based on the biomimetic precipitation of calcium phosphate on titanium surfaces by immersion in SBF. This method includes the heterogeneous nucleation and growth of bone-like crystals on the implant surface at physiological temperatures and pH [102]. This nucleation of the CaP on the titanium surface is induced by the chemical bonding of nano-sized clusters. [102].

The mechanical stability of the CaP coating requires a rough titanium surface. In addition, this method extends the variety of calcium phosphate phases that can be deposited, such as octacalcium phosphate or bone-like carbonate apatite [86]. It has been shown that such biomimetic coatings are more soluble in physiological fluids and resorbable by osteoclastic cells like dentin materials than high temperature coatings such as plasma-sprayed HAp [86, 103].

The osseointegration of titanium implants coated with biomimetic calcium phosphate has been investigated in pre-clinical comparative models. These studies have demonstrated a higher bone-to-implant contact (BIC) for biomimetic calcium phosphate coatings than for uncoated titanium implants [101].

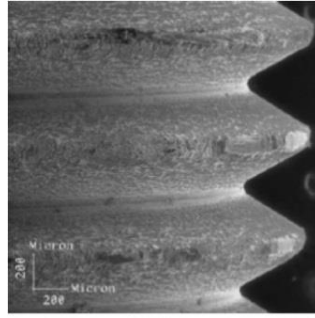


Fig.1.23. SEM image of HAp- coated implant (X50) [104]

3.4.7. Incorporation of biologically active drugs

The surface of titanium dental implants may be coated also with bone-stimulating agents to achieve a local enhancement of the bone healing process. Growth factors such as bone morphogenetic proteins (BMPs), TGF- β 1, platelet-derived growth factor (PDGF) and insulin-like growth factors (IGF-1 and 2) are some of the most promising candidates for this aim. [70].

Implants surface could also be loaded with molecules or drugs controlling the bone remodeling process. Incorporation of bone antiresorptive drugs, such as bisphosphonates, might be very useful in clinical cases lacking bone support, e.g. resorbed alveolar ridges. It was reported recently that incorporated bisphosphonate onto titanium implants increased the local bone density in the peri-implant region [105]. *In vivo* studies have mentioned that antiresorptive drug effect seems to be limited to the peri-implant region with only a little increase in dental implant osseointegration [105].

Interestingly, it has been demonstrated that coatings of implant surface by a different bioactive molecules influence osteogenic events. For instance, when RGD peptides doped to a bisphosphonate were chemically adsorbed on titanium discs, adhesion and proliferation of osteoblastic cells together with the biomineralization were notably optimized [106].

Antibiotic incorporation into implant coatings has also recently been investigated. Calcium-based coatings of an implant material can bind to antibiotics, such as cephalothin, carbenicillin, amoxicillin, cefamandol, tobramycin, gentamicin and vancomycin, which are able to release from the coating material. [107].

Progressive studies concentrating on the drug release, method of drug incorporation and chemical structures of the antibiotic that facilitate their incorporation capacity,

would be of great importance to develop a new antibiotic incorporated coatings for medical implants [108]

The complex regulation of growth factors during bone healing makes their delivery system very important for the success of osseointegration. So far, the immobilization of growth factors with calcium phosphate ceramics has commonly been performed by adsorption of proteins onto the surface of the materials [109] which leads to the release of the proteins upon connecting with a physiological environment [109].

CHAPTER II

Analysis techniques for the physicochemical characterization of TiO₂ functionalized surfaces.

The morphology and topography of the functionalized surfaces were characterized by scanning electron microscopy (SEM) [110]. The surface chemical composition was characterized by X-ray Photoelectron Spectroscopy (XPS) [111] and infrared spectroscopy (reflection-absorption mode) through core level binding energy and vibration modes. [112]

1. Scanning Electron Microscopy (SEM)

SEM is an analytical instrument that shows surface topography using monochromatic energetic electron backscattered from the sample. The electron beam can be focused by magnetic field from micro to nanometer level, enabling measurement of surface topography at the magnification of 10 to 500,000 [110, 113]. This technique is used to make a characterization of the samples surface micro-structure and nano-structure, with a fine visualization of surface defects [110].

By irradiating the sample with an electron beam in vacuum, secondary electrons and backscattered electrons allow to image the surface structure due to different electron emissivity where the surface is heterogeneous. As the primary electrons as well as high energy secondary electrons generate core level ionizations, characteristic X-rays are generated as indicated in (Fig.2.1) [113, 114]. This allows a chemical characterization of the sample surface (EDX) as the X-rays emitted from the surface are typical of the ionized atomic levels.

Nevertheless, as the electron beam penetrates the sample to a depth approximately of 1 μ m, the chemical information is not characteristic of the first atomic planes as it is the case for photoemission. The combined effect of elastic and inelastic scattering

controls the penetration of the electron beam into the solid. The resulting zone over which the incident electrons interact with the sample is known as interaction volume. The interaction volume has several important characteristics, which determine the nature of imaging in the SEM. (Fig.2.1). SEM image obtained upon detecting the secondary electrons, produced near the sample surface, reflects the fine topographical structure of the sample and depends strongly on the chemical nature (by the atomic number Z), the topography and the crystallinity of the surface. For each scan position of the incident beam, the secondary electrons are detected by an analysis system that can then be a two-dimensional image of the surface. [110].

A BSE image therefore reflects the compositional distribution on the sample surface. In general, high-resolution images ($\geq \times 10,000$) of samples can be achieved at the SEM mode. [113]

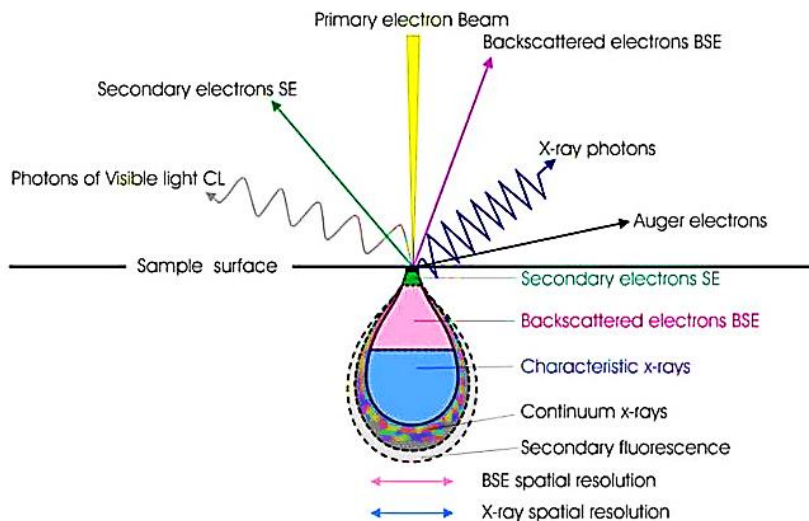


Fig.2.1. Interaction volume between material and electron beam

In this thesis, SEM images were realized with a field emission scanning electron microscope (FE-SEM, LEO) operating at 5.0 kV. The surface composition of the samples was analysed using energy dispersive spectroscopy (EDS).

2. X-ray Photoelectron Spectroscopy (XPS)

X-ray Photoelectron Spectroscopy (XPS), also known as Electron Spectroscopy for Chemical Analysis (ESCA), is a widely used technique to investigate the chemical composition of surfaces. XPS is based on the photoelectric effect using X-ray sources

and it analyses the chemical elements present in the first atomic planes of the material by identifying their core level binding energies [111].

This spectroscopy can provide the chemical composition at a sample surface as well as the type of the existing chemical bonds and their in-depth distribution when the analysis is coupled with sputtering [115]. However, XPS allows obtaining the chemical composition of the surface of a material within a depth of 10 nm [115]. As sampling depth is defined as inelastic free paths of photoelectrons in the material from which 95% of all photoelectrons are scattered by the time they reach the surface (3λ). λ depends on the kinetic energy K.E. of the photoelectron and the specific material and it's almost located at the range of 1 – 3.5 nm for Al $K\alpha$ radiation So the sampling depth (3λ) for XPS under these conditions is 3-10 nm where the angle can change between the sensor and the standard on surface from 0° to 75° .

In XPS, the sample is irradiated with low-energy ($\sim 1.5\text{KeV}$) X-rays, in order to induce photoabsorption. The emitted electron energy distribution is determined by means of a high-resolution electron spectrometer [115, 116]. The sample analysis is conducted in a vacuum chamber, typically $\sim 10^{-10}\text{Torr}$ to facilitate the transmission of the photoelectrons to the analyzer and avoid surface reactions/contaminations. [116]

In XPS, electrons are emitted from the surface as a result of a photoemission process. An electron is ejected from an atomic energy level by an X-ray photon, mostly from an Al- $K\alpha$ or Mg- $K\alpha$ primary source which emit 1253.6 and 1486.6eV respectively, and its kinetic energy is determined by the spectrometer which acts as a monochromator.

The characteristic parameter for the electron is its binding energy. The relation between binding energy, kinetic energy and X-ray photon energy is given by Eq. (2.1): [111]

$$E_B = h\nu - E_K - \Delta\Phi_{\text{work function}} \quad (2.1)$$

$h\nu$: Energy of the incident X-ray beam , **E_K** : Kinetic energy of the emitted electron , **E_B** : Binding energy of the electron in the atom . **$\Delta\Phi$** is the work function which corresponds to the energy difference between the Fermi level and the vacuum level. (Fig.2.2)

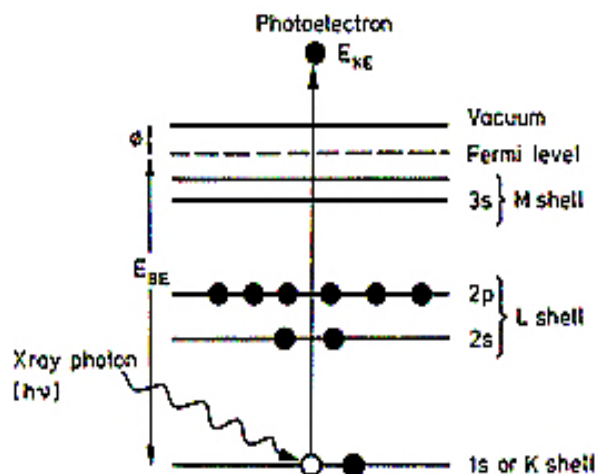


Fig.2.2. The photoemission process

From Eq. (2.1) it is clear that only binding energies lower than the exciting radiation (1486.6eV for Al-K α and 1253.6eV for Mg-K α) are probed. Each element has a characteristic electronic structure and thus a characteristic XPS spectrum. [115]. In fact, the observed binding energy is not directly the binding energy of the atom in the molecule or in the solid because some relaxation phenomena are induced during the excitation-emission process. Those relaxation phenomena are related to “other electrons” reaction due to the photoemission process and prove that the Koopmans theorem is infirmed in such multi electrons systems.

In XPS spectrum, a number of sharp peaks appear on a background. The background comes from photoelectrons that undergo energy and direction changes between photoemission from the atom and detection in the spectrometer. This background is usually called the inelastic tail and is characteristic of the electron escape depth (related to its kinetic energy) and the emitting atoms in-depth distribution. Usually, to obtain a pseudo-quantitative information, this inelastic tail have to be subtracted from the whole signal to isolate the sharp peak that can be related to atomic concentrations in the surface first nanometres. The most used method to do this is subtraction the well-known Shirley method. The observed peaks can be classified into three types: peaks originating from photoemission (i) from core levels, (ii) from valence levels at low binding energies (0 to 20eV) and (iii) from X-ray excited Auger emission. The identification of the elements present on the surface of the material is made from

peaks appearing on the global spectrum which is called "Survey". The (Fig.2.3), corresponding to a wide scan survey XPS spectrum of TiO₂ sample, illustrates the type of spectrum obtained where a series of peaks appears. The peak intensities measure how much of a material is at the surface, while the peak positions indicate the elemental and chemical composition. [116]

It's important to mention that XPS uses the spectroscopic notation: first the principal quantum number ($n = 1, 2, 3 \dots$), then $l = 0, 1, 2 \dots$ indicated as s, p, d ... respectively, and finally the j value given as a suffix ($1/2, 3/2, 5/2 \dots$). The K, L, M... are related to Auger peaks and in this respect it could be useful to indicate that photoelectron kinetic energy is depending on the source nature and the Auger electron kinetic energy is independent of the source nature. So by changing the X-ray source energy, it will be easy to distinguish between photoelectrons and Auger electrons [116].

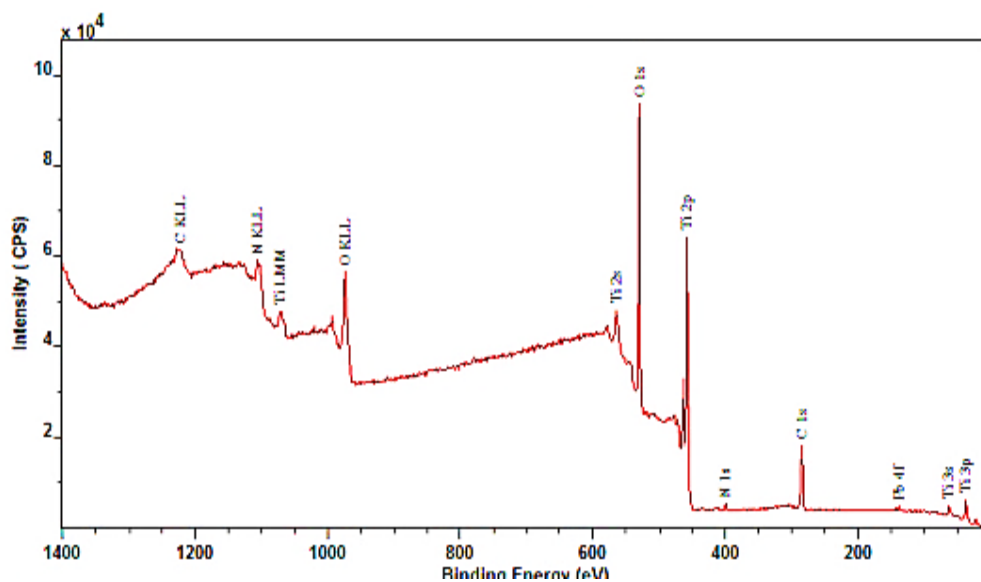


Fig.2.3. Example of XPS "Wide Scan Survey Spectrum" for TiO₂ sample

The chemical state, that's to say the number and the kind of nearest neighbours, affects the binding energy. Thus, difference in binding energy in the XPS spectrum can be observed and is called the chemical shift. Both initial and final states contribute to the chemical shift. For example, in a positive ion, the lack of electrons results in higher binding energy for the emitted electron, and the opposite effect for negatively charged ions. (Fig.2.4) shows the chemical shift of Ti 2p level when oxidized. The Ti2p binding energy goes from 453eV for Ti_{2p} metal to 458.5eV for TiO₂ identifying

the chemical state of the element. Actually, the ability to determine the chemical states is one of the main advantages of this spectroscopy and its most powerful ability is to do this for the ultimate atomic planes of the sample.

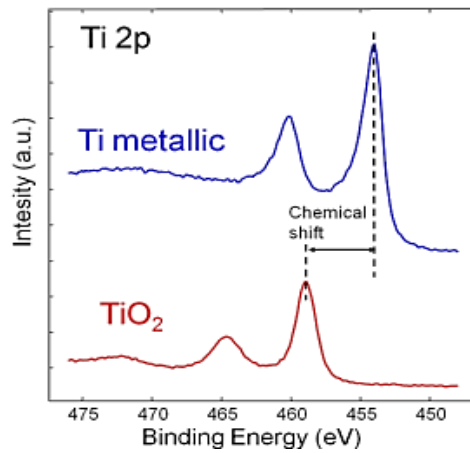


Fig.2.4. XPS peaks shift of Ti when oxidized.

To obtain accurate chemical information, it is essential to determine peak positions accurately. When dealing with small shifts between two different chemical states, overlapping peaks may occur in the spectrum.

(Fig.2.5) shows an overlapping between copper and aluminum core levels which requires a high resolution XPS and a deconvolution technique for data interpretation.

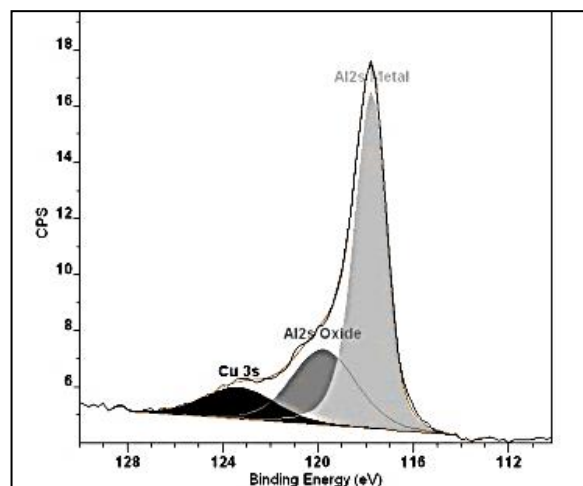


Fig.2.5. Deconvolution of overlapped copper and aluminum peaks.

Peak deconvolution and peak fitting tools are available in the commercial data handling systems, where peak shape, intensity and full width at half maximum as well as energy can be constrained parameters.

In the XPS spectrum, the relative intensities are governed by the ionization efficiencies of the different core shells, designated by ionization cross section. The line width, defined as the full width at half-maximum intensity (FWHM), is a convolution of several contributions: the natural width of the core level, the width of the X-ray line and the resolution of the analyser. [117]

In this work, we used a Thermo Scientific K-Alpha fully integrated, monochromated small-spot X-ray Photoelectron Spectrometer. The monochromated Al K α X-ray beam may be focused into a small spot providing an ultimate lateral resolution of 30 μm . A high-flux, low-energy ion source is integral to K-Alpha for depth profiling.

XPS measurements were also performed using a MAC II RIBER photoelectron spectrometer with non-monochromated Al K α excitation ($h\nu = 1486.6\text{eV}$). The compositions of the surface film were determined by measuring integrated photo-peaks intensities after a Shirley background subtraction. The peaks areas were corrected from sensitivity factors [120]. Survey spectra (overall XPS spectra) were acquired with an energy step BE of 1.0 eV, while BE was 0.05eV for core level windows. Acquisition time was 100ms per step in all the case. The analysis chamber base pressure was by $2.0 \cdot 10^{-10}\text{Torr}$.

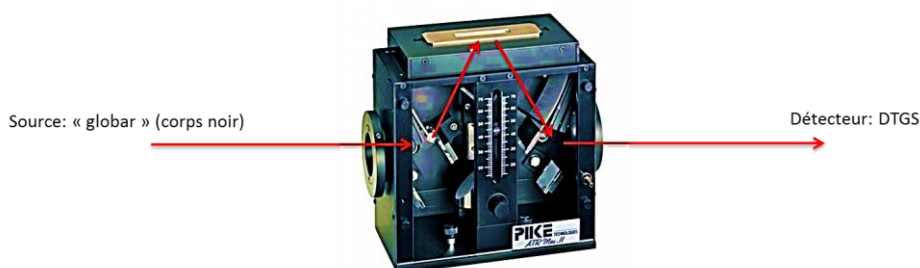
3. Infrared Reflection-Absorption Spectroscopy (IRRAS)

Infrared Spectrometer allows by the detection of characteristic vibrations of chemical bonds to make an analysis of organic or inorganic materials. Infrared spectrum represents a fingerprint of a compound with absorption peaks corresponding to the frequencies of molecular vibrations. In addition to this chemical identification, it can determine the amount of material present when used in transmission in the case of powders, liquid or gases. In that case, modern software equipped with powerful algorithms of spectral deconvolution and thousands of reference spectra, makes this spectroscopy an excellent tool for quantitative analysis. [112]. Infrared spectroscopy covers a wide range of techniques, from transmission to reflection (diffuse or specular) for gaseous, liquid or solid samples.

Infrared spectroscopy exploits the fact that the molecules have specific frequencies for which they vibrate in correspondence with discrete energy levels (vibrational modes). The resonant frequencies are determined by the normal modes corresponding to the

potential surface energy of the molecular electronic ground state. However, the resonant frequencies can be first related to the strength of the bond and the atomic mass.

In our studies we used the method of reflection-absorption to characterize the adsorption of molecules on the surfaces of nanostructured titanium. The spectrometric system consists of infrared spectrometer coupled to an infrared reflection-absorption device (VEEMAX) for measuring low concentrations of chemical compounds adsorbed onto reflective surfaces such as metals covered with a thin oxide film [119]. IRRAS technique is normally used for the characterization of thin films on highly reflecting metal substrates, and can also be applied for non-metals and even liquid surfaces, as shown by Desbat et al [119]. It is a specular reflection method in which the spectrum of a substrate coated with thin film is compared to the spectrum of a clean substrate, reflecting the signal from the adsorbed matter.



2.6. Reflection-Absorption mode of IR Spectroscopy

IRRAS spectrometers have become an established sampling method for films of thickness less than 100 nm. In Reflection-Absorption IR Spectroscopy, the IR beam is reflected from the front face of a highly-reflective sample, such as a metallic surface. Infrared radiation is emitted by a source called global which emits polychromatic light (black body source). After passing through the Michelson interferometer, the radiation is sent onto the sample at grazing incidence (from 5° to 10°). Then the light is reflected by the metal and is directed in specular way to a detector. (Fig.2.6)

Due to reflectivity on a metallic surface, only the vibrational modes that possess a component of the dipole moment perpendicular to the surface are "active" (reflection rules) and thus give an absorption band in the spectrum. IRRAS spectra of the film

constituents are generally presented as plots of reflectance-absorbance (RA) vs. wavenumber (cm^{-1}). (RA) is defined as $-\log_{10}(R/R_0)$ where R is the reflectivity of the film-covered surface and R_0 is the reflectivity of the clean substrate surface. [121].

Theory of Infrared Absorption

At temperatures above zero, all the atoms in molecules continuously vibrate with respect to each other. The vibrational modes of a molecule are quantized, so when the frequency of a specific vibration is equal to the frequency of the IR beam irradiating the molecule, photo-absorption arise and the molecule gets into a vibrational excited state. The major types of molecular vibrations are stretching and bending (Fig 2.7). When IR radiation is absorbed, the associated energy is used to amplify these types of motions, that's to say bond length stretching (2 centers) or bond valence angle bending (3 centers). The individual vibrational motion is usually coupled with other atomic motions, similarly to springs excitation when linked together. These combinations lead to the complex absorption bands observed in the IR spectrum. [112, 120]

As mentioned above, vibrations can involve either a change in bond length (*stretching*) or bond angle (*bending*) (Fig 2.7). Some bonds can stretch in-phase (*symmetrical stretching*) or out-of-phase (*asymmetric stretching*), as shown in (Fig 2.8).

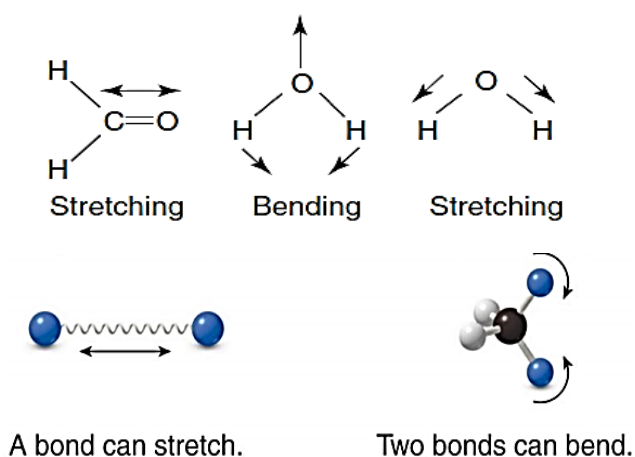


Fig.2.7. Stretching and bending vibrations

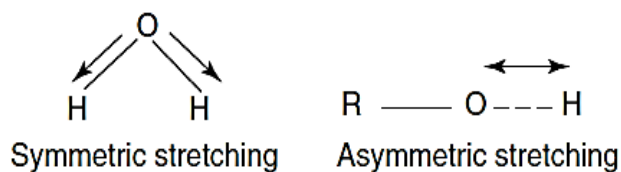


Fig.2.8. Symmetric and asymmetric stretching vibrations

Bending vibrations also contribute to infrared spectra and they are four types of bend (Fig 2.9). In the “school” case of CH vibrations, it is best to consider the molecule being cut by a plane through the hydrogen atoms and the carbon atom. Hydrogen can move in the same direction or in opposite directions in this plane, here the plane of the page. This results in *in-plane* and *out-of-plane* bending vibrations, as illustrated (Fig.2.10).

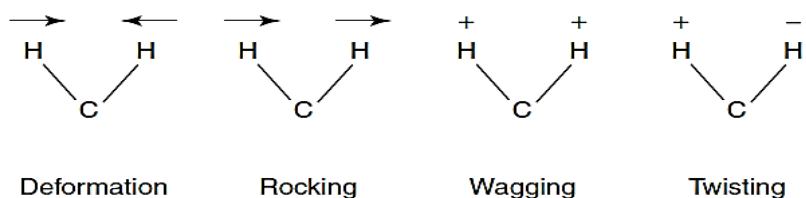


Fig.2.9. Different bending vibrations

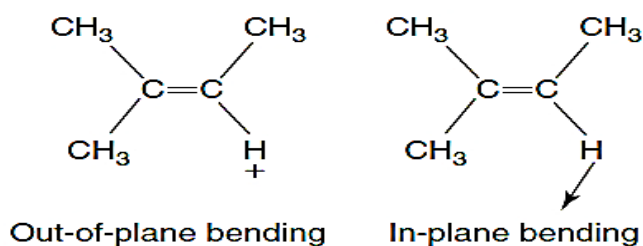


Fig.2.10. Out of plan and in plan bending vibrations

Infrared spectroscopy allows detection of molecule vibrations involving a variation of the dipole moment of the molecule. Thus, the most intense absorption bands are typically those of a strongly polarized bond.

For medium frequencies (typically 1000 to 4000 cm^{-1}), each specific variation of the dipole moment of a chemical bond occurs at a given frequency and varies a little with the other atoms of the molecule. These are the localized modes and the position and the intensity of characteristic bands therefore allow identification of chemical groups

present in the analysed material [112]. On the other hand, for low frequency modes, coupling with neighbouring atoms leads to vibration delocalization (collective modes) and are usually used as fingerprints for structure identification.

Interpretation of Infrared spectrum

Because it's important to have a relative scale for the absorption intensity and due to the fact that IR spectrometer is a single beam instrument, a background spectrum must be performed to subtract absorptions that are not characteristic of the adsorbed species [112] (Fig.2.11). These absorptions are due to substrate reflectivity and to interactions of the IR beam with matter on its path between the IR source and the detector. In fact, the background spectrum contains characteristics of the; the source, the beam-splitter, the absorption by the air (mainly due to CO₂ and water vapour) in the beam path, and the sensitivity of the detector at different wavelengths. As in reflexion-absorption mode, only the sample surface is modified, the subtraction of the background in the IR spectrum leads to absorption bands characteristic of the adsorbed matter.

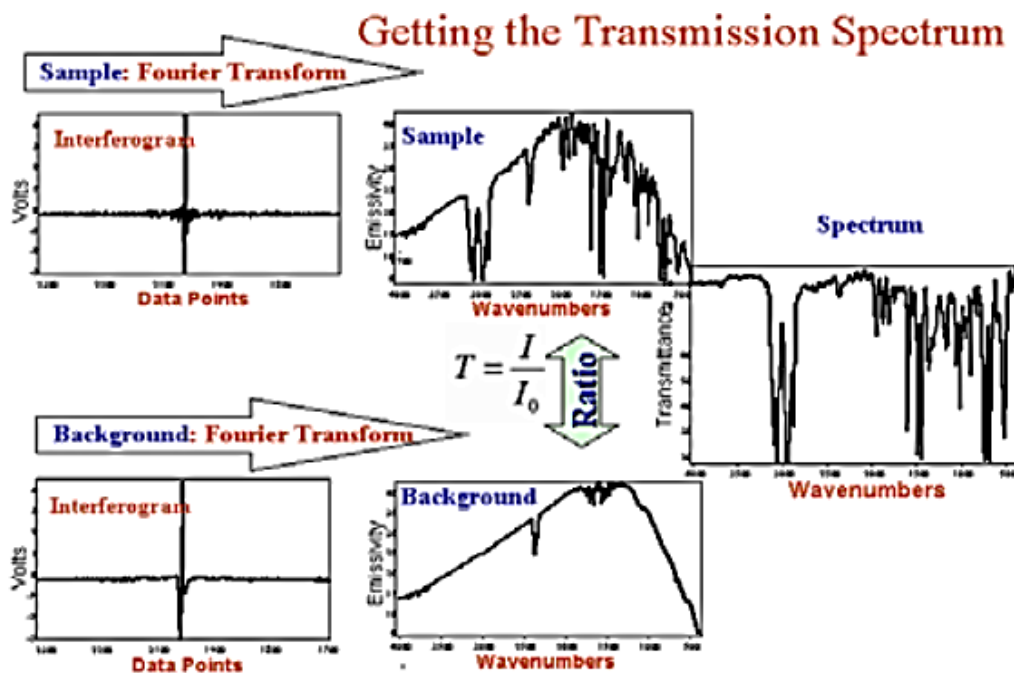


Fig.2.11. Background and sample spectra

IR absorption positions are most commonly presented as wavenumbers (ν) in cm^{-1} that determine the number of waves per unit length. Thus, wavenumbers are directly proportional to frequency, as well as the energy of the IR absorption.

Infrared radiation spans a section of the electromagnetic spectrum having wavenumbers from 14,000 to 10 cm^{-1} .

Near IR	Mid IR	Far IR
13000- 4000 cm^{-1}	4000-200 cm^{-1}	200-10 cm^{-1}

Our study focuses on the most frequently used mid IR region, between 4000 and 400 cm^{-1} (2.5 to 25 μm for wavelength). As mentioned previously, infrared spectrum is commonly obtained by passing infrared radiation through a sample and determining the absorbed part of the incident radiation at a particular energy. The energy at which any peak in an absorption spectrum appears corresponds to the vibration of a part of sample molecule. The interpretation of the infrared spectra is mainly based on the detection of characteristic peaks and their assignment to specific chemical groups.

To get qualitative information, we have to identify the wavelengths absorbed by the sample that are characteristic of the chemical groups present in the analyzed material. The same group may give rise to several types of vibrations and thus absorptions at different frequencies [112].

An IR spectrum is a plot of the amount of transmitted light versus its wavenumber. The IR spectrum is divided into two regions: the functional group region (at $\geq 1000 \text{ cm}^{-1}$), and the fingerprint region (at $< 1000 \text{ cm}^{-1}$) (Fig.2.12).

Bands in fingerprint region are the result of many types of vibrations that are characteristic of the molecule as a whole. This complex fingerprint region represents a unique pattern for each organic compound. The region is useful for comparing the spectrum of an unknown compound with the spectra of a known compound for identification purposes.

Where a particular bond absorbs in the IR depends on bond strength and atom mass. Stronger bonds (i.e., triple > double > single) vibrate at a higher frequency, so they absorb at higher wavenumbers. Bonds with lighter atoms vibrate at higher frequency, so they absorb at higher wavenumbers. (Fig.2.13)

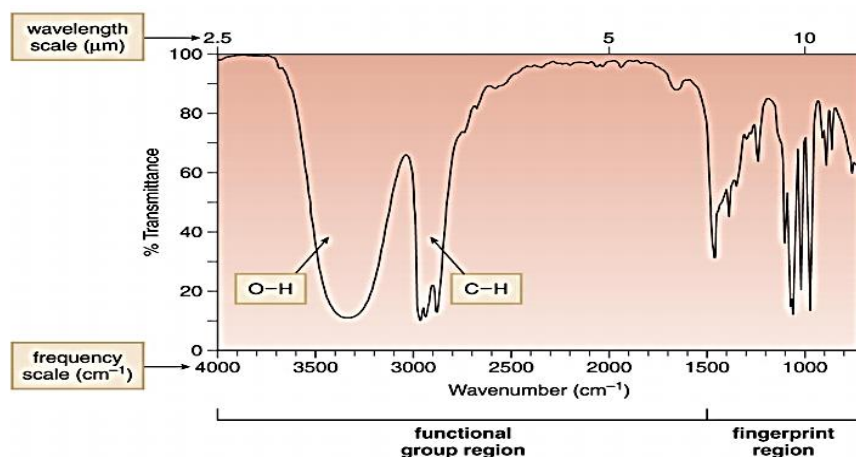


Fig.2.12. Functional group region and fingerprint region in IR spectrum

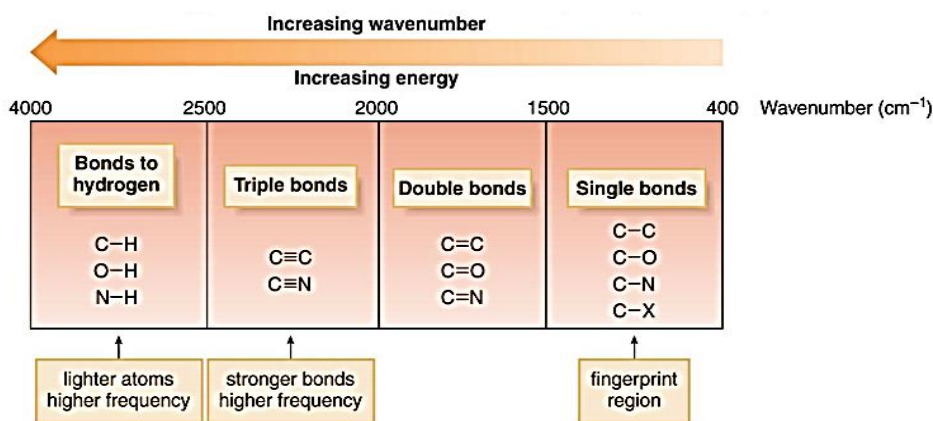


Fig.2.13. General trends in bond stretching absorption frequencies

Tables are used to assign the absorption at different chemical groups present in the spectrum. (Table 2.1) shows typical IR frequencies used for analysis of IR spectra. (Table 2.2) shows infrared absorption data for some other functional groups. In fact, the spectrometer software possess compounds library that can be used for bands identification.

The intensities of the absorption bands are correlated to the amount of chemical bonds present in the sample, but quantification can be quite difficult in IRRAS mode because of surface selection rules that favours vibration that have a strong dipole component perpendicular to the sample surface. Moreover, in the case of thick films (>50 nm), optical effects can be observed with bands deformation. In our case, adsorption only concerns a thin film deposited onto an oxide layer and such effect cannot be observed.

In conclusion, this method of analysis is used in our work to determine chemical bonds of IR-active molecules in bioactive layers deposited on a nanostructured TiO₂ substrate.

In this work, IR spectra were obtained by a NICOLET 6700 FTIR spectrometer equipped with a VEEMAX accessory allowing reflection-absorption experiment with an incidence angle of 20°. Spectra have been averaged over 128 scans and the resolution was set to 4.0 cm⁻¹.

CHARACTERISTIC INFRARED ABSORPTION BANDS OF FUNCTIONAL GROUPS

Class of Compounds	Absorption. cm^{-1}	Intensity	Assignment	Class of Compounds	Absorption. cm^{-1}	Intensity	Assignment	
Alkanes and Alkyls	2850-3000	s	C-H stretch	Carboxylic Acids	2500-3500	s, broad	O-H stretch	
	1450-1470	s	C-H bend		R-C(O)-OH	1710-1715	s, broad	C=O stretch
	1370-1390	m	CH_3 C-H bend		C=C-C(O)-OH or	1680-1710	s	C=O stretch
	1365 + 1395 (two bands)	m	$-\text{CH}(\text{CH}_3)_2$ or $-(\text{CH}_3)_3$ bend	Ar-C(O)-OH				
	715-725	w	$-(\text{CH}_2)_n$ bend	Esters	aliphatic 1160-1210	s-vs	O=C-O-C stretch	
Alkenes	3020-3140	w-m	=C-H stretch	acetates ~1240				
	1640-1670	vw-m	C=C stretch	aromatic 1250-1310				
	RCH=CH ₂	m + s	=C-H bend	R-C(O)-O-R	1735-1750	s	C=O stretch	
	(two bands)			C=C-C(O)-O-R or	1715-1730	s	C=O stretch	
	RR'C=CH ₂	s	=C-H bend	Ar-C(O)-O-R				
	cis-RCH=CHR'	m-s, broad	=C-H bend	R-C(O)-O-Ar	1760-1790	s	C=O stretch	
	trans-RCH=CHR'	s	=C-H bend	Acyl Chlorides				
RCH=CR'R''	s	=C-H bend	R-C(O)-Cl	1785-1815	s	C=O stretch		
Alkynes				Ar-C(O)-Cl	1770-1800	s	C=O stretch	
	R-C≡C-H	s, sharp	≡C-H stretch	Anhydrides				
	2100-2140	m	C≡C stretch	R-C(O)-O-C(O)-R	~1750 + ~1815	s,s	C=O symmetric & asym. stretch	
Alkyl halides	610-700	s, broad	≡C-H bend	Ar-C(O)-O-C(O)-Ar	~1720 + ~1775 (both two bands)	s,s		
	R-C≡C-R'	vw-w	C≡C stretch	Nitriles				
Alcohols	3265-3335	s, sharp	≡C-H stretch	R-C≡N	2240-2260	m-s	C≡N stretch	
	2100-2140	m	C≡C stretch	C=C-C≡N or	2220-2240	s	C≡N stretch	
	610-700	s, broad	≡C-H bend	Ar-C≡N				
	R-C≡C-R'	vw-w	C≡C stretch	Amines				
				R-NH ₂	~3400 + ~3500 (two bands)	w	N-H symmetric & asym. stretch	
Aldehydes	3300-3400	s, broad	O-H stretch		1580-1650	w-m	N-H bend	
	C=C-CH ₂ -OH	m-s	C-O stretch	RR'N-H	3310-33350	w	N-H stretch	
	R-CH ₂ -OH (1°) or	m-s	C-O stretch	Amides				
	C=C-CH(R)-OH	m-s	C-O stretch	R-C(O)-NH ₂	3200-3400 and 3400-3500 (two bands)	w-m	N-H symmetric & asym. stretch	
	RR'CH-OH (2°) or	m-s	C-O stretch		1650-1690	s, broad	C=O stretch	
C=C-CRR'-OH	m-s	C-O stretch		1590-1655	m-s	N-H bend		
RR'R''C-OH (3°)	m-s	C-O stretch		1640-1690	w-m	N-H stretch		
Ar-O-H	m-s	C-O stretch		1510-1560	s, broad	C=O stretch		
Ethers				R-C(O)-NH-R	1640-1690	s, broad	C=O stretch	
	R-O-R'	1085-1150	s		1640-1690	s, broad	C=O stretch	
	Ar-O-R	1020-1075 and 1200-1275 (two band)	m-s	=C-O-C sym. & asym. stretch		m-s	N-H bend	
Ketones				R-C(O)-NR'R''	1630-1680	m-s	C=O stretch	
	RR'C=O	1710-1720	s	Nitro Compounds				
	C=C-C(O)-R	1665-1685	s	R-NO ₂	~1550 and ~1370	s	N-O symmetric & asym. stretch	
Ar-C(O)-R	1675-1695	s		~1525 and ~1335 (both two bands)	s	N-O symmetric & asym. stretch		
four member	1770-1780	s	C=O stretch	Aromatic Compounds	3010-3100	m	Ar C-H stretch	
cyclic					1450-1600	m-s	ring C=C stretch	
five member	1740-1755	s	C=O stretch	monosubstituted	(two to four bands)	sharp		
cyclic					730-770 and	s	C-H bend	
six member	1710-1720	s	C=O stretch		690-710	s	C-H bend	
cyclic					(two bands)			
				<i>o</i> -disubstituted	735-770	s	C-H bend	
				<i>m</i> -disubstituted	750-810 and	s	C-H bend	
					690-710	s	C-H bend	
				<i>p</i> -disubstituted	810-840	s	C-H bend	

Intensity abbreviations: vw = very weak, w = weak, m = medium, s = strong, vs = very strong

Table.2.1. Characteristic IR absorptions of some functional groups for IRRAS spectra analysis

(<http://www.unm.edu/~orgchem/304Lpages/05IRchart.pdf>)

Functional Class	Characteristic Absorptions
Sulphur Functions	
S-H thiols	2550-2600 cm ⁻¹ (wk & shp)
S-OR esters	700-900 (str)
S-S disulfide	500-540 (wk)
C=S thiocarbonyl	1050-1200 (str)
S=O sulfoxide	1030-1060 (str)
sulfone	1325± 25 (as) & 1140± 20 (s) (both str)
sulfonic acid	1345 (str)
sulfonyl chloride	1365± 5 (as) & 1180± 10 (s) (both str)
sulphate	1350-1450 (str)
Phosphorous Functions	
P-H phosphine	2280-2440 cm ⁻¹ (med & shp) 950-1250 (wk) P-H bending
(O=)PO-H phosphonic acid	2550-2700 (med)
P-OR esters	900-1050 (str)
P=O phosphine oxide	1100-1200 (str)
phosphonate	1230-1260 (str)
phosphate	1100-1200 (str)
phosphor amide	1200-1275 (str)
Silicon Functions	
Si-H silane	2100-2360 cm ⁻¹ (str)
Si-OR	1000-11000 (str & brd)
Si-CH₃	1250± 10 (str & shp)
Oxidized Nitrogen Functions	
=NOH oxime	
O-H (stretch)	3550-3600 cm ⁻¹ (str)
C=N	1665± 15
N-O	945± 15
N-O amine oxide	
aliphatic	960± 20
aromatic	1250± 50
N=O nitroso	1550± 50 (str)
nitro	1530± 20 (as) & 1350± 30 (s)

Table.2.2. Infrared absorption bands for some functional groups; most of the absorptions cited are associated with stretching vibrations. Standard abbreviations (str = strong, wk = weak, brd = broad & shp = sharp)

(<https://www2.chemistry.msu.edu/faculty/reusch/virttxtjml/Spectrpy/InfraRed/infrared.htm>)

CHAPTER III

Functionalization of TiO₂ surfaces

1. Nanostructuring of TiO₂ surface

Recent trends in surface modification field are to modify titanium-based implants to possess nanometric surface features considering that natural bone is a nanostructured material [1]. Anodic oxidation method has been successfully used as a surface treatment for implants in the past few decades and it has some new advances recently. The first part of this chapter will present an overview of anodization and discuss processing parameters with a presentation of experimental results. The main focus will be on the unique 3-D tube-shaped nanostructure of TiO₂ that creates profound impacts on cell behavior. [56]

1.1. Fabrication of TiO₂ nanotube arrays by anodisation

The anodization technique was discovered in the early 1930's and was widely studied in the 1960's to enhance titanium implant osseointegration [2]. The anodic oxidation is a simple method that can be easily applied to prepare TiO₂ nanotubes whose diameter and length depend highly on the electrochemical conditions, such as the working electrode potential, temperature and the solution composition. [125]

In addition to the many physicochemical and biological advantages of nanotechnology mentioned in chapter I, and from mechanical and physical point of view, we are trying by nanostructuring the surface with TiO₂ nanotubes (nT-TiO₂) to create a negative relief pattern of the integration between bone and implant surface.

The anodic oxidation of titanium sample in a solution containing fluoride was first reported by Grimes et al [123]. Further studies were interested in controlling the nanotube morphology, length, pore size and wall thickness. [122, 126, 130]

The anodizing of Ti sample was initiated using an electrochemical cell of a reference electrode (calomel), facing a platinum electrode and the working electrode (titanium)

as the anode [123]. The aqueous medium is a solution of HF at 0.5% (by weight) and acetic acid in the proportions 1:7(Fig. 3.1). [125].

Anodization experiments are commonly carried out by electrolyte agitation which reduces the thickness of the diffusion layer at the metal/electrolyte interface, and ensures uniform current density and temperature along the Ti surface [124]. In Grimes et al work, they evaluated the anodizing titanium between 10 and 40 V in dilute (0.5–1.5 wt. %) aqueous HF solutions [123].

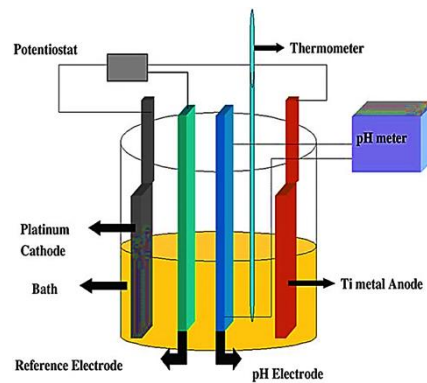
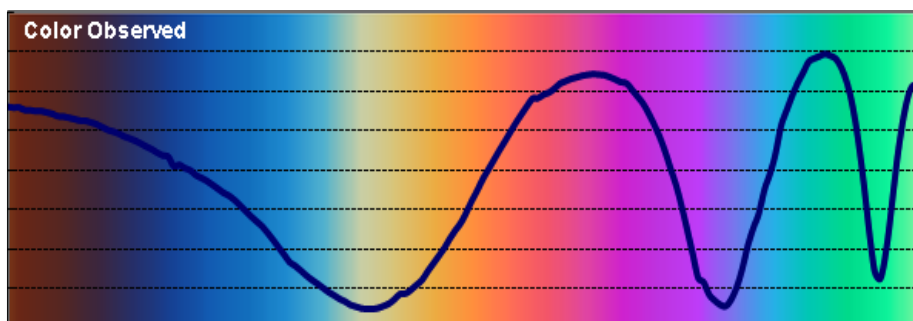


Fig.3.1. Illustrative drawing of an electrochemical cell

It was found that the diameters of nano-tubes were determined by applied voltage. The addition of acetic acid to the 0.5% HF electrolyte in a 1:7 ratio results in more mechanically tough nanotubes without changing in their shape and size [124,126]. During anodisation the color of the titanium oxide layer normally changed giving a more homogeneous coloring of the surface reflecting the thickness of the oxide thin film on the surface. (Tube length) (Fig.3.2)



Oxidized TiO ₂ Layer Thickness (nm)	10-25	25-40	40-50	50-80	80-120	120-150	150-180	180-210
Color	Golden	Purple	Deep Blue	Light Blue	Yellow	Orange	Purple	Green

Fig.3.2. Titanium anodizing color changes spectrum

1.2.Mechanism of nanotubes formation

The mechanism of TiO₂ nanotube formation in fluorine-ion based electrolytes is a result of three simultaneous processes: Ti oxidation to form titanium dioxide, the dissolution of Ti metal ions in the electrolyte, and the chemical dissolution of Ti and TiO₂ due to fluoride ions etching, which is enhanced by the presence of H⁺ ions as presented by the electrochemical reactions explained in the following parts [127]. TiO₂ nanotubes are not formed on the pure Ti surface but on the thin TiO₂ oxide layer naturally formed on the Ti surface. Therefore, nanotubes formation mechanism is related to oxidation and dissolution kinetics.

Schematic diagram of the TiO₂ nanotubes formation by anodisation process is shown in (Fig.3.3) [128]. The anodisation mechanism for creating the nanotubular structure is as follows:

- Before anodisation, a nano scale TiO₂ passivation layer on the Ti surface.
- Pit formation on the TiO₂ layer when applying a constant voltage. (8.5V in our work).
- As anodisation time increases, the pit grows longer and larger to become a nanopore.
- Nanopores and small pits undergo continuous barrier layer formation.
- After specific anodisation time (10 minutes in our work), completely developed nanotubes arrays are formed on the Ti surface.

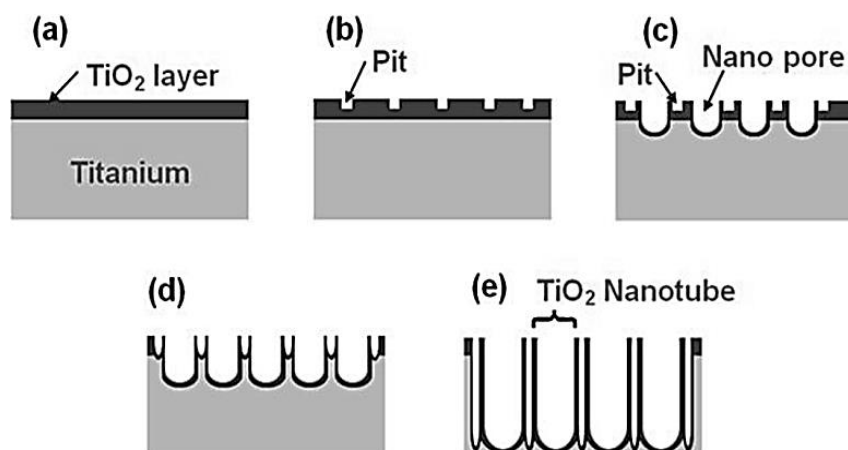


Fig.3.3. Schematic illustration of TiO₂ nanotube formation [128]

The electrochemical reactions of anodisation are:



The presence of F^- ions in the solution causes TiO_2 dissolution and this is represented by the following equation:



Pore growth (nanotubes size) grows due to the increase of the oxide layer at the base of the pores (pore-oxide interface layer) by the mechanisms (1) and (2) then the dissolution of this oxide by the mechanism (3). [124]

Previous reactions are connected to the evolution of the current vs. time diagram, and characteristic evolution for each mechanism. Mor et al [129] divided this diagram to five stages of nanotube formation:

Stage I: Initial formation of coherent oxide layer

Stage II: Pore formation

Stage III: Pore widening and connection

Stage IV: Nanotube growth

Stage V: Continued nanotube growth from dissolution and oxide growth

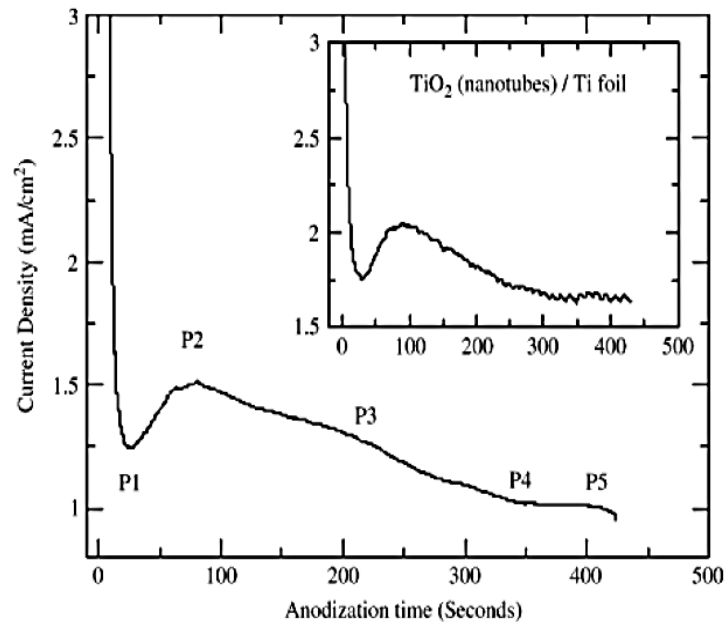


Fig.3.4. Anodisation behavior of a 400 nm. Ti thin film anodized at 10 V in HF-based electrolyte (acetic acid and 0.5 vol% HF mixed in ration 1:7) at room temperature. Inset shows a typical current density vs. time response observed for a titanium foil anodized at the same potential and electrolyte [129]

Based on the nanotube formation mechanism, many studies have evaluated the influence of various parameters on the nanotubes growth. [128,129] (Table.3.1)

Electrolyte pH and composition, anodization conditions, and size of the resulting nanotubes										
No.	Electrolyte ^a				pH ^b	V (V)	t (h)	D (nm)	L (μm)	Q ^c
	F ⁻	SO ₄ ²⁻	PO ₄ ³⁻	Cit						
01	0.1	1.0	—	—	<1	5	1	10±2	—	No NT
02	0.1	1.0	—	—	<1	10	1	40±5	0.28±0.02	NT
03	0.1	1.0	—	—	<1	15	1	80±9	—	NT
04	0.1	1.0	—	—	<1	20	1	100±11	0.48±0.03	NT
05	0.1	1.0	—	—	<1	25	1	110±12	0.56±0.04	NT
06	0.1	1.0	—	—	<1	30	1	—	—	No NT
07	0.1	1.0	—	—	<1	20	6.5	100±11	0.43±0.03	NT
08	0.1	2.0	—	—	<1	20	1	100±11	0.45±0.03	NT
09	0.1	1.0	—	0.2	1.3	10	20	30±5	0.32±0.03	NT
10	0.1	1.0	—	0.2	2.8	10	20	30±5	0.59±0.05	NT
11	0.1	1.0	—	0.2	2.8	15	20	50±5	1.00±0.05	NT
12	0.1	1.0	—	0.2	2.8	25	20	115±10	1.50±0.04	NT
13	0.1	1.0	—	0.2	3.8	10	20	30±5	0.80±0.06	NT
14	0.1	1.0	—	0.2	3.8	10	60	30±5	1.80±0.06	NT
15	0.1	1.0	—	0.2	3.8	10	90	30±5	2.30±0.08	NT
16	0.1	1.0	—	0.2	4.5	10	20	30±5	1.05±0.04	NT
17	0.1	1.0	—	0.2	4.5	25	20	115±5	4.40±0.10	NT
18	0.1	1.0	—	0.2	5.0	10	20	30±5	1.40±0.06	NT
19	0.1	1.0	—	0.2	5.0	25	20	115±5	6.00±0.40	NT
20	0.1	1.0	0.1	0.2	6.4	10	24	—	—	No NT
21	—	2.0	—	—	<1	10	24	—	—	No NT

Cit: citrate; t: time; D: inner diameter of nanotube; L: length of nanotube.

SO₄²⁻ is from addition of H₂SO₄ or NaHSO₄; PO₄³⁻ is addition of potassium hydrogen phosphate K₂HP₃O₄; Cit denotes citric acid from its salt, HO(CO₂Na)(CH₂CO₂Na)₂·2H₂O.

^a Electrolyte components are in mol/L. ^b pH<1 represents a 1.0 or 2.0 mol/L H₂SO₄ medium.

^c Quality Q of resulting nanotubes. NT: nanotubes uniformly across substrate.

No NT: No nanotubes or partly developed nanotube /porous structures.

Table.3.1. The influence of the chemical composition of the electrolyte, the pH of the solution, the potential and the duration of anodisation. [129]

Electrolyte composition plays a key role in determining the nanotubes morphology. [129]. The pH affects both the electrochemical etch and the oxide formation. Grimes et al [123], indicated that longer nanotubes can be formed in higher pH solutions that remain acidic. They also reported that the best pH range for formation of relatively long nanotubes is between pH 3 and 5; lower pH forms shorter but cleaner nanotubes, while higher pH values result in longer tubes that suffer from unwanted precipitates. Schmuki et al, 2007 [130] reported that wall thickness decreases with fluoride ion concentration, this behavior can be explained by a difference of the dissolution rate,

considering that these nanotubes grow as a result of a competition between an electrochemical oxide formation and chemical dissolution of oxide by fluoride ions.

For low F^- concentration, the dissolution of oxide is slow; therefore, the wall remains thick. Also, in low F^- electrolyte, the anodic current is smaller and the tube length is shorter [131].

Grimes et al [125] reported that wall thickness increases with decreasing solution temperature, thus, the spaces in the inter-pore areas fill and the tubes become more interconnected then the discrete tube-like structure approaches a nanoporous structure in appearance. Moreover, the length of the nanotubes increases with decreasing anodisation bath temperature [125]. (Table 3.2)

Anodisation temperature (°C)	Wall thickness (nm)	Tube length (nm)
5	3.4	224
25	2.4	176
35	1.3	156
50	0.9	120

Table.3.2. Average wall- thickness and tube-length of 10V TiO₂ nanotubes anodized at different bath temperatures. [125].

Another important parameter in the anodisation process is the applied voltage. By increasing the applied voltage, larger diameter nanotubes can be formed. [128] (Fig. 3.5) shows the relationship between anodisation potential E and outer diameter of the nanotubes d measured by cross-sectional SEM for various anodisation potentials between 1 and 100V. [130]

The outer diameter increases with the increasing of anodisation potential and the relationship can be linear according to Eq. (1): $d = 4.60E + 0.9$ (1) [130]

That was also confirmed for other fluoride concentrations. This linear relationship can be attributed to the fact that the thickness of anodic oxide film linearly increases with the potential in forming a compact oxide in the initial stage of tube growth [131].

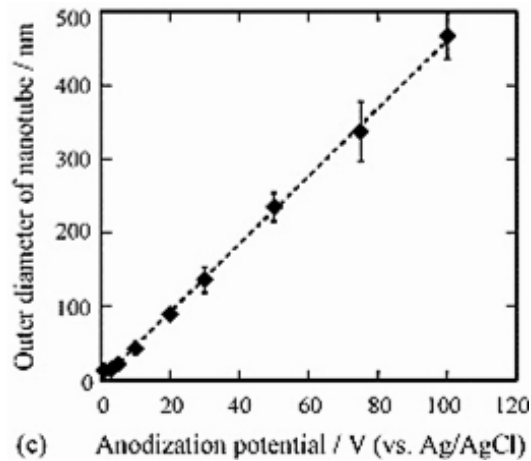


Fig.3.5. Dependence of outer diameter of nanotube on anodisation potential [130]

Mor et al [129], reported that anodisation voltage window for successfully achieving the nanotube arrays is 6–10 V for 0.25 wt% HF concentration, and 10–18 V for 1 % HF concentration.

Concerning the nanotube length, it becomes longer at more positive potential [128,131] (Fig.3.6). During the initial potential sweep, after an increase in anodic current an active–passive transition takes place resulting first in a porous surface oxide layer, and finally the current drops to a constant value while a self-organization process creates a highly ordered oxide structure [132].

During extended constant potential anodisation, the current decreases due to an increase in the diffusion layer thickness for the ionic species. However, for the anodisation times longer than 2h, the nanotube length becomes shorter because of the dissolution of nanotube wall [130].

1.3.Experiments of the present thesis for TiO₂ nanotubes fabrication

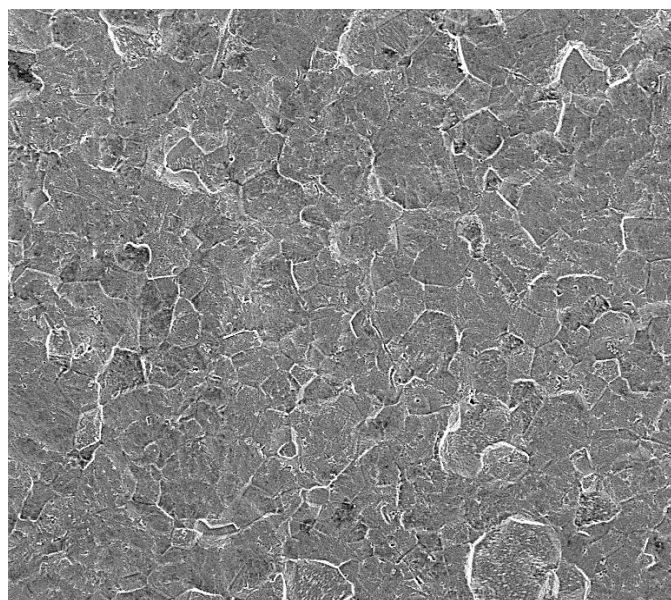
The Ti foils (99.9%) were polished down to 4000 grade SiC paper and then cleaned by sonication (180 s) in acetone-alcohol mixture (50%).

Titanium foils were anodized (EGG Princeton Applied Research potentiostat A263) using a three-electrodes electrochemical cell with a platinum foil as cathode. Samples were anodized at 8,5V anodizing voltage, in 0.5wt% HF aqueous solution at room temperature. The titanium samples were anodized for 600s with an electrolyte of acetic acid and 0.5% HF with 1:7 ratio [125].

Anodized titanium surface obtained presents amorphous TiO_2 nanotubes aligned perpendicularly to the sample surface. Mean tubes diameter is circa 35 nm and the wall thickness 2.0 nm as the operating potential is 8.5V. The observed color was purple to deep blue, which gives a thickness of about ≈ 50 nm. (Fig.3.2) Samples were rinsed and conserved in deionized water (22 MOhms) to be used later for CaP coating of TiO_2 nanotubes. Anodized titanium surface in HF solution presents amorphous TiO_2 nanotubes aligned perpendicularly to the sample surface (Fig.3.7, 3.8).

Actually we choose the previous experimental parameters to obtain nanotubes with such dimension (35nm diameter, 40-50nm length) because it was reported that nanotubes with a diameter between 30-70 nm favor bone reactions including gene expression and the adhesion of MC3T3-E1 on the implant. Whereas for nanotubes with a diameter >150 nm, a decrease of such interactions was observed [101].

The formation of a thin film of titanium oxide is confirmed by the IRRAS spectrum which appears a broad adsorption band towards low frequencies ($700 - 1000 \text{ cm}^{-1}$) and can be attributed to vibrational modes involving chemical bonds Ti-OH and O-Ti in a solid phase (Fig.3.9) [118]. Two small absorption bands can be seen in the spectral region around 3200 cm^{-1} and 1600 cm^{-1} . These bands can be attributed to adsorbed water or surface OH linked by H bonds and adsorbed carbonate species.



200 mm x 200 mm

Fig.3.7. SEM image of anodized TiO_2 surface of the order of 0.04 mm^2 (White lines on the image are grain boundaries revealed by acid etching of the sample)

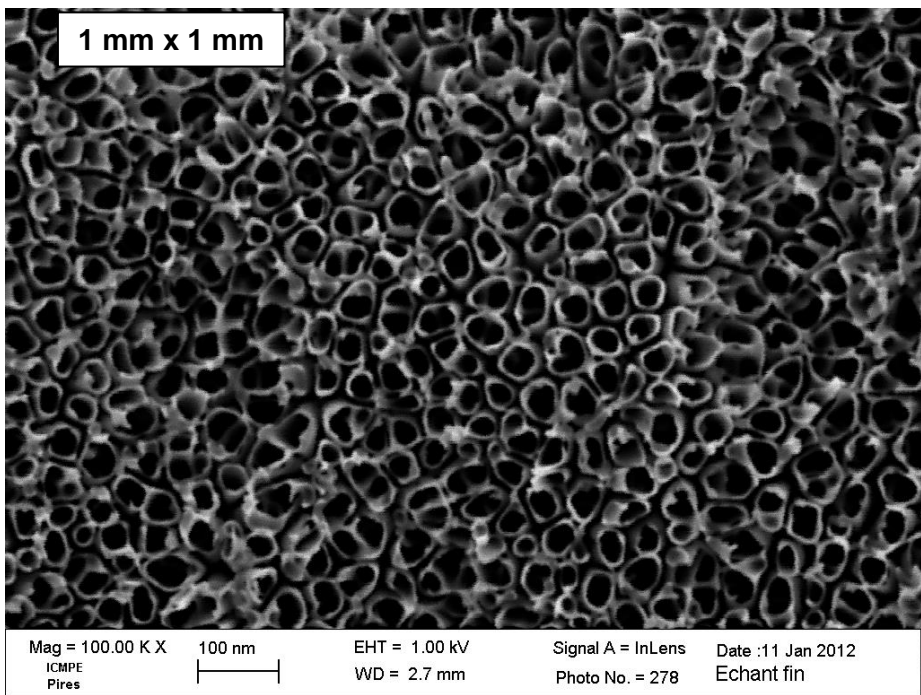
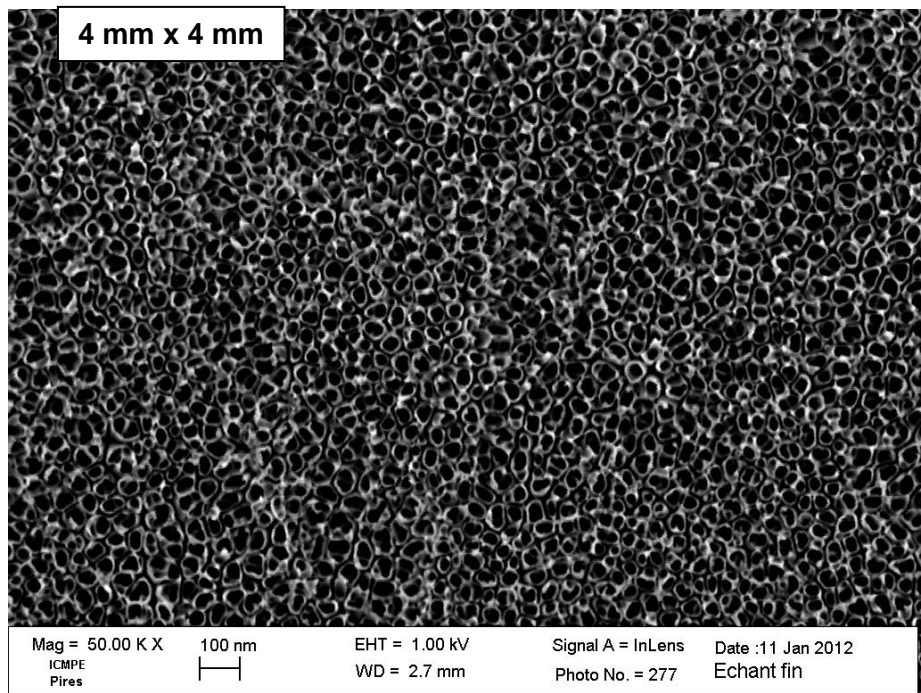


Fig.3.8. SEM images of TiO₂ nanotube (nT-TiO₂) arrays

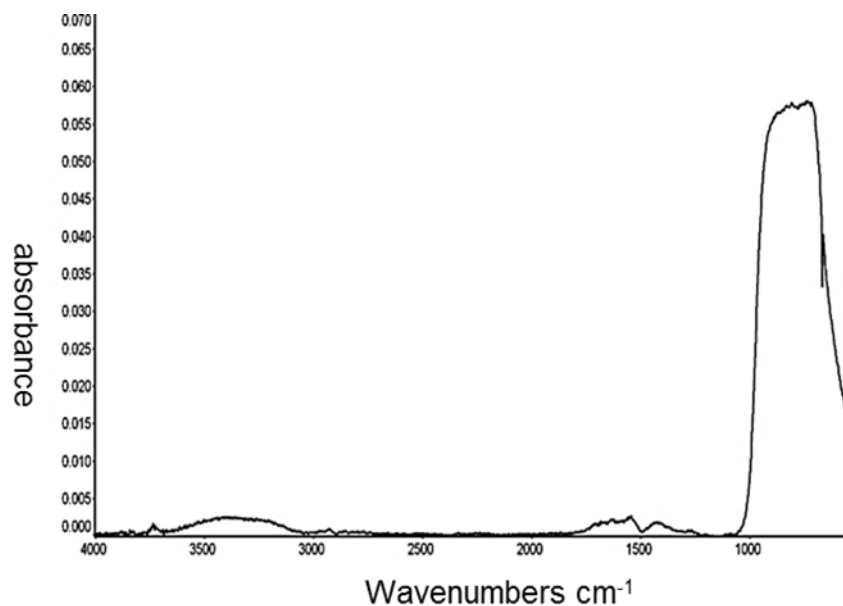


Fig.3.9. IRRAS spectrum of anodized TiO₂ surface

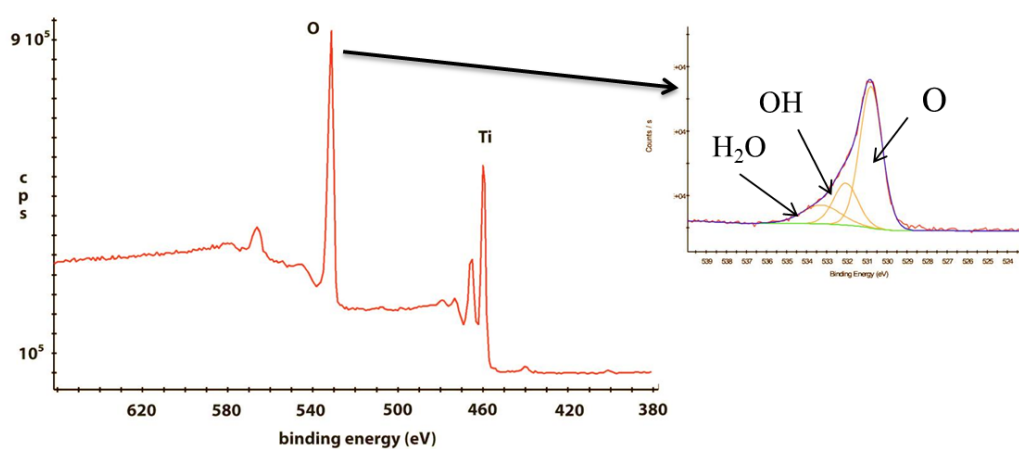


Fig.3.10. XPS spectrum of anodized TiO₂ surface with a deconvolution of O_{1s} peak

To confirm the chemical composition of the surface we realized XPS analysis with a deconvolution of oxygen peak that indicated the presence of OH and H₂O on the surface. After calculating the atomic percentages, we had the following percentages (Ti≈29%, O≈56%, OH≈15%) which indicated that TiO₂ nanotubes are slightly oxygen sub stoichiometric (TiO_{1.93}) but hydroxylated and hydrated as shown in the deconvoluted spectrum of O_{1s} (Fig.3.10).

2. Analysis of nanostructured TiO₂ reactivity toward phosphate

“Bioactive” implants are implants that contain elements or compounds such as calcium, magnesium, phosphorous, fluorine, sodium, strontium and calcium phosphates compounds which increases the bonding strength and anchorage speed of implants in bone [133, 134].

Phosphate exists at significant concentrations in biological systems, e.g., in blood at around 10.0 mol.L⁻¹ [135], and is expected to interact with metallic oxides surfaces of implants, changing their chemical nature and inducing osseointegration [136]. Many *in vivo* studies [137, 138] investigated the bone response to phosphate-incorporated titanium implants which showed higher removal torque value than non-incorporated cp titanium with a higher bone metal contact percentage. *In vitro* studies [139] reported that phosphorus-ion deposition increase corrosion resistance and biocompatibility of titanium implant.

In our experiment, the used phosphorus species were considered as small size molecules to be deposited on TiO₂ nanotubes. Actually, beside their important biological role, phosphorus species were deposited in our study to evaluate the nanostructured TiO₂ reactivity toward calcium-phosphate compounds and to test and observe phosphate adsorption process by such nanostructured surface to better control and understand the later deposition of more complicated compounds such as HAp.

Two methods of deposition were used. The first one was simply immersing samples in phosphorus solutions, rinsing with deionized water (DI) or using ultrasounds and then drying.

The second method was standard electrodeposition by using a classical three-electrode electrochemical cell with an aqueous solution of the studied molecule at room temperature and a constant potential. The electrodeposition technique is used to deposit cations and anions from the electrolyte following interfacial reactions that are induced by the imposed potential on the working electrode. As this method has been used to deposit CaP compounds in the next step of this work, it is interesting to investigate the action of imposed potential on the phosphate adsorption.

With electrodeposition method, the chemical composition of the coatings can be controlled by varying the ion concentrations in the electrolyte [142, 143].

In this study, the deposits composition and their growth rate were investigated by FT-IRRAS and XPS.

Phosphates are tetrahedral molecules, with symmetry dependent on the number of substituent on the O atoms. Observing IR spectra and for phosphorus species $(\text{H}_{(n)}\text{PO}_{(4)})^{(3-n)}$ ($n=0-3$), the region between 800 and 1300 cm^{-1} is a very informative region. It contains the majority of the stretching vibration modes (elongation $\text{P} \leftrightarrow \text{O}$) for P-O bonds. As phosphate shows four different vibrations; the symmetric stretching (ν_1), the symmetric bending (ν_2), the asymmetric stretching (ν_3) and the asymmetric bending (ν_4). The ν_1 (non degenerate symmetric stretching) and the ν_3 (triply degenerate asymmetric stretching) vibrations can be used to understand the molecular symmetry of the phosphoric acid and its adsorption complexes on metallic oxide surfaces. Herzberg [144] has placed the ν_3 and ν_1 vibrations for the tetrahedral PO_4^{3-} ion at 1082 cm^{-1} and 980 cm^{-1} , respectively; however, the frequencies can vary and we can remark degenerations and frequency shifts depending on the protonation of the phosphate or the local symmetry of the adsorption site. This behavior is observed in different organo-metallic compositions where the symmetry and strength of the chemical bond depend on the metal (ligand - metal) in the complex [145].

In this respect, it's important to mention the effect of pH and deprotonation on the symmetry and composition of phosphorus species. Phosphate has 3 pKa values ($\text{pK}_1=2.20$, $\text{pK}_2=7.2$, and $\text{pK}_3=12.3$), and the protonation significantly affects the molecular symmetry. The following illustration shows the predominance domain of phosphorus species according to pH, indicating that PO_4^{3-} are dominates at $\text{pH}>12$. (Fig.3.12) [146]

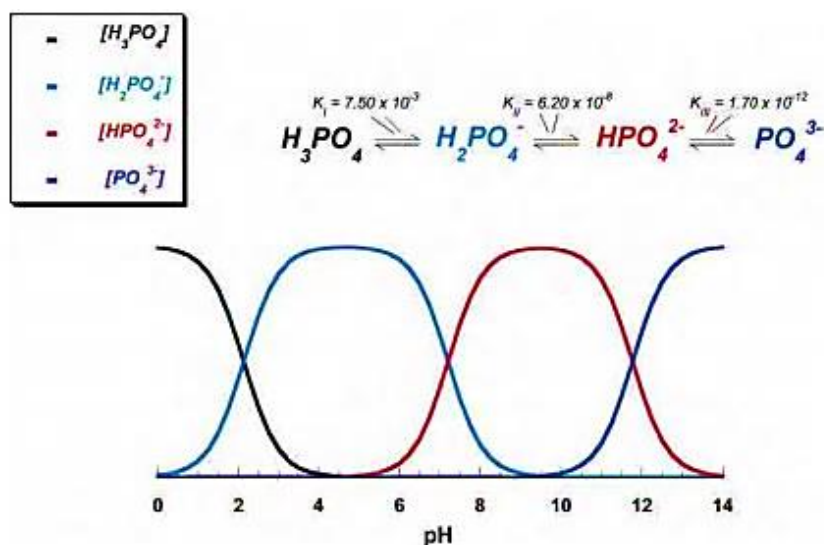


Fig.3.11. pH variation of ionic concentrations for phosphoric acid solutions [146]

Fully deprotonated phosphoric acid (PO_4^{3-}) at pH 11 has T_d symmetry. This tetrahedral molecule shows a single ν_3 asymmetrical vibration at $\approx 1006 \text{ cm}^{-1}$, and there is no activation of the ν_1 vibration. (Fig.3.13) shows the IR spectra of P solution species which are reproduced based on Tejedor-Tejedor and Anderson's research [147].

Protonation of this complex to monoprotonated (HPO_4^{2-}) leads to a symmetry reduction from T_d to C_{3v} , and the triply degenerate ν_3 vibration splits into two separate ν_3 bands located at 1078 and 990 cm^{-1} , and there is also ν_1 band activation at $\approx 850 \text{ cm}^{-1}$. Further protonation results in the formation of diprotonated phosphate (i.e., $H_2PO_4^-$), which leads to a reduction in the symmetry from C_{3v} to the C_{2v} . This symmetry reduction leads to splitting of the ν_3 vibration into three ν_3 bands at ≈ 1160 , 1074 , and 940 cm^{-1} , and the ν_1 band remains active and shifts to higher wavenumber at $\approx 870 \text{ cm}^{-1}$, so that a total of four bands are present for this phosphate species (Fig. 3.13). At $\text{pH} \approx 1.3$, the symmetry of the dominant phosphoric acid species is H_3PO_4 (C_{3v}) and the spectrum shows doublets of the ν_3 vibration at ≈ 1179 and 1006 cm^{-1}

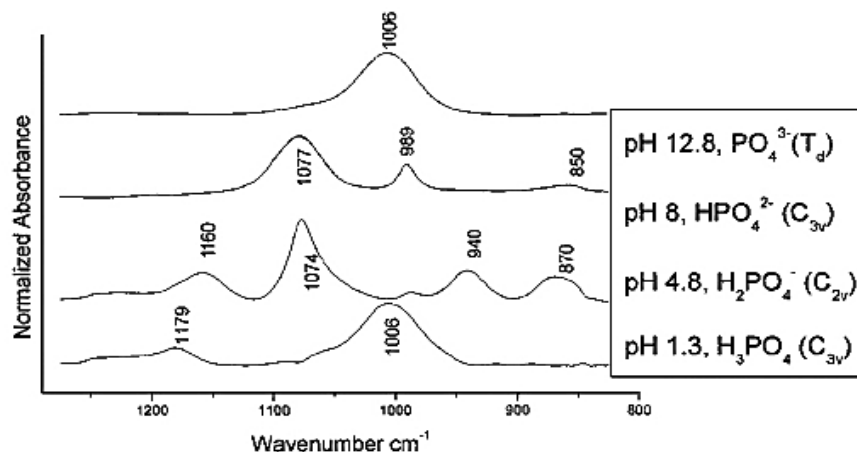


Fig.3.12. FTIR spectra of phosphoric acid at different pH values [147].

The relation between the number of IR active bands and phosphate symmetry can be used to interpret phosphate bonding configurations at mineral surfaces as adsorbed phosphate can be viewed as surface complexes. For example, when phosphate forms a non-protonated monodentate complex, the symmetry of the phosphate molecule is C_{3v} , and two ν_3 bands are expected to be present in addition to the active ν_1 band. When phosphate forms a bidentate complex, the symmetry of the surface complex is C_{2v} so that three active ν_3 bands should be present in addition to the ν_1 band. [145]

As mentioned before, in this work phosphate deposition is done by two methods; first, immersion of nanostructured TiO_2 samples in Na_3PO_4 stock solution ($C=1.64$ g/l) with a pH adjusted to 7.0. The adsorption was evaluated in different points of immersion time.

For the second method, standard electrodeposition, the same solution was used as electrolyte in a three electrodes electrochemical-cell (nanostructured TiO_2 sample, platinum electrode and calomel electrode). The phosphate electrodeposition was carried out in potentiostatic conditions at (-2.0V) for different durations.

The aim of this work is to provide *in situ* infrared spectroscopic evidences for the mechanism of phosphate adsorption on nanostructured surface, regarding the identification of the adsorbed species, the nature of the interaction between the species and the surface.

2.1. Experimental results

2.1.1. Phosphate Deposition by immersion

From IRRAS spectra for the immersed samples of nt-TiO₂ in phosphate solution, we observed broadband with several components that located at; 1030, 1100 and 1153 cm⁻¹ (Fig.3.13).

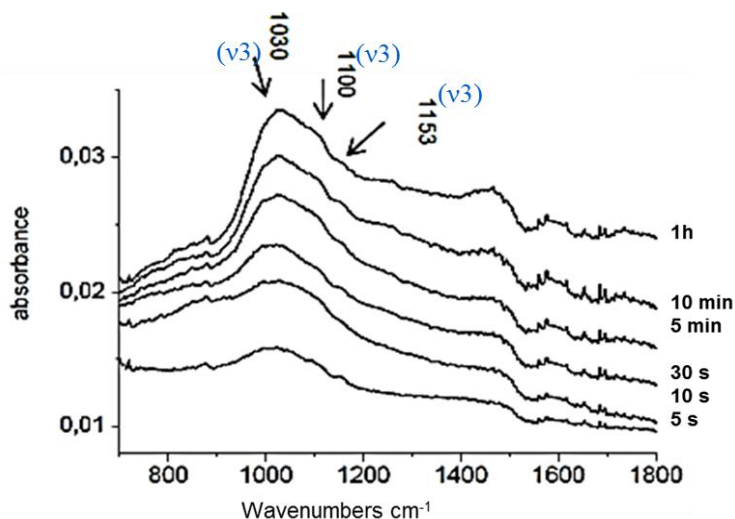


Fig.3.13. IRRAS spectra of immersed nt-TiO₂ samples in phosphate solution; the growth of adsorption intensity as a function of immersion time

Phosphorus species are bound to titanium ions via P–O– groups, forming a P–O–Ti bond. Precedent studies on other types of oxides reported that these bands could correspond to an adsorbed bidentate complex [148,149, 150].

For the bands at 1030 and 1100cm⁻¹ (Fig.3.13), the adsorbed complex was very similar to those observed by Michelmore et al [148,149] on non-nanostructured ZnO and TiO₂. Those peaks correspond to the asymmetric stretching vibrations of P– O for bidentate complexes with C_{2v} symmetry. Similar adsorbed entities characterized by bands located by 1030 and 1100 cm⁻¹ were also observed by Arai et al. and Tedjedor et al. on goethite and ferrihydrite [147, 159].

The peak at 980 cm⁻¹ observed by Michelmore et al [148], assigned to the stretching vibrations of P– O–Ti, isn't visible in our spectrum and this could be because the absorption bands are broad and overlapped with the peak at 1030 cm⁻¹. So we have realized a peak decomposition to define the absorbed species. (Fig.3.14)

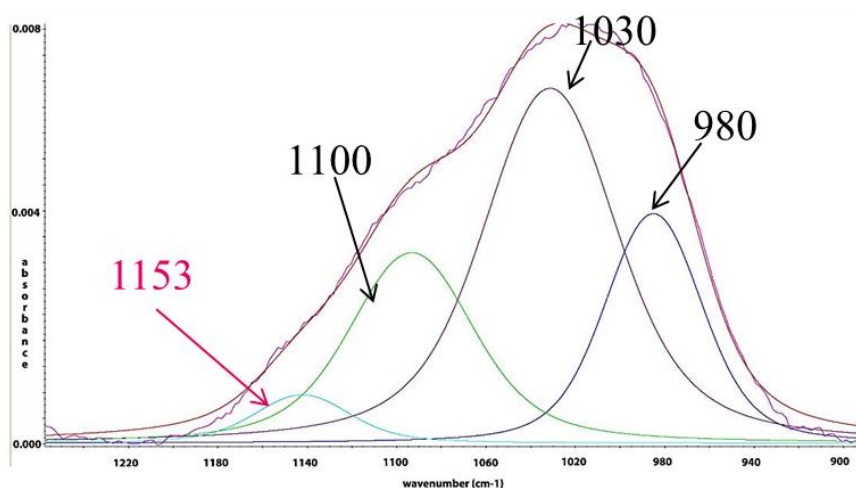


Fig.3.14. IRRAS deconvoluted spectra of phosphate band

Actually, from the analysis of the IRRAS spectra and as compared to the results of Arai et al. and Tedjedor et al. on goethite and ferrihydrite [147, 159], we have found that the three major peaks at 980, 1030 and 1100 cm^{-1} indicating phosphate is adsorbed on TiO_2 surface as a bridging bidentate surface complex with C_{2V} symmetry.

These results agree with Connor and McQuillan [151] who reported that phosphate binds strongly as bidentate surface species. In their results, the peak at 980cm^{-1} wasn't detected either. They also reported that spectra of the phosphate species adsorbed on TiO_2 surface are different from those of phosphate solutions where P–O bonds on the substrate were at lower frequencies (1030, 1100 cm^{-1}) than that in the solution (1077, 1155 cm^{-1}).

The band at 1153cm^{-1} wasn't mentioned in Michelmore et al studies but it was observed on hematite (iron oxide) by Persson et al. [150] where this high frequency band could correspond to an adsorbed structure with a highly ionic bonding (physical adsorption). The existence of adsorbed protonated complex is combined with a broadband absorption around 3200 cm^{-1} (OH hydrogen bonding).

These results can be supported by the fact that HPO_4^{2-} and $\text{H}_2\text{PO}_4^{2-}$ species are dominant for $\text{pH} = 7.0$ and can be adsorbed onto the oxide surface following deprotonation in an acid-base mechanism with surface hydroxyls.

2.1.2. Phosphate electrodeposition

Before presenting the obtained IRRAS spectra for such method, it's important to present the deposition mechanism of standard electrodeposition method applied in this work. (Fig.3.15) shows typical current density–time curves recorded during phosphate deposition at -2.0V . The value of current density decreased during the first steps of deposition and then increased rapidly. The cathodic current density shifts from -0.5 mA cm^{-2} to a nearly steady value, -11.3 mA cm^{-2} at -2.0V .

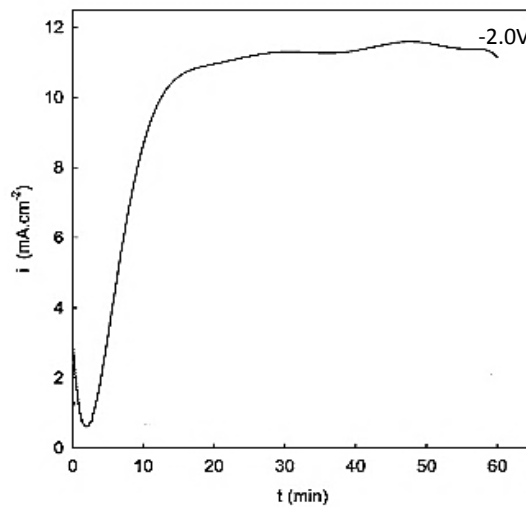


Fig.3.15. Evolution of cathodic current density vs. time resulting from -2.0V potential applied for phosphate deposition onto nanostructured TiO_2 sample

Accordingly, it's important to explain the mechanisms of deprotonation by cathodic reaction with OH^- of the surface. The local pH on the titanium surface is increased relatively to the phosphate solution due to the reduction of water under these experimental conditions:



Then the local phosphate ion concentration increase due to the hydroxide ion engagement reactions (2) and (3). This means that in the constant potential mode, the accumulation of OH^- led to an increased production of PO_4^{3-} ions (3).



From IRRAS spectra of electrodeposited phosphate (Fig.3.16), we can observe the same adsorption range observed for the immersion method with a major peak around

$\approx 1000 \text{ cm}^{-1}$ where components similar to the immersion case can be distinguished suggesting the same adsorption geometry complexes that were observed with immersion method.

But then, when continuing in the process (increasing electrodeposition time) we found a broad band with two dominant bands appear at 984 and 1100 cm^{-1} which correspond with the P-O asymmetric stretching vibration and ν_3 vibration mode for P-O-Ti bond.

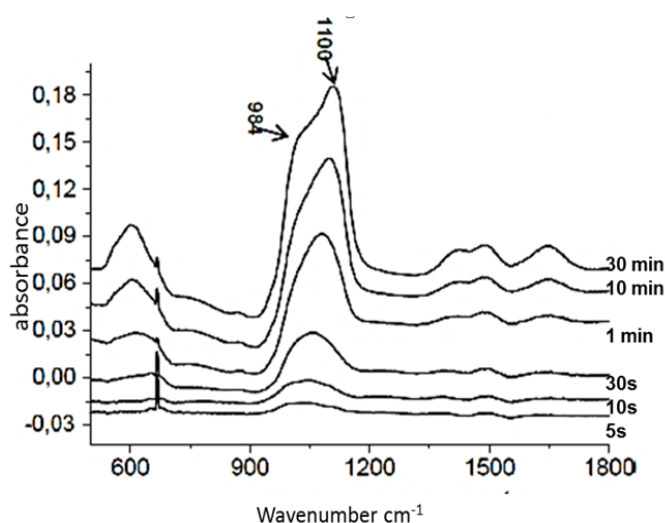


Fig.3.16. IRRAS spectra of electrodeposited phosphate on nt-TiO₂ at -2V

Arai et al. mentioned a monodentate mononuclear complex with C_{3v} symmetry [159] for this couple of absorption bands. We can also remark that the band located near 1153 cm^{-1} is not present as in the case of the immersion method. The protonated adsorbed species doesn't exist in this case as they can react with the hydroxyls produced during water hydrolysis.

In addition, we found that the adsorption intensity was much more important than in the immersion case ($\approx \times 10$).

3. Alkaline treatment of nanostructured TiO₂ surface

As surface charge plays a key role in enhancing the mineralization of apatite. Yamashita et al [152] reported that heterogeneous nucleation of CaP could only happen on negatively charged surface. However, at positively charged Ti oxide surfaces, competitive adsorption between phosphate and chloride ions from electrolyte was found to block the growth of calcium phosphate phases [153]. For that reason,

attempts have mainly focused on creating negative ions at the surface of Ti by chemical or physical methods. Common chemical methods use hydrogen peroxide or alkaline treatment.

NaOH treatment is popular among current dental implant investigators. By immersing implants in sodium hydroxide in relatively high temperatures ($\approx 60^\circ\text{C}$) then rinsing in distilled water. This results in the growth of a sodium titanate layer on the implant surface allowing calcium phosphates compounds deposition such as hydroxyapatite. [154]. The titanate gel layer obtained after these treatments bears negatively charged Ti-OH groups under physiological conditions, which facilitate the precipitation of Ca^{2+} and as the calcium ions accumulate on the surface, the surface gradually gains an overall positive charge. As a result, the positively charged surface combines with negatively charged phosphate ions to form a calcium phosphate compound [155]. Sodium titanate is well known for accelerating CaP formation in $(\text{CaP}_{\text{sol}})$ [102]. The surface acts as a site for the subsequent nucleation of calcium phosphates when immersed in CaP solution $(\text{CaP}_{\text{sol}})$. This involves an initial formation of Ti-OH by the release of sodium ions from the sodium titanate layer due to the process of ion exchange. This is followed by formation of calcium titanate as a result of reaction with the calcium ions from the solution.

Kokubo et al. [157] reported an enhancement of the bioactivity and bone-bonding ability of titanium implants treated with an alkali hydroxide solution.

3.1.SEM and XPS experimental results for alkaline treatment

In our experiments we have treated TiO_2 samples with 1 M NaOH solution at 60°C , after that the samples were rinsing with distilled water , dried and conserved for CaP coating.

(Fig.3.17) represents TiO_2 nanotubes after NaOH treatment for 10 minutes and shows the deposits on the sample substrate. A ring of deposits is formed around the nanotubes neck or edges; “Ring-like shape”.

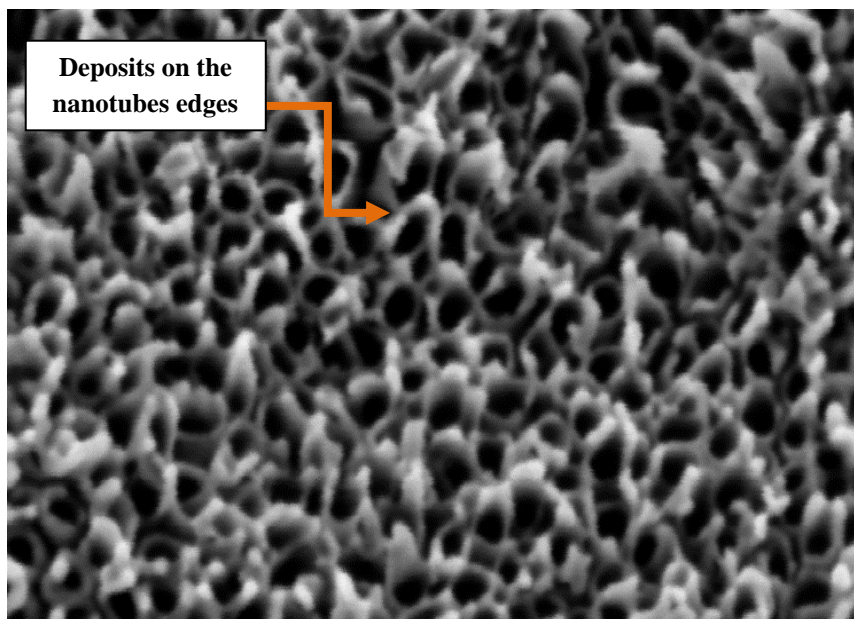


Fig.3.17. SEM image of (nT-TiO₂) treated with NaOH

To investigate the chemical composition of the deposits, we realized XPS analysis of the surface (Fig.3.18) and calculated the atomic percentages (Na 9%, Ti 23%, O 47%, OH 21%) which suggest the following formula for the sodium titanate on the nanotube edges: Na₂Ti₃O₅(OH)₄ + 2(TiO₂).

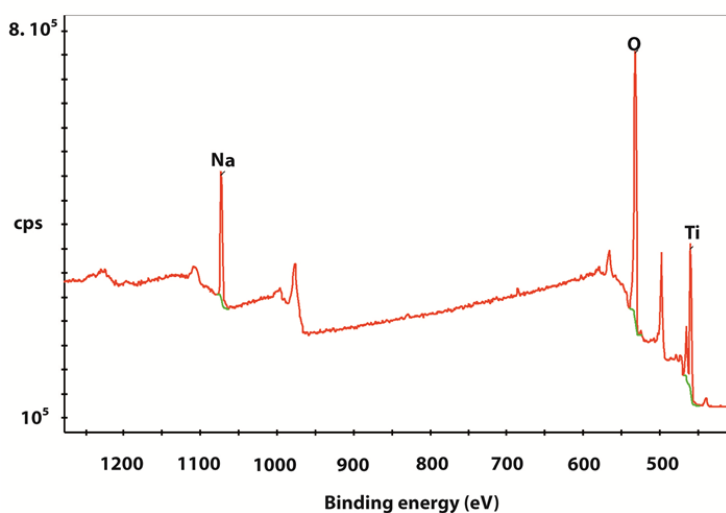


Fig.3.18. XPS spectrum of NaOH treated TiO₂ surface

In (Fig.3.19) we can see XPS spectrum of the O_{1s} electron binding energy for nT-TiO₂ treated with NaOH for different durations; 5, 10 and 15 minutes. In the first spectrum Oxygen peaks O_{1s} appears after 5 min of treatment, a peak can be seen at 531eV and

related to Ti-O whereas in the second and third spectra and when getting further in treatment duration for 10 and 15 minutes, we can observe that Ti-OH peak at 532eV developed with an equal or even higher [Ti-OH]/ [Ti-O] ratio, which indicates the further formation of Ti-OH groups on the surface as a function of processing duration.

In this part of work we evaluated the NaOH pretreated nanostructured surfaces for the deposition of phosphate by both immersion and electrodeposition methods to observe the influence of NaOH pretreatment on such adsorption.

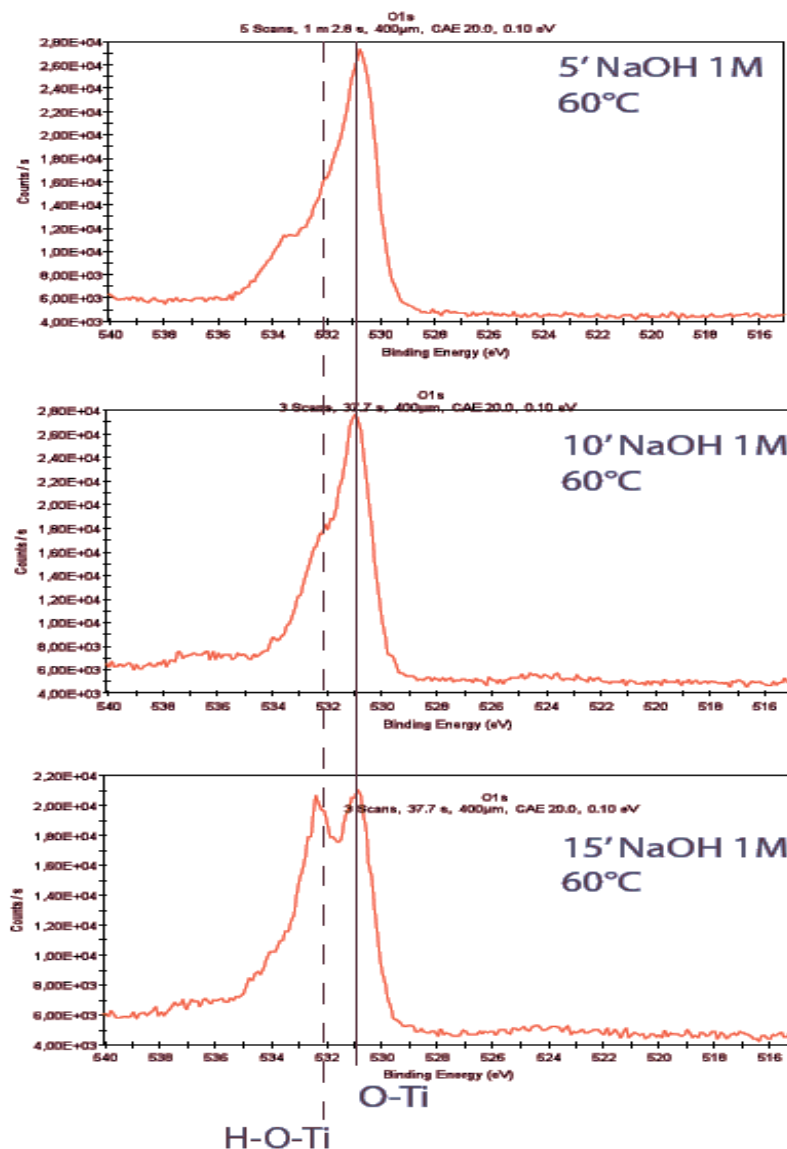


Fig.3.19. XPS spectra of nanostructured TiO₂ surface treated with NaOH as a function of time (5min, 10 min and 15 min).

3.2. NaOH pretreatment effect on phosphate adsorption onto TiO₂ nanotubes

(Fig.3.20) shows the IRRAS spectra for the phosphate adsorption onto NaOH pretreated titanium nanotubes by immersion and electrodeposition at -2V.

In both spectra we can observe growth of phosphate deposits with similar adsorption intensity as compared to deposits onto non-treated (nT-TiO₂) previously presented.

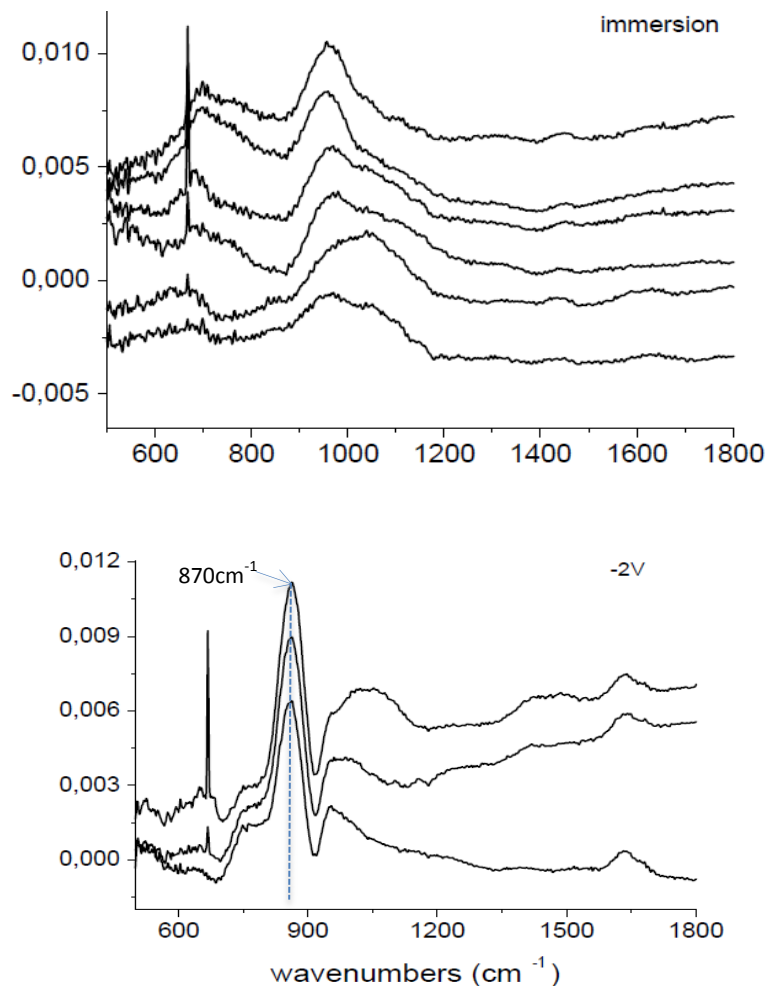


Fig.3.20. IRRAS spectra of deposited phosphate on nt-TiO₂ by immersion and electrodeposition with NaOH pretreatment

Nevertheless, one can observe a modification of the evolution with the deposition time of the absorption band shape for immersed samples when pretreated with NaOH.

At low coverage, a broad band composed of peaks near 1040, 1110 and 1145 cm⁻¹ can be clearly seen and presents the same components as for the immersion on nt-TiO₂.

For higher coverage, the main broad peak is around 960 cm^{-1} and this can be related to a modification of the adsorption geometry with immersion time.

From these observations we can suggest that in a first step, bidentate complexes are adsorbed onto the surface which transform to monodentate species when phosphate surface density increases.

When deposition is realized by electrodeposition, one can observe a completely different behavior. A sharp absorption band localized at 870 cm^{-1} dominates the IR spectrum with a low intensity broad band located near 1050 cm^{-1} .

Such a spectrum with a dominant strong absorption band located at low frequency has been observed by Persson et al. [150] in the case of orthophosphate adsorbed onto goethite at basic pH (12.8). This observation correspond to the results of Raj et al. [158] and Arai et al. [159] for adsorption in a basic pH indicating the existing of a third complex tridentate.

Raj et al have realized DFT calculations for different phosphate modified titania and only tridentate complexes give rise to a main absorption band located near 900 cm^{-1} .

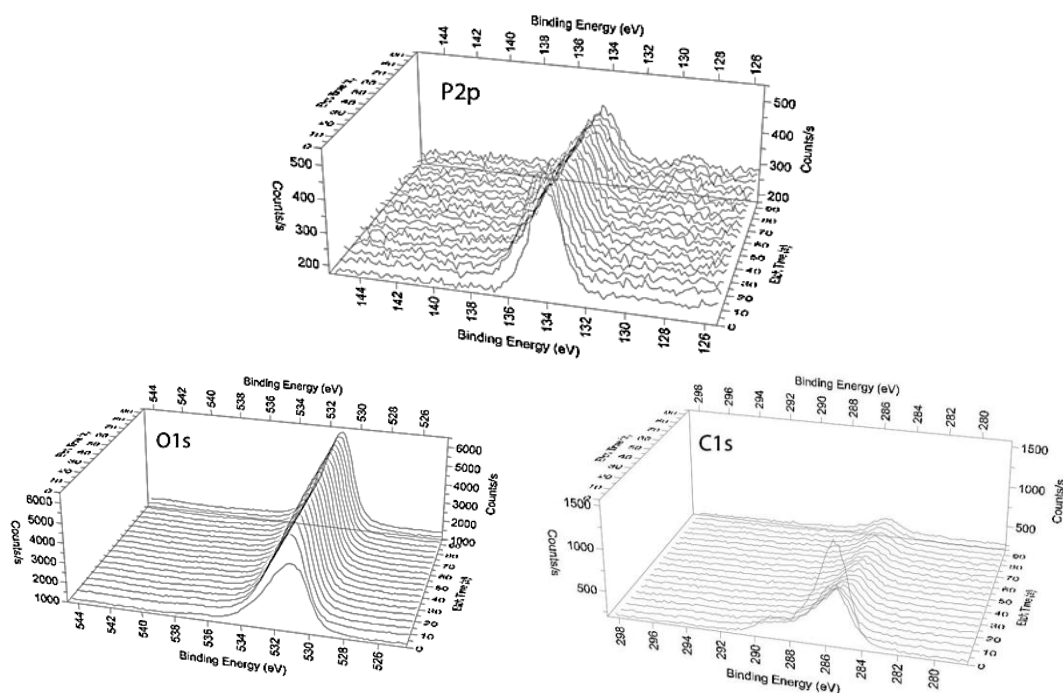


Fig.3.21. XPS spectra recorded during depth profiling of phosphate adsorbed onto nt-TiO₂ (immersion)

In order to investigate if the adsorbed phosphate are localized inside the tube or only adsorbed on the tube edges, we have performed an XPS depth profiling with Ar⁺ ion sputtering (3.0 KeV). (Fig.3.21) The estimated sputtering depth is 0.3 nm.s⁻¹ on Al₂O₃ thin film. In each case, the P_{2p} signal remain constant even after a sputtering of 30.0 nm, meaning that the phosphate adsorbed entities are located on the nanotubes wall. We can observe a carbon contamination mainly located on the tube edges.

4. Functionalization of nanostructured TiO₂ surface with calcium phosphate and Strontium-doped Calcium phosphate

As mentioned in chapter I, and due to the fragile nature of bulk CaP ceramics, it cannot be used in orthopedic or prosthetic devices because they tolerate high functional pressures during their expected lifetimes. Still, as CaP coatings of metallic implants, they permit the amelioration of implants bioactivity and osteoconductivity as these compounds are very similar chemically to inorganic bone matrix [160].

Upon implantation, these CaP coatings dissolve and release Ca²⁺ and HPO₄²⁻ which are easily recycled by the body. Such dissolution leads to the precipitation of biological apatite nanocrystals. This biological CaP layer will promote cell adhesion and differentiation into osteoblast, and also enhance the synthesis of mineralized collagen and the extracellular matrix of bone tissue. As a result, these CaP coatings promote a direct bone-implant contact without intervention of connective tissue layer leading to a proper biomechanical fixation of dental implants.

Actually, such attempts to improve bone-bonding by titanium-based implants coating are commonly accomplished by plasma spraying which unfortunately had demonstrated high long-term failure ratios. The vertically aligned TiO₂ nanotubes on Ti substrate help in improving the binding between apatite coating and Ti substrate.

Functionalization of the nanostructured TiO₂ surface by CaP coatings and Sr doped CaP coatings is an interesting approach to improve the properties of the implant coating and thereby increase the possibility for a positive bone response *in vivo*. Therefore, in our work we applied pulsed electrodeposition to deposit CaP compounds as this method has many advantages over plasma spraying and which will be discussed in this chapter.

This section investigated the ability of nanostructured Ti surface to induce CaP and Sr-doped CaP nucleation and growth *in vitro* via electrodeposition method with discussing of the coatings composition. Samples were characterized by SEM, XPS and IRRAS.

4.1. Calcium Phosphate compounds

Calcium phosphate compounds are resorbable noncytotoxic materials that create chemical bonds between implant substrate and host bone to enhance the implant osseointegration. These compounds can also serve as drug delivery systems when doped with important bio-elements such as Sr and Zn and participated with antibiotics and proteins.

The major advantages of the CaPs include biocompatibility and resorbability *in vivo* [161]. Upon implantation, these materials act as osteoconductive scaffolds but, as time passes, they degrade and are replaced by new bone during the remodeling process [161].

CaPs degradation occurs by the combination of two processes; first *in vivo* dissolution, which depends on their composition and particle size [68]. The second process is cellular resorption mainly by osteoclasts which is advantageous since it mimics the natural process of bone remodeling, in which osteoclasts resorb bone and then osteoblasts secrete bone matrix [162]. Bone substitutes regeneration and bio-resorption rate depends on several factors such as porosity, composition, solubility and presence of certain elements that release during the resorption of the ceramic material and facilitate the bone regeneration [160].

Actually, CaPs and bone mineral are comparatively different in composition and degree of crystallinity. Bone mineral is a calcium compound and contains carbonate substitutions and some other ions which present in bone mineral such as magnesium (Mg^{2+}), sodium (Na^+), potassium (K^+), fluoride (F^-), and chloride (Cl^-) ions.

It has been reported that the most appropriate chemical formula for biological HAP is $(Ca, M)_{10}(PO_4, Y)_6(OH, X)_2$ where M represents a substitution cation and X and Y represent substitution anions [65].

All current formulations of calcium orthophosphate cements are divided into two major groups, depending on the end-product of the reaction, apatite and brushite cements. The final product of the cement determines the solubility and therefore in vivo bio-resorbability. [163].

Depending on the calcium/phosphorus (Ca/P) molar ratio and solubility of the compound, we can obtain different calcium phosphate compositions and crystallographic phases (as reviewed in chapter I). In general, the lower the Ca/P ratio, the more acidic and soluble the calcium phosphate phase.

Presence and incorporation of calcium phosphate precursors with aqueous solution stimulates various chemical transformations, where initial calcium phosphates crystals

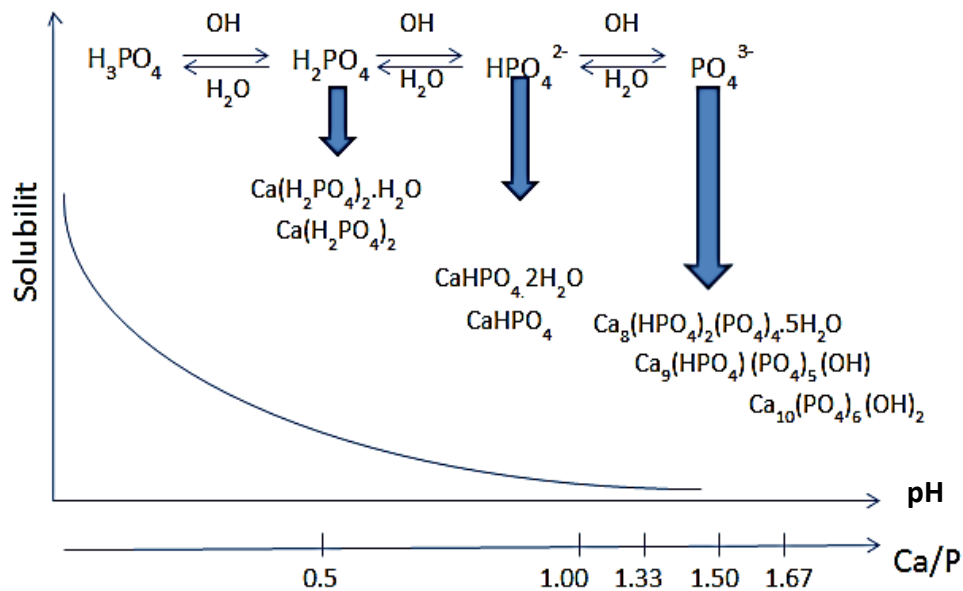


Fig.3.22. Decrease in solubility of calcium phosphates with increasing Ca/P ratio. [160]

dissolve rapidly and precipitate into crystals of hydroxyapatite HAp or brushite-like composition DCPD with possible formation of intermediate precursor phases such as ACP and octacalcium phosphate OCP (Fig.3.22) [160,164].

Actually, those metastable intermediate precursor phases can participate in the crystallization process. Moreover, the *in vivo* presence of peptides, proteins, and other inorganic compounds also affect the crystallization, making it difficult to predict the probable formed phases. [64]

Hydroxyapatite HAp is the most stable phase and the least soluble and it is formed in neutral and basic pH [164]. In more acidic solutions, DCPD and octacalcium phosphate OCP are often formed.

Brushite-like cements have attracted attention because they are resorbed *in vivo* much faster than apatite ones. Moreover, brushite-like compositions are metastable under physiological conditions and brushite based cements have relatively shorter setting times and considered to be ideal for *in vivo* resorption rate [163, 164].

However, it's important to mention that brushite and OCP could form possible precursors before they transform to apatite. Although brushite and OCP are often detected during *in vitro* crystallization, they have not been found in normal *in vivo* calcifications, suggesting the formation of an initial amorphous calcium phosphate phase (ACP) followed by transformation to apatite. [165]

4.2.Strontium Substituted Calcium Phosphate

Recently, ionic substitution in CaP (mainly α , β -TCP) ceramics, by bio-elements such as magnesium (Mg), strontium (Sr) and zinc (Zn), have been of great interest because of their important role in the biological processes after implantation [166]. The presence of foreign ions into calcium phosphate structure can alter many structural, physicochemical and biological properties, such as lattice parameters, crystallinity, solubility in the setting liquid, resorption and bone bonding capability [166].

The substitution of a foreign ion also depends on the nature and size of the ion and its crystallographic site. It was reported that ion substitutions can happen in a CaP crystal structure if the valence of the replacing ion is within one unit of that of the ion being replaced and if the radii of the two ions are similar [167].

Mg, Zn and Sr match both requirements and these ions can occupy the same site in a crystal. [167]. The current tendency is to obtain calcium phosphate bioceramics partially substituted by bioactive elements that enhance the bio-properties of the resulting implant coating, taking into consideration the influence of these elements on the bioactivity of TiO₂ implants.

Many researches were interested in the strontium (Sr) incorporation into the CaP structure due to its role in the calcifying of bone that is represented in osteoporosis and its deposition ability into the mineral structure of bone [168].

The presence of Sr can enhance endosteal and trabecular bone formation without affecting bone mineralization and reducing bone resorption which can directly influence the mechanical properties of bone, increasing the bone strength, while maintaining the bone physiological balance. Moreover, Sr can stimulate osteoblast differentiation and inhibit osteoclastogenesis when used in a dose dependent manner. [169]

Strontium (Sr) was shown to decrease osteoclast activity by about 30%, and to induce osteoclast apoptosis as reported by Baron et al [170] by resorbing pit assay in isolated rat cells resulting in a decrease in bone resorption *in vitro*. Notably, the inhibition of bone resorption by strontium is not complete, leaving physiological regulation of bone cells to occur. (Fig.3.23)

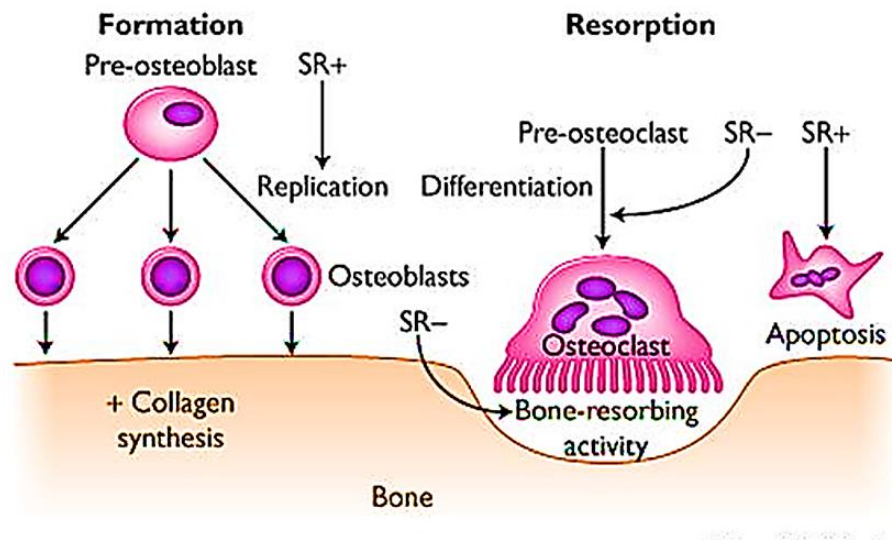


Fig.3.23. Strontium (Sr) anti-resorbing and bone-forming effects [168]

Furthermore, strontium increases alkaline phosphatase activity (ALP), a marker of osteoblast differentiation, and enhances collagen synthesis [171]. This indicates that strontium stimulates bone formation *in vitro*, which classifies this agent as a bone-forming drug in a dose dependent manner [171]. Beside its chemical analogy to Ca, Sr is a bone seeker element. In dental enamel, Sr was also found to stabilize the apatitic structure and induce higher resistance to degradation by bacterial acids. [172].

From a crystal-chemical point of view, the incorporation of Sr^{2+} led to an expansion of lattice parameters, because Sr^{2+} has an ionic radius (1.13 Å) higher than that of Ca^{2+} (0.99 Å), thus, its incorporation in bone crystals increases the length of Sr-hydroxyl

bond more than that of Ca-hydroxyl. This in turn results in a decrease in the lattice energy, which is vice versa proportional to the cohesion distance and, therefore, a subsequent decrease in crystallinity. Thus, Sr incorporation in bone mineral may lead to the modifications in lattice parameters, crystal size, and crystallinity of bone mineral [173]. For example, Kannan et al. [166] observed a linear expansion of lattice constant values with the increase in Sr concentration that was settled in the β -TCP structure.

Moreover, doping by Sr^{2+} ions also influences the nucleation and growth and composition of CaP, Heughebaert et al [174] indicated that traces of Sr^{2+} ions have been shown to reduce the overall rate of CaP crystallization and delay the transformation of amorphous CaP to apatite phases.

Actually, doping CaP coating by Sr would help in taking advantage of both strontium and CaP for osseointegration. It was reported that CaP coating has been mostly realized by soaking the samples in SBF solutions [175,176]. This process generally takes long immersion duration (hours to few days) to precipitate CaP on the TiO_2 nanotubes, with a low surface bonding strength [65]. TiO_2 surface is mostly negative in simulated biological environments (pH 7.4), thus it's electrostatically capable of attracting positively charged ions such as calcium. Cationic Ca^{2+} reacts then with negatively-charged PO_4^{3-} and CO_3^{2-} to form a CaP containing surface layer which finally crystallizes to bone-like apatite [178]. Because this reaction occurs in an environment similar to that of natural apatite, it was reported [178] that such coating method may strengthen the bone-bonding better than those made by other methods such as plasma spraying. In addition, the nanotube arrays also participate in increasing surface roughness and provide surface area for the later hydroxyapatite coating deposition. Nanotubular structure serves as an excellent anchorage for CaP coating which improves the mechanical bonding of the implant to the bone.

Calcium phosphate CaP coating of Ti substrate by electrodeposition has been investigated as one of the simplest and most effective CaP coating methods [177]. So taking advantages of nanostructured, NaOH pre-treated TiO_2 samples, we tried to deposit CaP and Sr doped CaP onto those surfaces by pulsed electrodeposition method and make a physicochemical evaluation of such functionalized surfaces.

4.3.Pulsed Electrodeposition

In this work, we realized the CaP and Sr-doped CaP deposition from acidic aqueous solutions by pulsed electrodeposition at room temperature applied by Kar et al. [179]. Anodized samples were initially pretreated with 1M NaOH solution for 10 minutes at 60°C and introduced into the electrolyte for CaP deposition. The electrolyte was basically a calcium phosphate solution (CaP_{sol}) obtained by mixing 2.20g of (CaCl₂,6H₂O) with 2.20g of (Na₃PO₄,12H₂O) in 1000 ml of deionized water. The pH solution was adjusted to 4.0 using HCl to avoid CaP precipitation.

For Sr doped CaP solutions (CaP.Sr_{sol}), three percentages of Sr were evaluated (10%, 20%, 30%) by adding respectively 0.27g, 0.54g or 0.81g of (SrCl₂, 6H₂O) to the previous CaP solution. This leads to CaP solutions with [Ca²⁺]= 0.01M, [PO₄³⁻]=0.006M and [Sr²⁺] = 0.001, 0.002 or 0.003M. Strontium chloride hexahydrate was purchased from Fluka. Calcium chloride dihydrate and trisodium phosphate dodecahydrate were purchased from Sigma-Aldrich.

A typical three-electrode electrochemical cell is used. A periodic pulse potential was carried out by scanning the potential between 0.0V and -2.0V forming potential pulses (PP) that was repeatedly set and started at -2.0V for 0.5s and immediately followed by 0.0V relaxation potential for 0.5s. The pulsing cycle is schematically illustrated in (Fig.3.24).

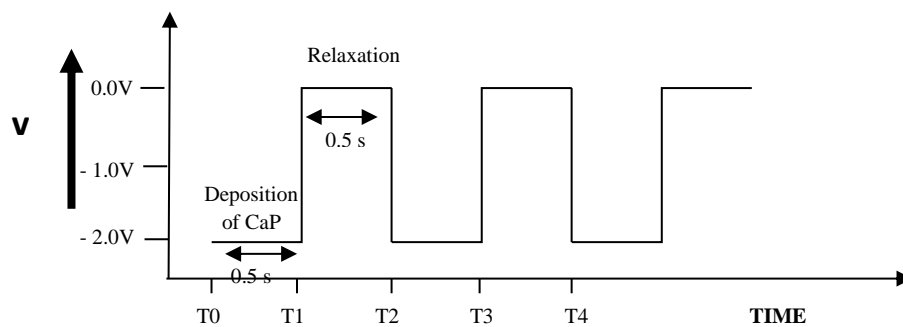
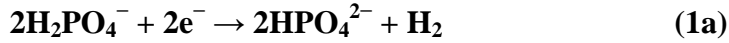


Fig.3.24. Current versus time illustration during the CaP coating (Potential Pulses)

When polarizing TiO₂ samples in cathodic direction, significant cathodic current is observed at -2.0V. This is because of the deprotonation or the reduction of acid phosphates to phosphate (reactions ((1a), (1b)) and reduction of protons or water (reactions ((2a), (2b)).



Reactions (1a) and (2a) could be achieved only in acidic pH solutions as in the present investigation with a pH~4.0.

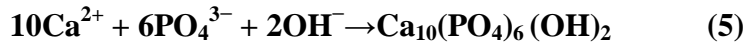
When a surface is polarized, different types of CaP depositions can be obtained depending on the pH near the surface. For example, Brushite type deposit is expected when HPO_4^{2-} specie is dominant near the interface due to the reaction:



During negative potential pulse, H_2O hydrolysis leads to hydroxyl creation near the surface increasing the CaP precipitation. Because when OH concentration increases, the acid phosphates are completely converted to phosphates by reaction (4):



From these reactions, it can be observed that formation of the enough quantity of hydroxyls ions is necessary for deposition of CaP according to the reaction (5):



The reaction (5) occurs when the OH^- ions are adsorbed on the cathode surface [180]. In the absence of the sufficient concentration of hydroxyl ions, octacalcium phosphate (OCP) or brushite precipitation could occur. The hydroxyl ions are available from the water reduction reaction (2b). [180]. When a high cathodic current density was pulsed, Ca^{2+} ions were attracted to the surface and presence of the hydroxyl and phosphate ions resulted in the electrodeposition of CaP according to the reaction (5).

The type of CaP deposited onto the surface should strongly depend on the pH of the solution as well as on the ions concentrations near the interface.

4.4. Experimental Results

4.4.1. Surface Characterization By Scanning Electron Microscopy SEM

(Fig.3.25) shows SEM images of the Ti nanostructured surface (nT-TiO₂) at different deposition time; (a) raw nT-TiO₂, (b) electrodeposited CaP after 500 potential pulses (PP), (c) after 1000 PP and (d) after 3000 PP.

As it can be seen on (a), (b) and (c), the deposits are growing on the outside edges of the TiO₂ nanotubes “Ring-like shape”, indicating that tubes edges are the most reactive sites of the nT-TiO₂ surface and that they act as an anchor of the coating and improve mechanical interlocking between the coating and the substrate.

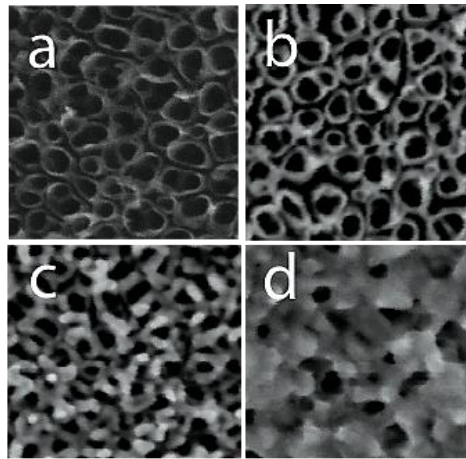


Fig.3.25. SEM images (5.0 KeV) of nT-TiO₂ surfaces taken before and after CaP pulsed electrodeposition. (a) Raw nT-TiO₂ surface (b) CaP deposition after 500 potential pulses (PP) (c) 1000 PP (d) 3000 PP

Going further in the deposition period, we got a high coverage ratio and the nucleation of the coatings became progressive so for high coverage ratios, CaP nano-particles anchored to tube edges get bigger and gathered to finally cover approximately the whole surface. (Fig 3.25.d)

As can be seen, the calcium phosphate coating obtained under these conditions is quite uniform. This effect is primarily due to the influence of periodic pulses on mass transport of hydroxyl ions that are generated as a result of the electrolysis. The period between pulses allows ions concentrations relaxations near the interface. From a crystal growth point of view, nanotubes edges are very reactive area as compared to tube walls and they are considered as preferred areas for adsorption process and act as

steps on a plane surface. Actually, for better biological results, it would be preferable not to cover the surface totally with coatings, because having porous voids between the coatings allows the mechanical interlocking between the TiO₂ nanotubes and the living bone because of the larger surface area and the irregular surface, thus we can gain the both mechanical and biochemical integration and binding between the functionalized TiO₂ implant surface and the surrounding bone. In addition, by comparing constant potential and pulsed potential conditions, we have found that incorporation of a pulsed potential as in Shirkhazadeh [183] provides coatings with superior uniformity, topology, and adhesion.

4.4.2. Surface Characterization By Infrared Spectroscopy IRRAS

CaP deposit growth has also been investigated by IRRAS allowing a chemical characterization of the CaP clusters according to their size.

In our experiment, the infrared spectra (Fig.3.26) are dominated by the broad absorption band located near 1000 cm⁻¹ which is characteristic of phosphate vibration. We observed that the band shape evolves with the coverage ratio, i.e. with the anchored CaP nano-particles size intensity. Actually, this band is mainly composed of two peaks (1030 cm⁻¹ and 1100 cm⁻¹) with the higher wave-number peak at 1100 cm⁻¹ that becomes dominant for high CaP coverage ratio with also a weak shoulder in the 800-900 cm⁻¹ range. These bands are assigned to ν_1 and ν_3 modes of phosphate entity.

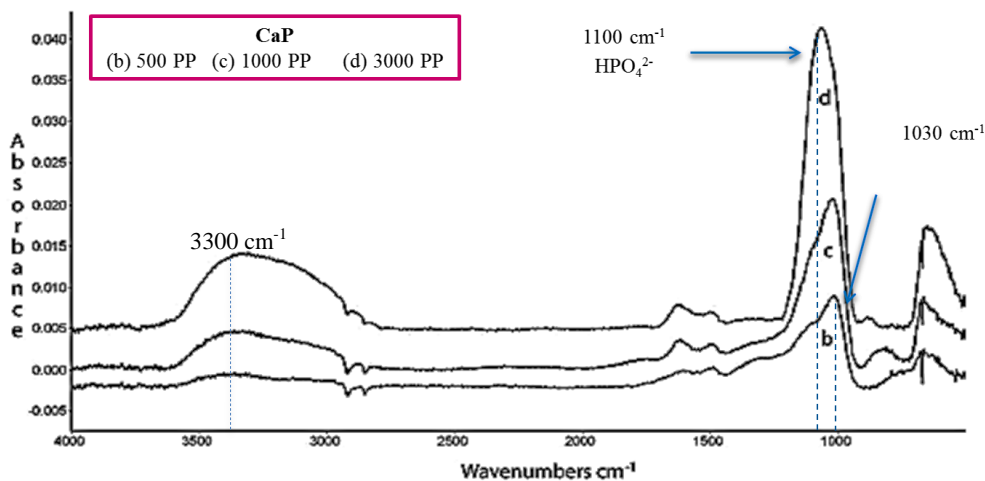


Fig.3.26. IRRAS spectra of nT-TiO₂ surfaces after CaP pulsed electrodeposition. (b) 500 potential pulses (PP) (c) 1000 PP (d) 3000 PP. Both phosphate and OH vibration bands are visible at respectively 1100 and 3300 cm⁻¹

As these two bands are located at higher wave-number comparing to free HPO_4^{2-} , we suppose a bidentate coordination as for PO_4^{3-} [184].

As the CaP clusters size increase, the 1100 cm^{-1} completely dominates the IR spectra.

This band can be attributed to HPO_4^{2-} in poorly crystallized CaP compound [184].

The IRRAS spectra (Fig.3.26) also reveal a broad absorption band located by 3300 cm^{-1} that is correlated with stretching mode hydrogen bonds (OH or H_2O).

Low intensity peaks by 1500 cm^{-1} were observed which could be attributed to carbonates.

The obtained spectra, and the symmetric and asymmetric vibrations at $1030\text{--}1100$ and 900 cm^{-1} confirmed the amorphous apatitic nature of the CaP films formed on the substrates for different coverage ratios.

Actually, it's important to mention here that Ca^{2+} ions lead to an increased amount of adsorbed phosphate. This additional adsorbed phosphate would come from the formation of surface complex consisting in a bidentate phosphate bound to amorphous TiO_2 , with Ca^{2+} binding to the already adsorbed phosphate.

However, (Fig.3.27) reveals that IRRAS spectra are completely different for Sr doped CaP coating. For all spectra (Fig.3.27, a, b, c and d), at least four bands are clearly visible in the phosphate vibration modes region: $885, 1120, 1180, 1243\text{ cm}^{-1}$.

The spectrum includes, also, peaks at 1550 cm^{-1} due to CO_3^{2-} ions, which probably came from contamination by atmospheric carbon dioxide during the preparation and washing.

According to Casciani et al, [185] these phosphate bands can be attributed to CaHPO_4 . The band located at 1243 cm^{-1} is associated with the ν_5 P- OH local in plane bending mode of HPO_4^{2-} group in CaHPO_4 compound [186], the peaks at $885\text{ cm}^{-1}, 1120, 1195\text{ cm}^{-1}$ are characteristic of delocalized mode of CaHPO_4 compound. [187, 188]

Compared to Casciani infrared spectra [185], the absorption bands of (Fig.3.27) are much larger, probably due to a less disordered compound in the case of the electrodeposited coating.

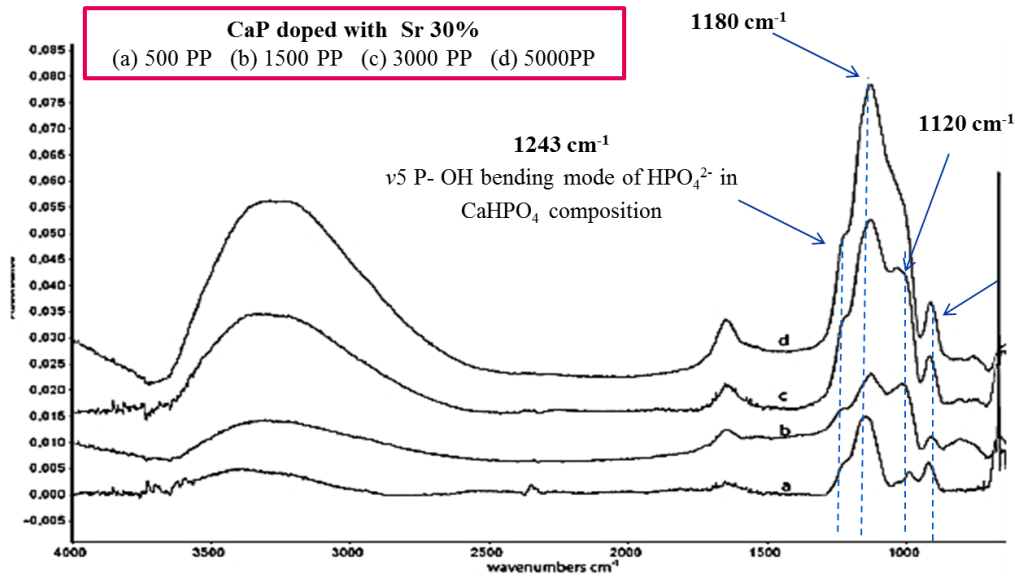


Fig.3.27. IRRAS spectra of 30% Sr doped CaP coating for 500PP, 1500PP, 3000PP and 5000PP (a, b, c and d respectively). While the broad band characteristic of bounded OH is still evident (OH stretching), the phosphate band presents a different structure when Sr^{2+} is substituted to Ca^{2+} .

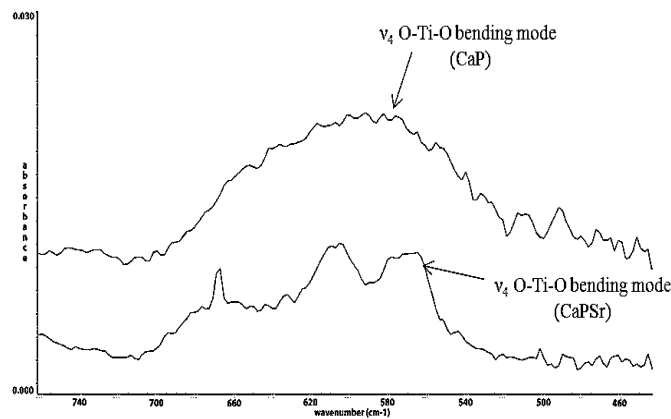


Fig.3.28. IRRAS peaks corresponding to ν_4 O-Ti-O bending mode for CaP and CaPSr

In our study we didn't use XRD (X-Ray Diffractometer) to characterize the deposits because the coating layer is very thin and the deposits quantity is very small thus XRD won't be sensitive to characterize such coated surfaces. But Faralay et al. [182] reported a significant correlation between the crystallinity index measured by IRRAS (The width of the peak 604 cm^{-1} which corresponds to ν_4 O-Ti-O bending mode in phosphate) and the crystallinity measured by X-ray diffraction. Thus, we can observe in (Fig.3.28) a wide large peak in non-doped CaP deposits indicating an amorphous composition while in the case of Sr doped CaP deposits we can observe two thin peaks indicating a crystalline composition and they are characteristics to brushite compositions.

3.4.2. Surface Characterization By X-Ray Photoelectron Spectroscopy

To get more information about the chemical composition of the coatings and to obtain the elemental ratios in the surface, samples were characterized by XPS spectroscopy. Concerning XPS experiments, all spectra show a positive energy shift of 1.7eV referenced to the C_{1s} peak at 285.0eV and the energy scale has not been corrected. (Fig.3.29) presents XPS spectra of 500 PP (a) and 3000 PP (b) CaP deposited onto nT-TiO₂. On these spectra, we observe that the substrate Ti signal ($2p_{3/2}$ core level) is lower in (Fig.3.29 (b)), meaning that it is covered by the adsorbed compound. Ca_{2p} , P_{2p} and O_{1s} core level signals at Ca_{2p} (348.2eV), P_{2p} (134.2eV), O_{1s} (532.2eV) confirm SEM and IR spectroscopy observations, i.e. a calcium phosphate compound has grown on top of the nT-TiO₂ surface.

XPS survey spectra also reveal the presence of carbon contamination C_{1s} (286.7eV) and a small component at (290.6eV) due to carbonate. As Ar sputtering (not shown) strongly reduces the C_{1s} peak, we conclude that the carbon contamination is mainly localized at the ultimate surface of the coating.

The chloride ions Cl_{2p} (199.5eV) peak was assigned to the adsorption of Cl^- ions at the outermost surface [190]. These adsorbed Cl^- may facilitate the electrostatic adsorption of Ca^{2+} and thus trigger the heterogeneous precipitation of a CaP phase by enhancing the negative charge of the surface. [189]

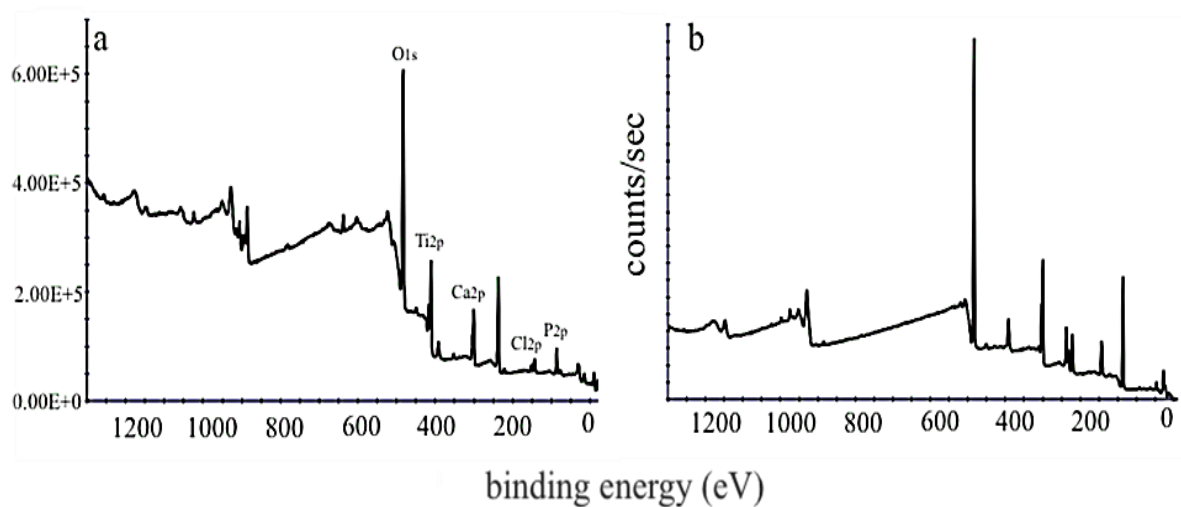


Fig.3.29. XPS spectra of nT-TiO₂ surfaces after pulsed electrodeposition (PP) of CaP (a) 500 potential pulses (PP) and (b) 3000 PP

To get further inside the coatings chemistry, higher resolution core level spectra (0.05eV steps) have been investigated, and especially for the $P_{2p} + Sr_{3d}$, O_{1s} , and Ca_{2p} core levels. Results are presented in (Fig.3.30) and (Fig.3.31).

In (Fig.3.30), the O_{1s} peak clearly presents a broad structure that can be deconvoluted into basic Gaussian components characterized by FWHM (Full Width at Half Maximum) of 2.1eV. In the case of pure CaP coating, 5 peaks are present to realize the O_{1s} deconvolution, while for mixed Sr-CaP coatings, the O_{1s} structure is thinner, and only 3 peaks are needed. In each case, the higher binding energy component, located at around 534.2eV, is attributed to H_2O species [191]. This is coherent with a highly hydrated compound. The two peaks near 532.2eV and 533.0eV can be assigned to O of P-O and O of P-OH respectively. For these two components an area ratio of 3 is obtained by the deconvolution process, thus we can conclude a mono-protonated $(HO-PO_3)^{2-}$ entity. In the case of the pure CaP coating, we can assign the peaks at 530.8eV and 529.0eV to hydroxyls [191,192,193] or O-Ca bounds that are not present when Sr ions are incorporated into the film.

The Sr_{3d} overlaps with P_{2p} core level giving a broader structure by 134.0eV (Fig.3.30). Nevertheless, these two peaks structure can be easily deconvoluted with a peak located at 134.2eV (P_{2p}) and a broader peak (FWHM = 3.2eV) located at 136.4eV (Sr_{3d}).

Concerning the Ca_{2p} core level, the two peaks structure ($2p_{3/2}$ at 348.2eV and $2p_{1/2}$ at 351.8eV) is shown in (Fig.3.31). As for the O_{1s} level, the Ca_{2p} doublet clearly presents a broadening with new components that reveals additional chemical bonds in the case of pure CaP coating (Fig.3.29.a) that are not present when Sr is added into the film.

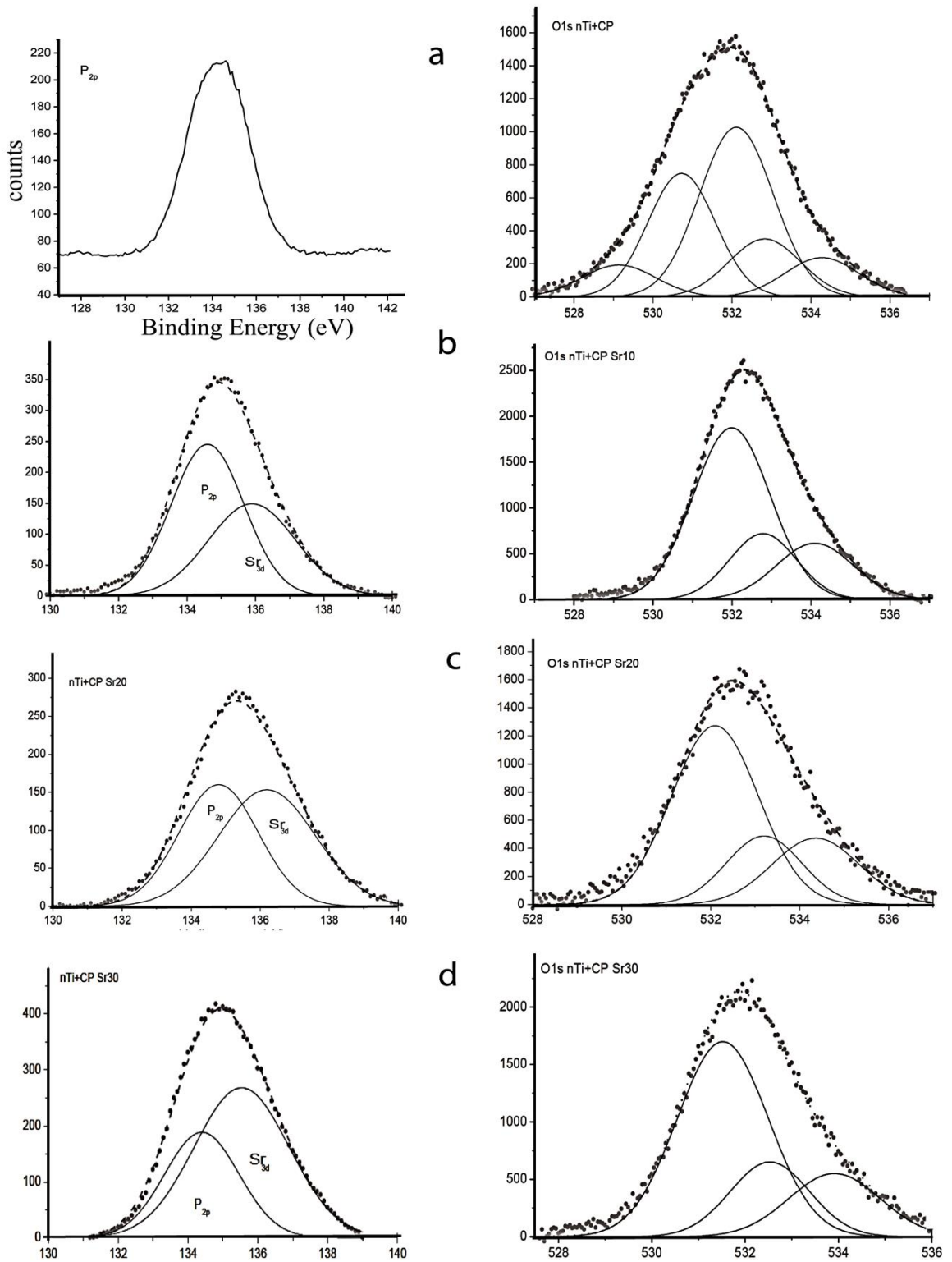


Fig.3.30. P_{2p} and O_{1s} XPS spectra of nT-TiO₂ surfaces coated with CaPSr_x for 3000 PP with respectively Sr_{3d}: 0% Sr (a), 10% Sr (b) , 20% Sr (c) and 30% Sr (d)

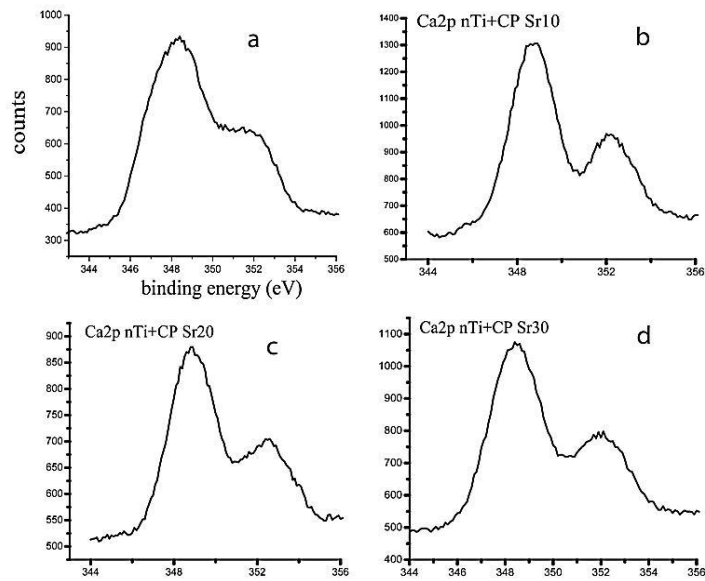


Fig.3.31. Ca_{2p} XPS spectra of nT-TiO₂ surfaces coated with CaPSr_x for 3000 PP with respectively: 0% Sr (a), 10% Sr (b), 20% Sr (c) and 30% Sr (d) (% Sr atomic percentage referred to Ca). One can notice the larger width of the Ca_{2p} levels for pure CaP coating.

Peaks area are corrected by sensitivity factor [194] given in (Table 3.3), where we can tentatively interpret semi-quantitatively our results and we obtained the following surface concentrations ratios that are presented in (Table 3.4).

XPS line	O _{1s}	Ca _{2p}	P _{2p}	Sr _{3d}	Sr _{3p}
S factor	0.66	1.05	0.36	1.48	0.92

Table.3.3. Sensitivity factor table from UKSAF [194]

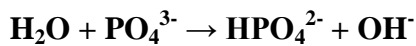
	[O]/[P]	[O]/[Ca]	[Sr]/[Ca]	[Sr]/[Ca]+[Sr]	[O _{H2O}]/ [O _{tot}]	[O-P]/[HO-P]
CaP pure	5.40	4.25	0.00	0.00	0.16	2.95
CaP Sr10%	5.90	6.00	0.18	0.15	0.21	3.10
CaP Sr20%	6.15	5.90	0.31	0.23	0.22	2.85
CaP Sr30%	6.20	6.15	0.46	0.32	0.23	2.90

Table.3.4. Element concentrations deduced from peaks area corrected with sensitivity factors.

From (Table.3.4), we can conclude that the Sr/Ca ratio in the deposited film agrees with the solution concentrations, this fact was difficult to be noticed as many chemical or physical factors can enhance one element deposition in the electro-deposition

process. Getting further inside XPS quantification and compound chemistry identification, we can deduce from (Table.3.4) that for pure CaP, calcium to phosphorus ratio is around $[Ca]/[P]=1.30$. As mentioned previously in the present thesis, many different amorphous calcium phosphates (ACPs) can exist and are mainly distinguishable by their $[Ca]/[P]$. In alkaline conditions, hydrated amorphous tricalcium phosphate (α -TCP, $[Ca]/[P] \approx 1.5$) is most widely found by precipitation in aqueous solutions [196]. When the pH becomes more acidic, ACPs may contain HPO_4^{2-} ions giving a compound characterized by lower $[Ca]/[P]$ value which remains >1.0 . Crystalline CaP phases like OCP and calcium-deficient apatite have been observed [197].

Moreover, ACP composition can change with ageing as proposed by Heughebaert et al [198] and internal hydrolysis between PO_4^{3-} and H_2O can occur in ACP gels, leading to HPO_4^{2-} and OH^- ions formation [198]. This type of reaction can exist during our pulsed electrodeposition process. This technique is based on water electrolysis, which induces a local increase in pH at the cathode where the metal substrate to be coated is placed. When the electrolysis bath contains a metastable calcium and phosphate solution this pH rise increases the concentration of PO_4^{3-} . Under these conditions homogeneous precipitation can occur at the cathode. It's also suggested that during the cathodic pulse (-2.0V), water reduction produce a high hydroxyl concentration near the n-TiO₂ electrode surface in an acidified solution that contains $H_2PO_4^-$ and HPO_4^{2-} entities, leading to a complex precipitation with HPO_4^{2-} and OH^- ions. (Fig.3.32):



In the case of an amorphous disordered compound (α -ACP) elaborated in alkaline medium, with calcium deficiency, a range of composition of α -ACP can be represented by the following formulae : $Ca_{9-y}(PO_4)_{6-x}(HPO_4)_x(OH)_{x-2}$. From the ratio $[Ca]/[P] \approx 1.30$ found by XPS, we can expect a compound like $Ca_4(HPO_4)_3(OH)_2$, $Ca_4PO_4(HPO_4)_2(OH)$ or $Ca_4(PO_4)_2(HPO_4)(OH)$ [195]. From O_{1s} and P_{2p} deconvolution, we can expect the rich OH compound $Ca_4(HPO_4)_3(OH)_2$.

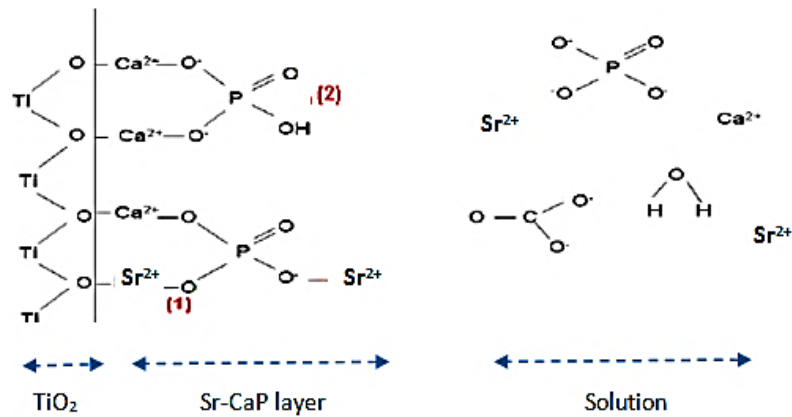


Fig.3.32. Proposed mechanism of CaP nucleation in the presence of Sr^{2+} at TiO_2 substrate (1) Sr^{2+} substitutes Ca^{2+} in the lattice structure or absorbs directly on the surface (2) Protonated PO_4^{3-} ions after adsorption at calcium sites.

The situation of the Sr doped CaP deposition is rather different and the $[\text{Ca}]/[\text{P}]$ ratio is by 1.0, so we must have a compound like $\text{Ca}_x\text{Sr}_{(1-x)}\text{HPO}_4$ in accordance with the O_{1s} and P_{2p} deconvolution.

The difference of compound chemistry and structure between pure and Sr doped CaP coating is not surprising as foreign ions like Sr^{2+} ions can strongly affect CaP compounds structure and stability. In fact X^{2+} cations like Sr^{2+} , Zn^{2+} or Mg^{2+} are known to favor the less compact calcium phosphate structure (TCP, lamellar DHCP) compared to the more complex HaP phase [199,200]. For example, the Sr^{2+} ionic radii is about 12% higher than the Ca^{2+} one, which gives greater steric constraint adaptability in less compact structures.

It can be noticed too that $[\text{O}]/[\text{P}]$ ratio or $[\text{O}]/[\text{Ca}]$ are greater than 4.0 meaning that the coatings are hydrated (H_2O in the formula). From the O_{1s} deconvolution, we observe $[\text{O}_{\text{H}_2\text{O}}]/[\text{O}] \approx 0.20$ which means that 20% of the oxygen signal is coming from H_2O for almost all compounds studied in this work.

This difference of chemical structure induced by Sr is also attested by a chemical shift on the O_{1s} and P_{2p} core levels when strontium is incorporated in the deposit. For low $[\text{Ca}]/[\text{P}]$ calcium to phosphorus ratio like in DCPD, Chusuei observed an increase of 0.5eV for O_{1s} and P_{2p} binding energy between ACP and DCPD, while the Ca_{2p} peak is located at the same binding energy [201]. When we refer binding energies to the Ca_{2p} level (avoiding change in work function between samples), we find that O_{1s} and P_{2p}

binding energy are respectively shifted of +0.4eV and +0.5eV for the strontium doped deposit.

From IRRAS and XPS spectra we can conclude that the incorporation of Sr into the CaP favors a CaP compound similar to DCPD ($\text{CaHPO}_4 \cdot 2\text{H}_2\text{O}$) or DCPA (CaHPO_4) (Dicalcium phosphate dehydrate/ Dicalcium phosphate anhydrous), meanwhile the pure CaP coating looks like an amorphous apatite-like compound (ACP).

Actually, for pure CaP coatings, ACP is found in several composite materials used in odontology as a remineralising phase for enamel and dentine and in toothpaste formulations as a remineralising agent for early carious lesions. It was also reported that ACP showed better osteoconductivity *in vivo* than apatite and its biodegradability was higher than that of tricalcium phosphate ($\text{Ca}_3(\text{PO}_4)_2$) [201].

For Sr doped CaP coatings, the substitution of Ca^{2+} by Sr^{2+} ions in the apatite lattice is a very important heteroionic substitution since it is known to interfere with the calcification mechanism [202]. Furthermore, Dorozhkin [203] investigated the incorporation of Sr in the α -TCP crystal structure reporting increased lattice parameters of the Sr-doped CaP in comparison to the Sr-free CaP. The lattice strains due to Sr substitution favored the milling process and made the coating more reactive. Comparing to other (CaP) phases which exist in human bone, DCPD and DCPA cements have a higher solubility than hydroxyapatite (HAP) at physiological pH, with a good resorption rate *in vivo*. [204]. Also, such cements have good performance *in vivo*, where the cement resorption is soon followed by new bone formation. Histological measurements indicated good biocompatibility of these compounds, with almost complete absence of inflammatory cells [205].

DCPD particles are found in the non-collagenous organic matter around non-mineralized collagen fibers, and it is believed that these particles serve as the reservoir of calcium and phosphate ions for subsequent mineralization. [206, 207] Furthermore, Villareal et al. [208], reported that higher alkaline phosphatase (ALP) activity was remarked with DCPD compositions compared to HAP, which can be reflected in positive effect on the osteoblastic population and bone apposition.

Summary

In this chapter, vertically aligned nanotube arrays of titanium oxide on the surface of titanium substrate have been prepared by anodization, then we have evaluated phosphate adsorption onto nanostructured and NaOH pretreated TiO₂ surfaces observing stronger bonds between phosphorous molecules and nanostructured surfaces when pretreated with NaOH.

CaP coating is deposited on anodized titanium by pulsed electrodeposition in an electrolyte containing calcium and phosphate ions. The surface morphology of TiO₂ nanotube promotes mechanical interlocking between CaP and TiO₂ where deposits are anchored around and between the tubes. The deposition method helps in the improvement of bonding strength as well.

Moreover, we noticed that the initial adsorption is around nanotubes edges, which confirms that titanium surface nanostructuration allows the creation of new surface sites with specific reactivity and are considered as preferential adsorption site for CaP and located on the nanotubes edges as revealed by SEM.

Chemical composition of the adsorbed thin films has been observed by XPS and IR spectroscopies. Both IR and XPS spectra have clearly shown that the addition of Sr into the CaP layer favor Ca_{1-x}Sr_xHPO₄ compound similar to DCPA or DCPD, while the pure CaP coating looks like an amorphous apatite-like compound (α -ACP). Thus, applying pulsed electrodeposition enabled us to obtain a powerful chemical functionalization of nanostructured titanium surface with bioactive compound that is anchored on the nanotube edges which are considered as the most reactive nucleation sites on the (nT-TiO₂) surface. The addition of strontium has the double advantage of supporting the mechanisms of cell multiplication and of giving an inorganic phase more easily bio-resorbable than HAP.

Such depositions could be considered as controlled bioactive coatings on (nT-TiO₂) that have positive effects when used for new implant design.

CHAPTER IV

Protein adsorption onto functionalized TiO₂ surfaces

1. Protein adsorption onto implant surface (biological effect)

Protein reactions are the first phenomena that occur when a foreign material is inserted into living body and is believed to be a major factor in controlling later cellular adhesion.

Following implantation, implant surface gets in contact with the blood coming from the injured vessels in the implant bed [23] and the biomolecules reach the surface in milliseconds. Proteins adsorb first onto the surface, then change their conformation, denaturize and desorb from surface leaving their place to other proteins that have more affinity to the surface. The main role of this protein layer is the attachment of functional cells in the healing process and osseointegration. Many proteins such as fibronectin, vitronectin, laminin, serum albumin and collagen facilitate the attachment of osteogenic cells on titanium surfaces. [209]

Proteins are made up of different sequences of amino acids which exhibit different characteristics such as being polar, non-polar, positively or negatively charged which is determined by having different side chains. Thus, attachment of molecules with different protein for example, those containing Arginine-Glycine-Aspartate (RGD) sequences are expected to improve cell adhesion when placed into its physiological environment [210]. The sensitivity of cellular interactions to interfacial proteins probably is due to the presence of cell surface receptors for specific proteins and those receptors interactions are enhanced by the concentration of proteins at interfaces.

However, it was reported that protein adsorption is sensitive to specific physicochemical properties of the implant surface [23, 210]. Therefore, protein binding capacity with implant surface is considered to be so important for successful osseointegration, since surface properties influence the protein adsorption. In this respect, implants surface modification by protein adsorption is used to enhance their

biocompatibility and thus their design as a bioactive material. Surface chemistry and topography can then be controlled to allow the adsorption of specific proteins which are required for cell colonization when the implant is placed in physiological environment. (Fig.4.1)

Recently, many investigations [211, 212, 213] have focused on understanding the effect of implant surface characteristics on the protein dependent mechanisms of cellular activities and bone matrix deposition, to develop novel implant surfaces.

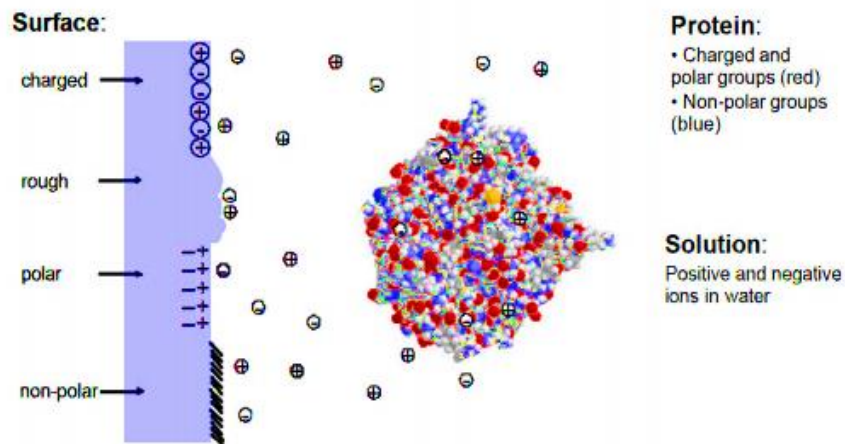


Fig.4.1 Schematic view of protein interactions with characterized surface

It was reported that only topographical features with dimensions similar to those of surface-bound proteins (nanometric scale) can significantly affect their morphology and activity [211]. For this reason, recent studies have focused on the influence of nanometric surface features on the adsorption of proteins. The creation of nanoporous structure results in a greater surface area which provides more binding sites and controlled nanoscaled topography [209, 211].

For titanium dental implants, surface spontaneously adsorbs great amounts of various proteins from body fluids in an unspecific manner, resulting in complex interactions with different types of cells and platelets. Such unspecific events may also present foreign body responses causing an acute inflammation which can develop to chronic one if macrophages fail to destroy the pathogens that merge to form a foreign-body giant cell which quarantines the implant.

By coating an implant with extracellular matrix proteins ECM, macrophages will be unable to recognize the implant as non-biologic. The implant is then capable to

continued interaction with the host, and thus, influencing the surrounding tissue. For instance, the implant may improve healing by secreting specific drugs such as growth factor. [212]

More recently, researchers have focused on the application of biomimetic CaP coating as a protein carrier system. Although CaP has been used for protein delivery in the past, most of the therapeutic agents are simply adsorbed onto CaP surfaces and then dissociate from CaP in a “burst release” fashion [213]. In comparison, when proteins are co-deposited with CaP crystals in the biomimetic coating process, a sustained protein release is resulted as the coating slowly degrades in vivo [214,215].

Other studies used BSA (Bovine Serum Albumin) as a model protein to analyse the protein uptake onto the ceramics and the release of the protein from the carrier material [216]. BSA was also used because it has a similar size of growth factors.

It was reported that [216, 217] albumin is released by osteoblast cells exist in healing sites and this raise in albumin increases the proliferation of surrounding cells indicating that surface modification with BSA led to significant improvement in osteoblast-like cells binding to an electrodeposited CaP coating. Similar observations, but for MC3T3-E1 cells, were reported by Wen et al [218] who have found that adsorption of BSA to the surface of conventional and nanophase ceramic (including hydroxyapatite) influences the activity of bone cells because BSA may have a specific binding interaction with hydroxyapatite which result in an improvement in the osteoblast cells bioactivity. Thus, it might be possible to develop better CaP coated biomaterials through an incorporation of BSA into porous mineral matrix to improve cell adhesion and proliferation [218, 219].

Due to the complex reactions of growth factors during bone healing, the quantitative and temporal framework of their delivery is very important for successful osseointegration. However, it was reported that the immobilization of growth factors with calcium phosphate ceramics has mostly been accomplished by adsorption of proteins onto the surface of the materials. [220].

Moreover, Wen et al [218] reported that the presence of the adsorbed protein layer should mediate the formation of apatite layers and enhance the cellular response to the material.

Data reported [217, 218] that BSA may have a specific binding interaction with calcium phosphate compounds which could improve the bioactivity of osteoblast cells.

Though many researches focused on the studying of physicochemical features effects of the CaP coating as carrier system of proteins, the role of dopants such as cations (Sr^{2+} , Zn^{2+}) in modifying protein adsorption onto functionalized TiO_2 surfaces for dental implants has rarely been studied.

As indicated in the previous chapter of this thesis, addition of strontium as a dopant changes the composition of CaP coatings. Incorporation of strontium in CaP lattice results in DCPA like cement instead of apatitic one. Due to the fact that DCPA cements are much more bioresorbables than apatitic ones, they can offer good opportunities to use them as a carrier for controlled release of drug and biomolecules.

In this part of work, we will investigate the influence of TiO_2 surface chemistry previously studied on the adsorption of a model protein which is found in high concentrations in the blood medium, the albumin.

In this work we used BSA (Bovine Serum Albumin) at a relatively low concentration (0.1 g.L^{-1}) compared to blood concentration (50.0 g.L^{-1}). We used XPS and Infrared spectroscopy to characterize the surface interaction after immersion in an aqueous solution for a given period of time.

At each step, the sample is rinsed in deionized water and analyzed by IRRAS, allowing us to evaluate the amount of protein absorbed as a function of immersion time. For each point, the shape of the infrared spectrum gives us a clue of the evolution of the secondary and tertiary structure of the protein.

As the pH of the physiological environment of the implant vicinity can vary (especially when the inflammatory process starts with a very acidic pH), we decided to look at the influence of this parameter on the adsorption process. Actually, the pH of the solution is a critical parameter since it will affect the charge distribution of the protein and the surface.

The pH is particularly important because the secondary and tertiary structures of the protein are strongly pH dependent, as we will see in the next paragraph. We have

chosen three pH values; acidic pH of 4.5, neutral pH of 7.0 and a basic pH of 10.0, as the N earth shape form of BSA cover this large pH range.

Proteins are linear biological polymers for which the monomeric units are amino acids. (Fig.4.2). Twenty different amino acids are used to make proteins, each distinguished by the identity of the “R” group. The amino acids are linked to form a polymer by linking the amino group of one amino acid with the carboxylic acid group of another amino acid to form a peptide bond. (Fig4.2) [221]

A polypeptide consists of a backbone and sidechains. The backbone comprises the amide nitrogen, the alpha carbon and the carbonyl carbon that are participated by each amino acid unit whereas sidechains comprise the “R” groups.

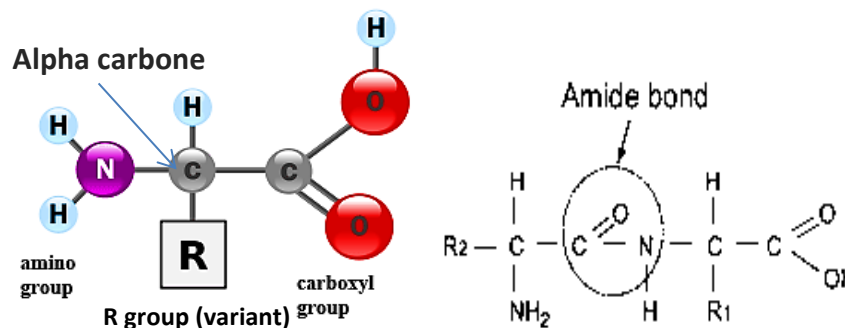


Fig.4.2 The structure of amino acid; the basic building block of proteins (left), the amide bond (right)

Proteins are distinguished from each other by the number of their amino acids units and by the identity and sequential order of the amino acids. The numbers vary from 50 to hundreds of amino acid units.

Few polypeptides are considered proteins. For a polypeptide to be considered a protein it must be able to fold into a well-defined 3-dimensional structure. This is usually a requirement for protein function. [221]

When a protein folds to form a well-defined 3-dimensional structure it exhibits three levels of structure: primary, secondary and tertiary.

Primary structure refers to the linear sequence of amino acids which is genetically determined and often modelled as beads on a string, where each bead represents one amino acid unit. (Fig.4.3)

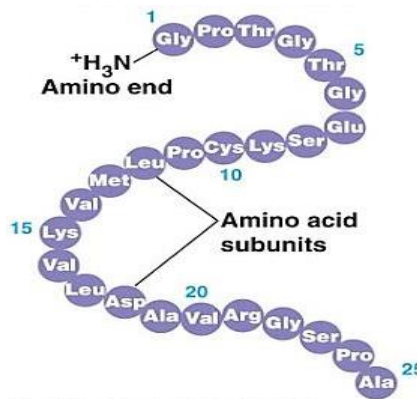


Fig.4.3. Protein primary structure

Secondary structure is "local" ordered structure created via hydrogen bonding within the peptide backbone. The types of secondary structure include **α -helices** and **β -sheets**, which allow the amides to hydrogen bond very efficiently. Both are periodic structures. [222]

In α -helix, the polypeptide backbone is wrapped up in a right-handed helix where the hydrogen bonding occurs between successive turns of the helix. In β -sheets, the strands of polypeptide are stretched out and lay either parallel or antiparallel to one another. The hydrogen bonds form between the strands. (Fig.4.4) [221]

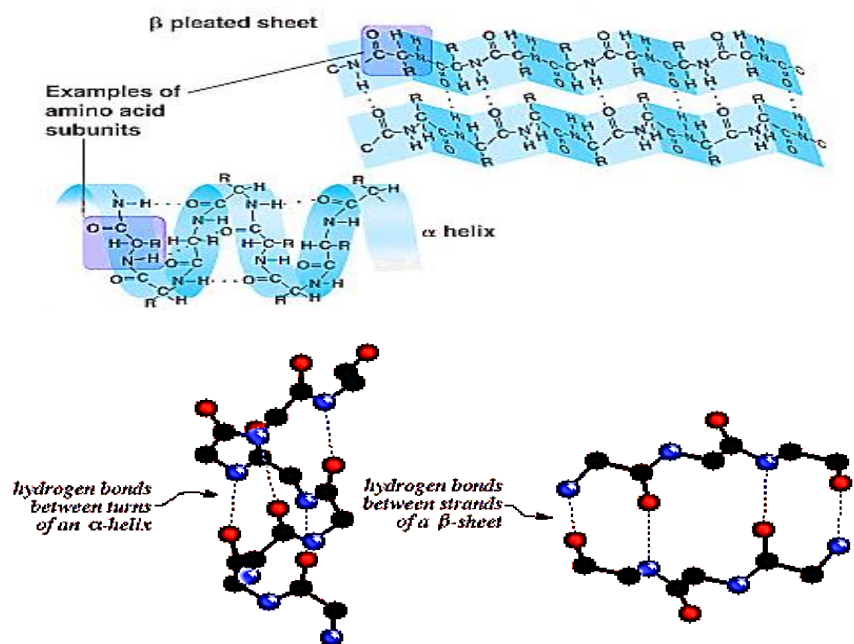


Fig.4.4 Secondary structure of proteins

The other elements of secondary structure include **β -turns** and **unordered** structure. β -turns are sharp turns that connect the adjacent strands in an antiparallel β -sheet. Unordered structure is generally a catch-all for regions that do not fall into one of the other categories. These are loops which form near the surface of proteins and join the other elements of secondary structure. [222]

Tertiary structure is the "global" folding of a single polypeptide chain. The most important factor in determining the tertiary structure of globular proteins is the hydrophobic effect. Hydrogen bonding involving groups from both the peptide backbone and the side chains are important in stabilizing tertiary structure [222]. Tertiary structure arises when various elements of secondary structure pack tightly together to form the well-defined 3dimensional structure. However, the shape is maintained permanently by the intra- molecular bonds; hydrogen bond of one hydrogen atom shared by two other atoms, Van der Waals force is the weak force that incurs when two or more atoms are very close, disulphide bond which is a strong covalent bond formed between two adjacent cysteine amino acids that stabilizes the tertiary shape of a protein, and ionic bond as electrostatic interaction between oppositely charged ions (Fig.4.5)

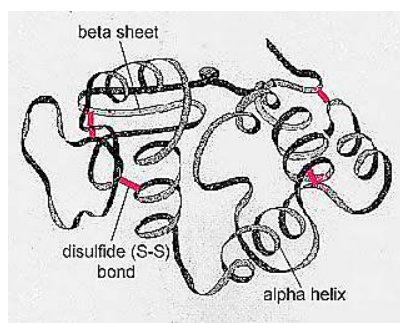


Fig.4.5 Tertiary structure

Finally, there's another protein structure which is **quaternary structure** that arises when a number of tertiary polypeptides joined together forming a complex, bio-active molecule.

Bovine serum albumin

Bovine serum albumin (BSA) is a globular, heart-shaped (at physiological pH) extracellular protein representing the main component of the blood transport system with a typical concentration of 50 g/l and providing the transport of a range of physiologically compounds like calcium. BSA is pretty much used for protein adsorption studies since its structure is close to the human serum albumin (HSA) structure [223].

The molecular weight of BSA is 66kDa with an isoelectric point of 4.7 [224]. BSA is built from 583 to 607 amino acids such as aspartic and glutamic acids, lysine, and arginine. It is also characterized with high content of cysteine. (Table 4.1) shows the amino acid composition of BSA.

BSA consists of 55-67% α -helices, 21% β -sheet, and the rest are turns. The secondary and tertiary structures of BSA depend on pH where a pH~4.3–8 keeps a triangular or heart shaped structure of BSA molecule with around 60% α - helix structure and the rest β -sheet and turns.

Amino Acids	Number of residues	
Aspartic acid	41	41
Arginine	23	26
Asparagine	13	14
Glutamic acid	59	58
Glutamine	20	21
Histidine	17	16
Lysine	59	60
Serine	28	32
Threonine	34	34
Alanine	46	48
Isoleucine	14	15
Leucine	61	65
Methionine*	04	05
Phenylalanine	27	30
Tryptophan	02	03
Tyrosine	19	21
Valine	36	38
Cysteine*	35	35
Glycine	16	17
Proline	28	28
Total	582	607

Table 4.1 Amino acid composition of BSA [225]

At pH less than 4.3, the BSA molecule unfolds into a form with 45% α -helix and further unfolding to an expanded form is observed with the decreasing of pH value. In the basic solutions with pH more than 8, the BSA molecule forms of \sim 47% α -helix. [224]

Actually, many physicochemical characteristics of substrates and media should be taken in consideration as they affect BSA-binding capacity, for example, chemical composition (ions in solution), pH of the solution, surface topography, surface hydrophobicity, surface roughness, and surface charge/potential.

The pH of the solution is an important factor that affects the electrostatic interactions during the adsorption processes. Some studies showed that a decrease in pH led to an increase in the acidic protein form adsorption and binding affinity [226]. Depending on the pH of the solution, proteins become charged which affects their binding with surface reactive sites. In this respect, it is important to mention that in the presence of calcium and phosphate ions, the adsorption BSA onto bare titanium surface is a function of protein concentration and pH level, which suggests possible conformational changes of the protein molecule [227]. (Fig.4.6)

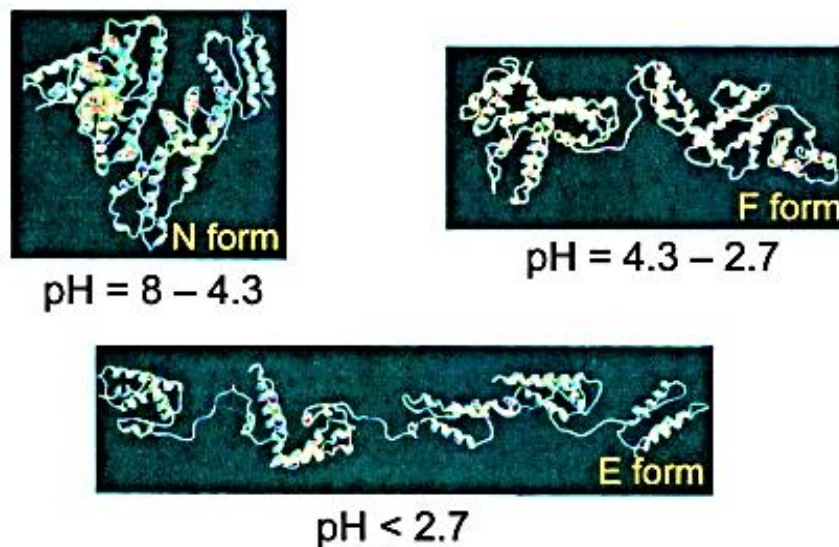


Fig.4.6 Different conformations of BSA as a function of pH (N form = Native, F form = Fast, E form = Expanded)

Surface charge has a great influence on the protein adsorption mechanism and kinetics as well. Ahmed et al, [228] studied the influence of surface potential on the kinetics of

BSA adsorption on a biomedical-grade 316LVM stainless steel surface, and indicated that when surface potential becomes more negative, both the BSA initial adsorption rate and the surface concentration saturation increased.

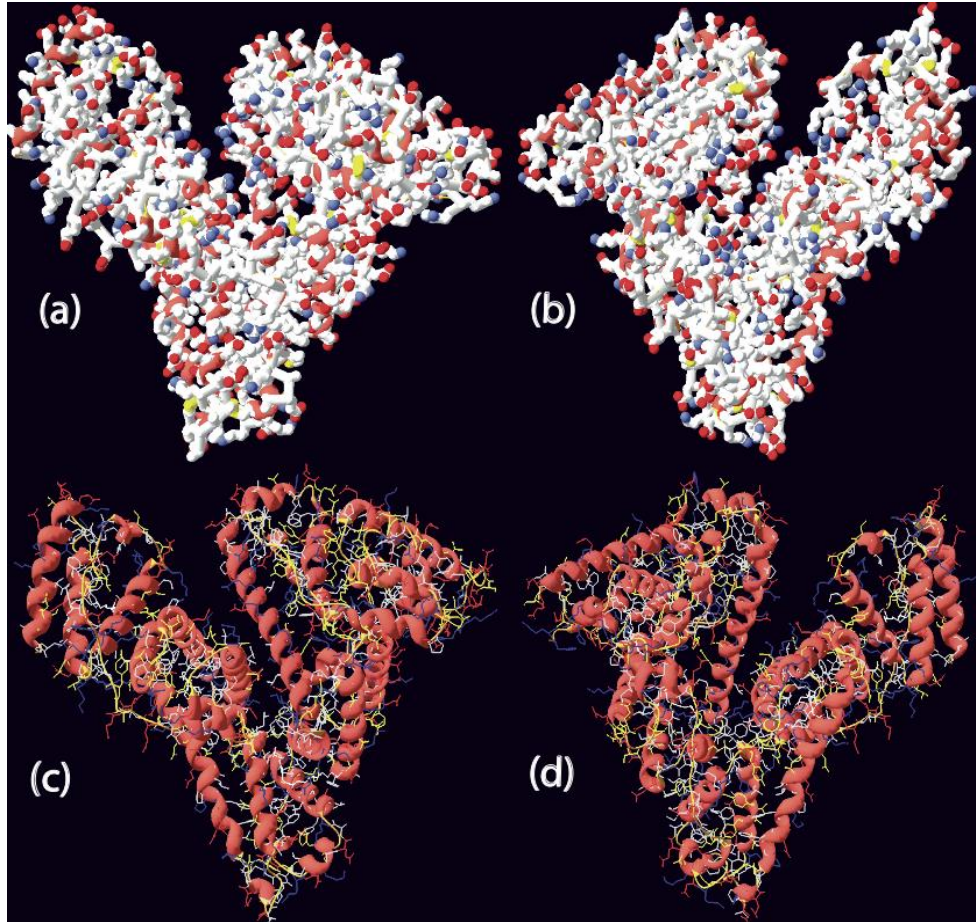


Fig.4.7 N form of the globular structure of BSA. Figures (a) and (b) shows a diagram of "ball & sticks" type with negatively ionized groups (COOH) in red and positively ionized groups (R-NH₂, for example) in blue. (a) and (b) show a front and back view of the form N. (c) and (d) show a representation of the secondary structures with α -helices and side chains (acidic =red, basic=blue). We notice the relatively homogeneous distribution of potentially positive and negative charges on the molecular surface. Representations obtained with Swiss pdb viewer 4.01.

In our work, we chose to work with the globular form (which is N-form) over a wide pH range from 4.3 to 10. In this domain, we can estimate the overall global charge of the protein which we already aware of its amino acid sequence and the characteristic pKa for the individual side group: arginine (12.5), histidine (6.0) lysine (10.5), aspartic acid (3.9) , cysteine (8.2), glutamic acid (4.1) and tyrosine (10.5). These local charges, which correspond to the deprotonation of the acid groups or the protonation

of basic groups of the side chains, are relatively homogeneously distributed on the surface of the globular protein. A molecular representation of this distribution is given in (Fig 4.7).

The ionicity of each one of ionized amino acids can be obtained by knowing the pKa of the side chain groups. We have represented in (Fig 4.8) the global charge of the molecule as a function of pH of the solution in which it is located. The total charge was simply calculated from the number of ionized amino acids of each species present in this protein sequence and according to the pKa (pKa variation zone ± 2). The isoelectric point is around 5.5.

(Fig.4.8) shows that in the pH range 4.0 to 5, the BSA has an important number of positively charged side chain groups from +12 to +90. In the pH range 6 to 8, the charge gets low and varies from +10 to -10. While for more basic pH solution, the total charge of negatively charged side chains reaches -105 with a pH value of 12.

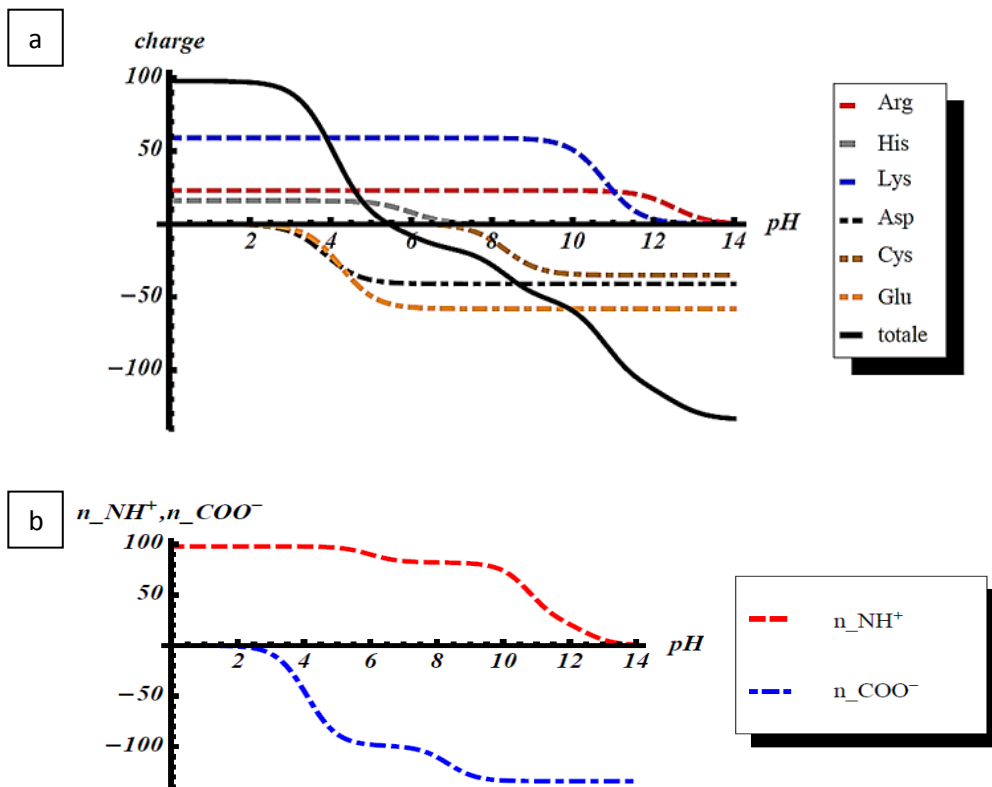


Fig.4.8 a. Evolution of the side chains charge and BSA total charge as a function of the pH of the solution. **b.** BSA positively and negatively charged groups number as a function of the pH of the solution.

Therefore, we have evaluated later in this work, the adsorption of the globular BSA N-form for solution in which it is generally positively globally charged (pH=4.5, total charge= +20), global slightly charged (pH = 7.0, total charge= -20) or highly negatively charged (pH=10, total charge= -60).

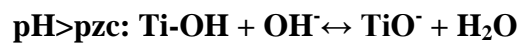
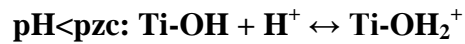
In this consideration, we have to mention that the concept of "total charge" of the protein is only a partial view of reality and correspond simply to the global charge of the ionization of acidic and basic side chains of amino acid groups. Actually, in the solution, the counter-ions join locally their protonated or deprotonated functions by purely electrostatic bonds (to ensure "locally" electrical neutrality). This association forms the first layer that strongly bound to the protein in the double layer model (dense layer of Helmholtz (then called Stern layer)) [228]. This combination then form a set of electric dipoles which are localized on the molecular surface and are capable of interacting with the surface of another molecule or the surface of a solid. This surface of the solvent ions that tightly bound to the ionized groups of BSA is surrounded by a diffuse layer (Gouy-Chapman layer) where the ions, well ordered adjacent the Stern layer, are much freer therefore easily moved during adsorption phenomena.

During adsorption on an oxide surface, electrostatic interactions will occur. The description of the local charges and dipoles that result in aqueous solution can be considered as attractive or repulsive forces on the microscopic scale. When the oxidation of a metal, the highly electronegative oxygen, attracts electrons in chemical bonds with the metal and thus finds itself negatively charged, while the metal atoms found them positively charged.

The chemical nature of the surface (surface anionic and cationic sites) can induce greater protein–surface interactions through either electrostatic or hydrophilic interactions [229]. The charged ions or groups on the substrate can bond the charged functional groups in the protein molecules to dominate the protein adsorption. As seen before, bovine serum albumin (BSA) has a high content of charged amino acids and can easily be adsorbed onto oxide surfaces like TiO₂ or deposited CaP nanoparticle by electrostatic interaction (charge-charge or dipole-dipole).

In the same way as we described the ionicity of the molecular surface of the BSA, we can describe the ionicity of the oxide surface. An important physical parameter (macroscopic) is the point of zero charge (PZC or IEP). This is defined as the pH of the solution (pH_{IEP}) for which the overall charge of the surface is zero [230] (as many positive charges as negative charges to acid-base direction Bronsted)

When the pH of the solution, in which the solid surface is immersed, is lower than the pH_{IEP} , we obtain a positive global charge, while for pH values higher than pH_{IEP} , we obtain a negative global charge. Thus, the pH of the solution influences both the state of charge of the BSA and the surface of the oxide.



For titanium oxide TiO_2 , the PZC is about 5-6 for a non-nanostructured solid [231]. In the case of nanoscale objects, the electronic structure due to the low dimensional, gives particular surface sites that can have a very different reactivity.

Bavykin et al [232], have shown that the PZC of TiO_2 nanotubes is close to 3.0, which means a pH more acid than for traditional forms of anatase type or rutile for macroscopic samples. For the different forms of calcium phosphates, PZC is basic, in the range 8.0-10.0. For calcium phosphate doped with strontium, the PZC is by 9.0 [233]. Thus, in our work, we will look at adsorption process of BSA on an “acidic” surface (nt- TiO_2) and two basic surfaces (CaP.nt- TiO_2 and Sr.CaP.nt- TiO_2).

Note that for deposits made in this work, the low dimensionality can significantly change the value of PZC. The interpretation of adsorption phenomena cannot be limited to a simple analysis of the global charge of two adducts as other factors may be involved in the phenomenon of adsorption of a poly-charged macromolecule onto an oxide surface. In particular, the ions associated with the ionized groups that can act as bridging ions between the surface and the protein with elimination of one of the two ions associated with interacted functional groups. Furthermore, the protein, used in our work, is considered as a "soft" protein, that is deformable depending on the surrounding environment. Thus, it can adapt its spatial conformation to favor certain favorable interactions with the solid surface and to optimize the adsorption energy.

This geometric change in "form" may also be correlated with structuring of ions situated at the solid-protein interface to optimize bonds of 3 centers of type (- + - or + - +).

According to W. Norde [234], the two aforementioned factors (change of conformation and structure of the ions in the interfacial zone) are predominant in the analysis of the enthalpy of adsorption. The adsorption energy related to the conformational changes and the loss of secondary structure of the protein is endothermic and reaches the minimum at the isoelectric point in the case of the interface HSA/polystyrene [234]. For the energy contribution of the organization of ions at the interface protein/surface, an important exothermic value is observed. Note that entropic factors, including solvent reorganization near the interface can be determinant in adsorption processes.

Concerning the influence of the ions that are present in the solution on the adsorption phenomena, it's also important to mention that the titanium oxide or CaP phase solubility and crystallinity are also important parameters for influencing the properties of the solution near the interface [235].

Surface topography determines the scale of the surface area that interacts with the protein molecules. More surface area can provide more interaction sites for protein adsorption. Meanwhile, pore size can control protein adsorption. For example, Fujii et al [236], reported that zinc-substituted HAp (Zn-HAp) nano crystals with some Zn content was more appropriate for β 2-microglobulin (β 2-MG) adsorption than for BSA adsorption, which is attributed to the pore size presented on Zn-HAp being suitable for β 2-MG adsorption. Actually, many researches were performed to investigate BSA adsorption onto different oxides surfaces because protein adsorption mechanism is very complicated and many factors are included in this process. (Fig.4.8)

For example, Zeng et al. [227] investigated BSA adsorption onto CaP and titanium surfaces as compared to germanium surfaces. This author reported that the higher increase in BSA adsorption was seen for BSA adsorbed onto a CaP surface, rather than on titanium (Ti) and germanium (Ge) surfaces, with a greater loss of α -helical

structure due to stronger electrostatic interactions with the highly ionic surface of CaP that attracts protein and exerts a greater force on its functional groups.

Dasgupta et al [237], evaluated the BSA adsorption by Zn and Mg doped hydroxyapatite to control the release of protein and reported that a decrease in α -helix content in doped and undoped BSA-HA which indicates that BSA's secondary structural integrity was distorted due to its interaction with HA crystal lattice. Also the amount of BSA uptake was found to be the highest for Zn doped HA-BSA nanopowder, while undoped HA-BSA nanopowder exhibited the lowest amount of BSA uptake which indicates that the addition of dopants significantly altered the quantity of adsorbed BSA and release behaviours of HA nano carriers. Zn doped HA-BSA nanocarriers being the least crystalline, released BSA at the fastest rate followed by Mg doped HA-BSA nanopowder and undoped HA-BSA nanopowders.

In this part of our work, we will investigate the influence of surface functionalization achieved in the first part of this thesis on protein adsorption phenomena such as BSA. The double functionalization; topographic modification (nanotubes) and chemical (grafting doped or undoped calcium phosphate) gives a solid surface where the nature and the ionicity of reactive sites, which depend on the pH of the aqueous solution, is different from untreated titanium surface. It is therefore essential to study how these changes affect the early stages of cell colonization, namely the adsorption of biomolecules such as BSA. We have chosen to study the adsorption of BSA at the liquid-solid interface (temporal tracking according to contact time) by infrared spectroscopy as it has the potential to demonstrate both the presence of this molecule at the interface and the changes of structure and/ or adsorption geometry by modification of vibrational spectrum. The XPS is used to control the final state of the surface once the adsorption kinetics achieved.

2. Protein analysis by IR spectroscopy

IR spectroscopy offers the possibility of identifying the most physiologically relevant conformation of a peptide or protein, thus it was used in this part of work as a main analytic device to investigate protein/surface adsorptive interactions. The application of IR spectroscopy to protein analysis is based on the assessment of the amide bands. Characteristic bands in the infrared spectra of proteins include the Amide I and Amide II that appear from the amide bonds between amino acids. [221].

The most sensitive spectral region to the protein secondary structural components is the amide I band ($1700\text{--}1600\text{ cm}^{-1}$), which is due almost entirely to the C=O stretch vibrations of the peptide linkages (approximately 80%) coupled with little in-plane NH bending (<20%) (Fig 4.9). The frequency of this vibration band depends on the nature of hydrogen bonding involving the C=O and NH [238]. The nature of the amino acid side-chain strongly affects the amide I which only depends on the secondary structure of the backbone. Thus, the amide I band is best suited to determine the secondary structure of proteins.

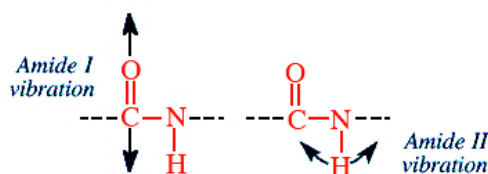


Fig.4.9. Vibrations of Amide I and Amide II bands in IR spectra of proteins.

The amide II band, ($1500\text{--}1600\text{ cm}^{-1}$), is attributed to in-plane NH bending (40–60% of the potential energy) and to the CN stretching vibration (18–40%). Amide II is affected by side-chain vibrations but the correlation between secondary structure and frequency is not that accurate when compared to the amide I region. [238, 239]

However, in the infrared region ($1200\text{--}1400\text{ cm}^{-1}$), signal of amide III vibration could be observed. This vibration is the combination of the NH bending and the CN stretching with small contribution from the CN in-plane bending and CC stretching vibration. Amide III is less useful for studying the secondary structure of proteins because its effect by side chain and the backbone vibrations varies considerably. Amide III signal in FTIR is weaker than amide I and amide II [238].

The correspondance between protein secondary structure and amide bonds

The band in the range $1650\text{-}1660\text{ cm}^{-1}$ is assigned to α -helix in aqueous environments. According to Fu et al [240], α -helix region attains 1661 cm^{-1} . The vibration of β -sheet can be seen in the region ($1620\text{-}1640\text{ cm}^{-1}$) and can be affected by varying strengths of the hydrogen bonding and transition dipole coupling in different β -strands.

The secondary structure of protein can be also determined from the amide II band, but the correspondance between IR spectra and secondary structure is more complex than in the amide I region because bands in the amide II region have not been well studied. In amide II region, bands between $1540\text{-}1550\text{ cm}^{-1}$ are considered as α -helix and the β -sheet vibration is the range $1520\text{-}1530\text{ cm}^{-1}$. β -turns can be seen around 1568 cm^{-1} . However, the important assignments of IR bands are given in (Table 4.2) [227]

IR region	Wavenumber cm^{-1}	Secondary structure
Amide I	1620-1640	β -sheet
	1645-1652	Random or unordered
	1650-1658	α -helix
	1662-1690	β -turn
Amide II	1520-1530	β -sheet
	1540-1550	α -helix
	1568-1580	β -turn
Amide III	1220-1250	β -sheet
	1250-1270	Random
	1270-1295	β -turn
	1295-1340	α -helix

Table.4.2. Protein band assignments in the IR spectrum [227]

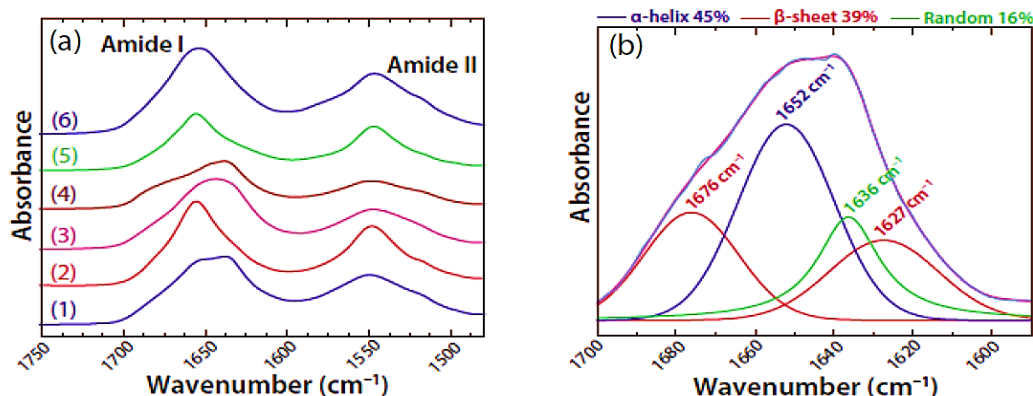


Fig.4.10. (a) IR spectrum of different type of proteins (1) α -Lactalbumin, (2) Hemoglobin (3) α -Chymotrypsin (4) Alcohol dehydrogenase (5) Human serum albumin (6) 6 α -1-Proteinase inhibitor. And (b) an example of the deconvolution of the amide I band into its components depending on the secondary structures. [241]

In our study, bovine serum albumin (BSA) was used as model protein to evaluate its adsorption onto the functionalized nanostructured TiO₂ surfaces. The use of infrared spectroscopy proves to be a valuable tool to monitor changes in protein structure based on certain parameters such as the coverage rate on the surface, the pH of the solution or the chemical nature of the adsorbent surface.

In order to make a qualitative characterization of the adsorption of BSA according to physical parameters such as the nature of the surface or the pH of the solution, we measured different infrared spectra depending on the amount of BSA adsorbed onto the surface of our samples.

One of the first observations is the intensity of the amide I band located in a spectral region 1600-1700 cm⁻¹. We can also compare the intensity of this characteristic band to the total intensity of amide I and amide II, the ratio of absorption bands can be related to structure modification and / or adsorption geometries.

From the evolution of the intensities (areas of the absorption bands) we can plot $I=f(t)$. On this curve, we can reveal the maximal intensities I_{max} at coverage saturation and the slope of the tangent at the origin that is related to the adsorption speed for low coverage.

From the measurements amide I and amide II band intensities we can define a parameter **R** corresponding to the intensity ratio I_{AI} / I_{AII} . It has been shown by Rothschild et al that **R** value is related to the average orientation of helix α relatively to the surface on which it is adsorbed [242].

In the case of a single helix, where it is lying on the surface ($\theta = 0^\circ$), a strong absorption of the amide I band is expected while for amide II it is a low intensity. In the case of a perpendicular direction to the surface plane, the intensity of the amide II band is expected to increase strongly as compared to the intensity of the band amide I [243].

Note that this parameter **R** gives us only average information on the molecular orientation or of BSA as this protein consists of several segments of this type of secondary structure with random or statistic orientation which is strongly anisotropic for the N form of BSA (see Fig. 4.7). In the case of denaturation, on the contrary, most

of the helixes are oriented in the direction of the axis of elongation of the protein i.e. parallels to the surface for this flat adsorption geometry.

In the case of films with highly organized molecular layer, the ratio R can be expressed in terms of the angle between the axis of the helix and the surface plan. Ignacio et al give the following relationship: [243]

$$R[\theta] = K \frac{\frac{1}{2}(3\cos^2\theta - 1)(3\cos^2\theta_I - 1) + 1}{\frac{1}{2}(3\cos^2\theta - 1)(3\cos^2\theta_{II} - 1) + 1}$$

Wherein θ represents the angle of the helix axis to the surface normal axis, θ_I is the angle at the dipole moment of the vibrational transition of the amide I band and θ_{II} angle of the dipole moment of the transition of the amide II band [244]

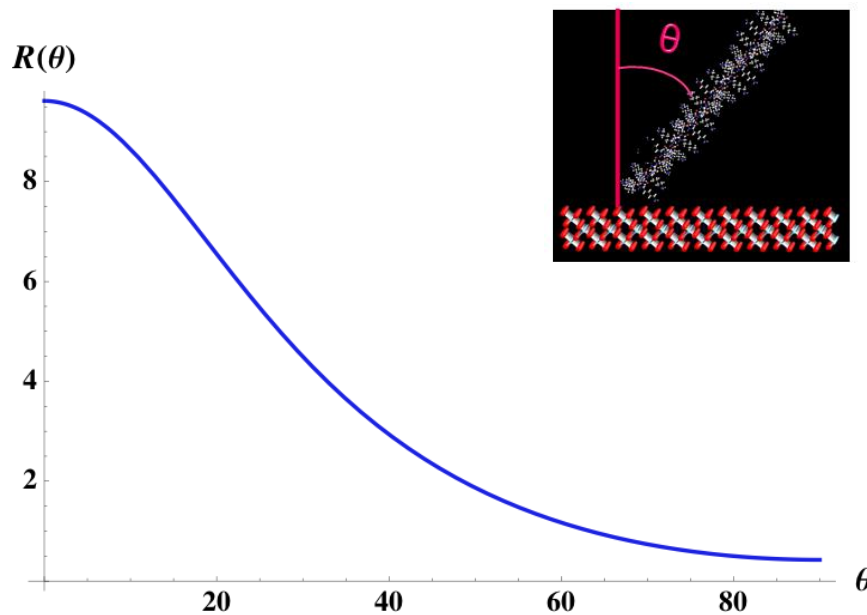


Fig.4.11. Evolution of R parameter according to the average angle of helix α to the surface normal axis [243]

For these two most probable configurations of adsorption, when the protein does not undergo any change of secondary and tertiary structures, the average value of the parameter R can be estimated from the distribution angle given in (Fig.4.12) and curve of evolution of parameter R according to the angle given in (Fig.4.11) using a formula of the type:

$$\bar{R} = \sum_{\alpha} R(\theta_i) P(\theta_i) = \sum_{\alpha} R(\theta_i) \frac{N(\theta_i)}{N_{tot}}$$

Where $N(\theta_i)$: the number of helix α with θ_i angle to the surface. N_{tot} : the total number of helix α

In the case of a configuration of "End on" adsorption, we find $R_{EO}=2.3\pm 0.1$, whereas in the case of adsorption "Flat", we obtain $R_F=3.0\pm 0.1$.

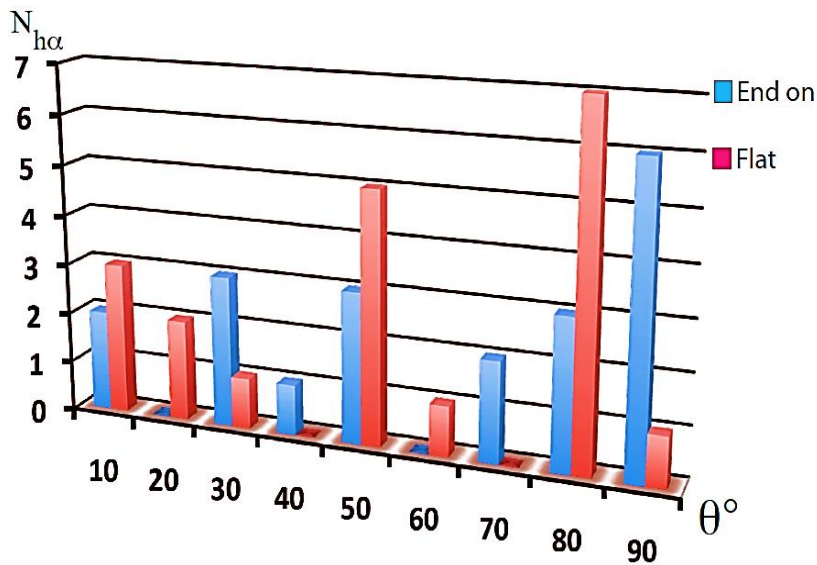


Fig.4.12 Distribution of the orientation of helices α according to the vertical axis of the N form of the BSA for an adsorption: «End on» (axis of the form N perpendicular to the surface) and «Flat» (axis of the form N parallel to the surface).

The variation of the parameter R is weak but significant but for these two extreme cases of adsorption geometry without changing the conformation of BSA. In the case of adsorption with "denaturation" and passage from the N form to a form of type E or F (unfolded protein) (Fig.4.6), R value is around ≈ 1 which indicates that a majority of helices α with their axis close to the parallel direction with the surface and this case often happens when interaction with surfaces.

3. Experimental results of BSA adsorption onto functionalized TiO₂ surfaces

In this work, we've evaluated the BSA adsorption onto uncoated TiO₂ nanotubes (nT-TiO₂), nanotubes coated with CaP, and nanotubes coated with Sr doped CaP (electrodeposition; 1000 potential pulses) using different pH values for BSA solution in order to explore the influence of the charge state of both surface and BSA molecule. BSA was deposited onto TiO₂ surfaces by immersing samples in a BSA stock solution (0.1 g/l) in distilled water and the pH value was adjusted with NaOH and HCl solutions. After a time step of several seconds of samples immersion in the BSA solution, samples are rinsed and dried and analysed by IRRAS. This operation is repeated until we obtained an intensity saturation of the absorption band that corresponds to the adsorbed BSA amide bands. The amount and the structural change of adsorbed protein is analysed through the amide I intensity and components as well as the R parameter previously defined.

The kinetic monitoring of infrared spectra in the region of the principal modes of vibration of the BSA is shown in (Fig.4.13, Fig.4.14, and Fig.4.15) for respectively following functionalized surfaces of TiO₂ (Blank nT-TiO₂, CaP. nT-TiO₂, Sr.CaP.nT-TiO₂ (30% Sr)). The trends are the same for different deposits of Sr.CaP so for sake of clarity we only present those with (Sr 30%). In each figure, the adsorption at acid (4.5), neutral (7.0) and basic (10.0) pH is presented. For each kinetic, we presented the infrared spectra for immersion time of 5s, 10s, 20s, 30s, 60s and 120s. The last immersion time gives a signal close to saturation.

In each case, we observe a signal evolution that depends on both the nature of the surface and the pH value as revealed by the intensity level and the distribution of bands which compose the amide I band. A more detailed analysis, including the composition of the amide I band, is therefore desirable and was realized from the 4 components mentioned above.

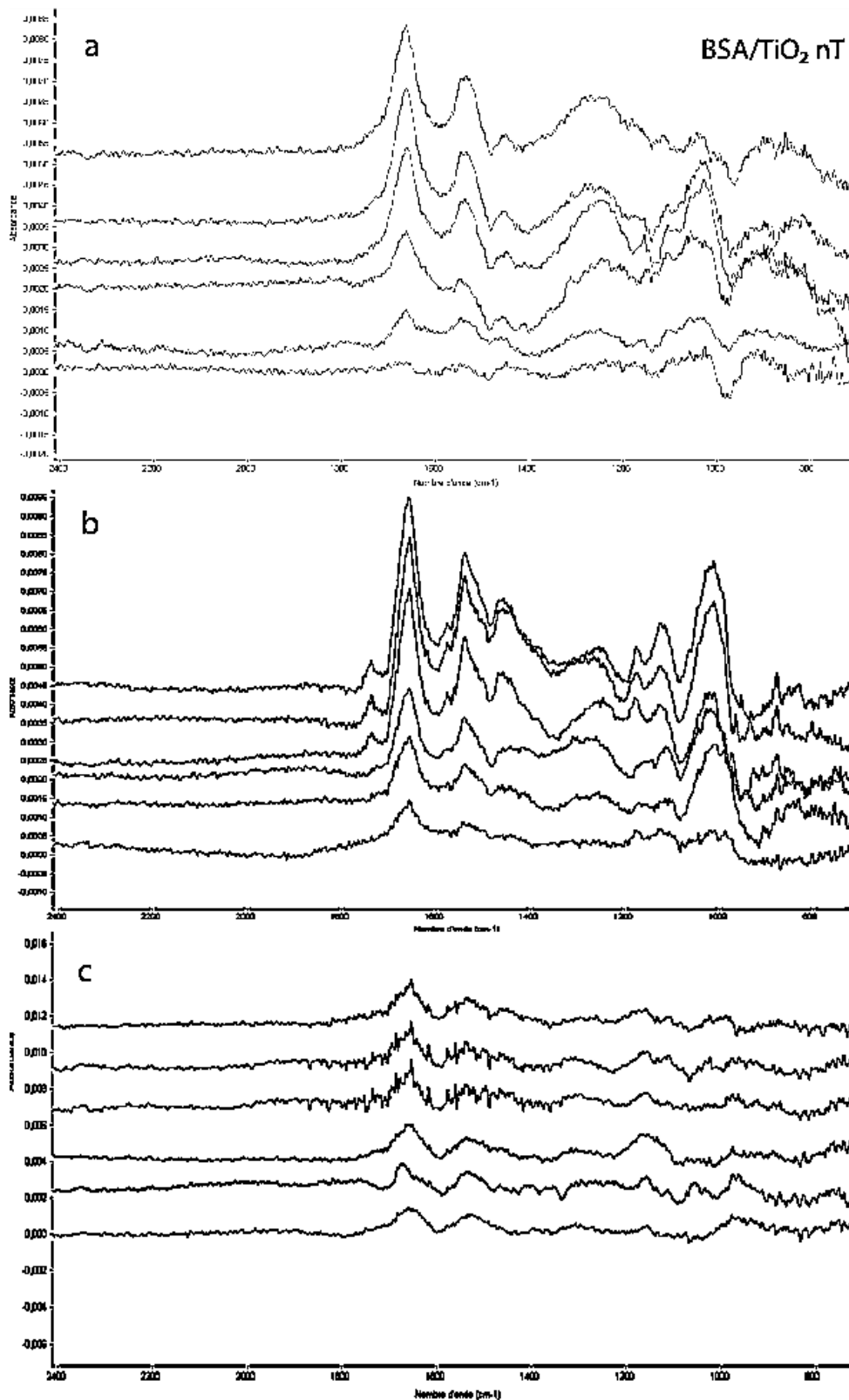


Fig.4.13. Evolution of the IR spectrum as a function of deposition time on nT-TiO₂ surface. (a) pH = 4.5 (b) pH = 7.0 (c) pH = 10. From bottom to top, 5s, 10s, 20s, 30s, 60s and 120s.

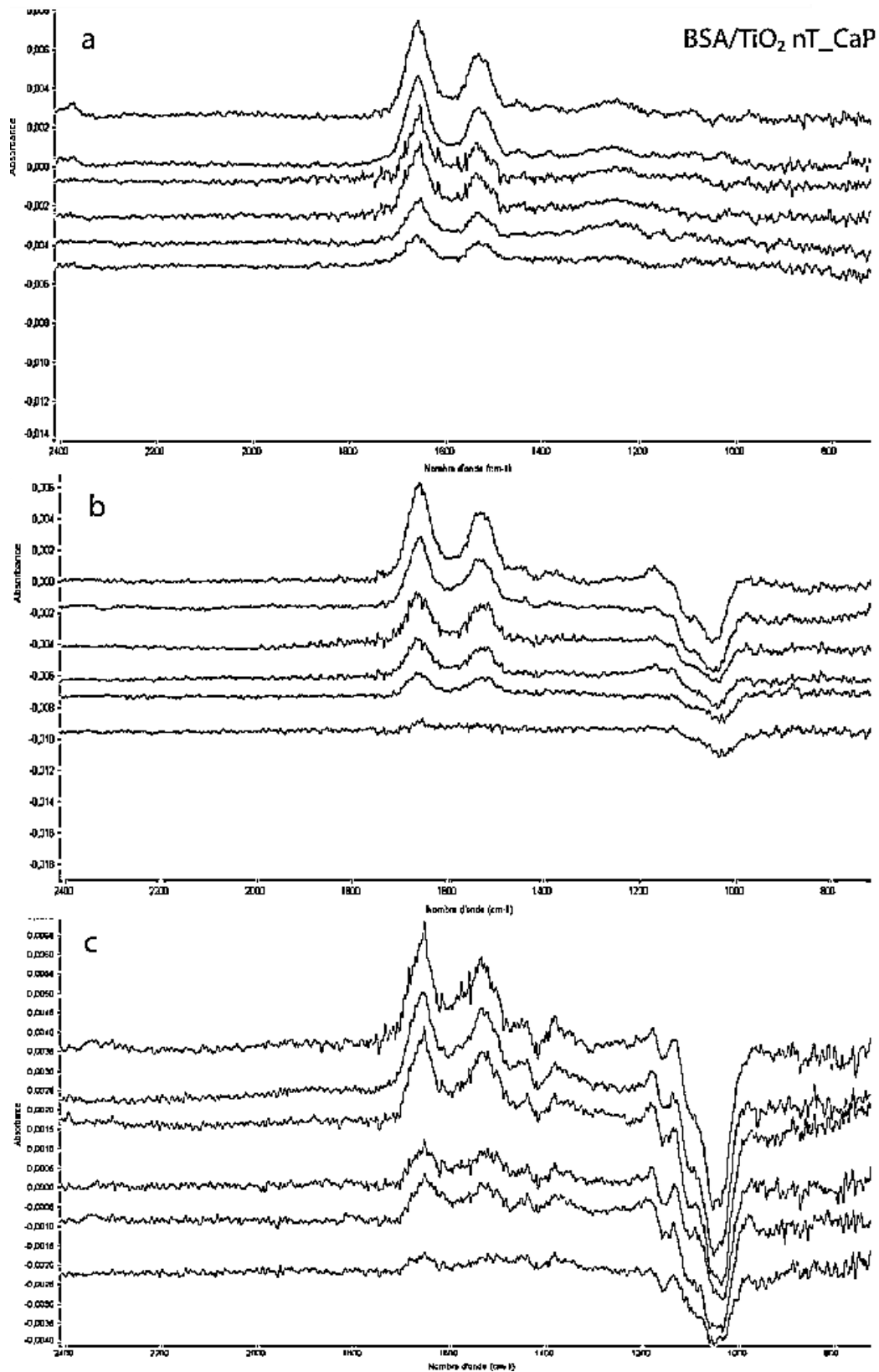


Fig.4.14. Evolution of the IR spectrum as a function of deposition time on CaP.nT-TiO₂ surface.
 (a) pH = 4.5 (b) pH = 7.0 (c) pH = 10. From bottom to top, 5s, 10s, 20s, 30s, 60s and 120s.

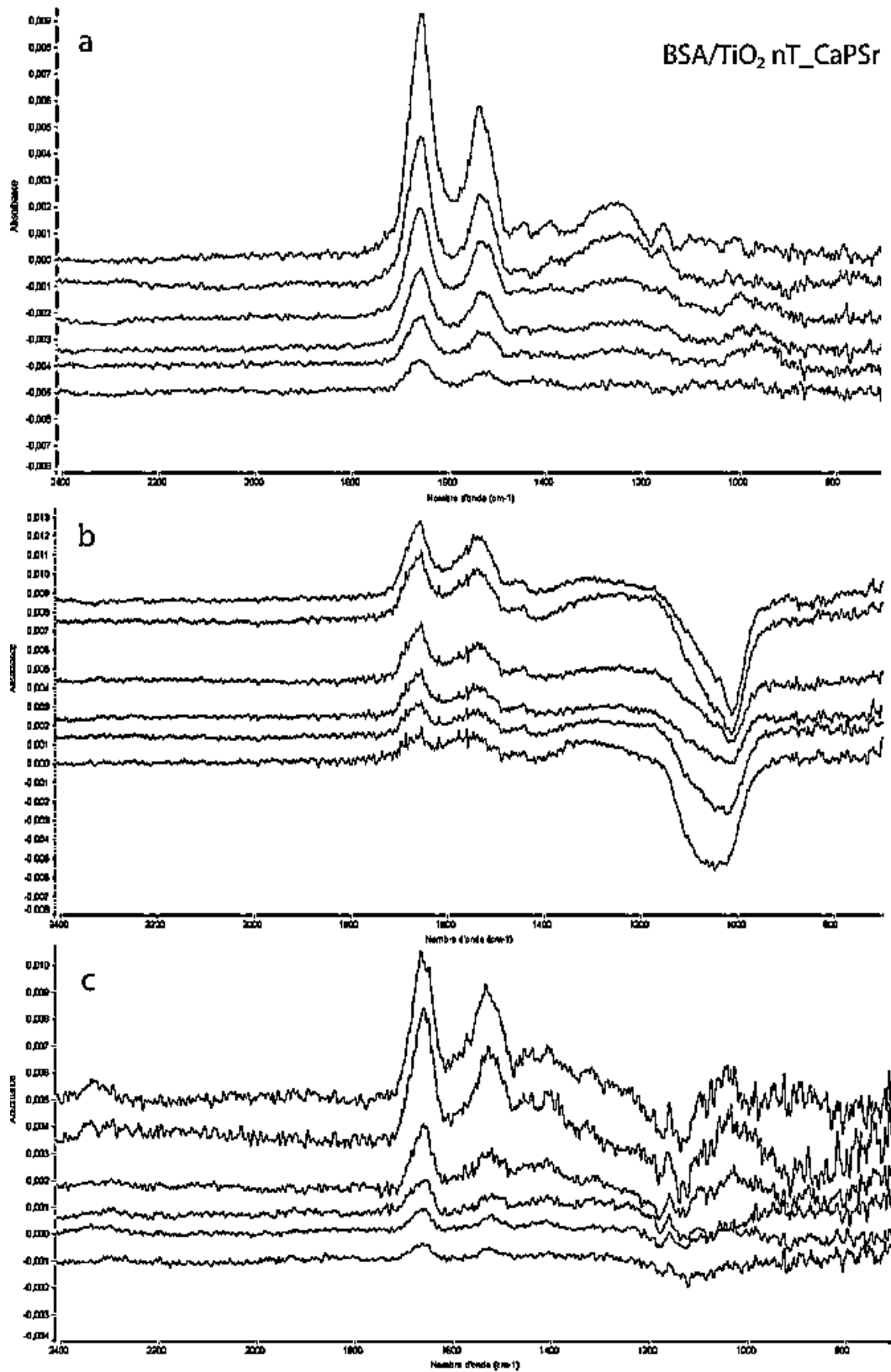


Fig.4.15. Evolution of the IR spectrum as a function of deposition time on Sr.CaP.nT-TiO₂ surface.

(a) pH = 4.5 (b) pH = 7.0 (c) pH = 10. From bottom to top, 5s, 10s, 20s, 30s, 60s and 120s.

To achieve this spectral decomposition, we used the OMNIC software by setting the values of the vibrational frequencies and the width at half height of each band with defined constraints ($\pm 4.0 \text{ cm}^{-1}$ and for the frequencies $12.0 \pm 3.0 \text{ cm}^{-1}$ for widths). The bands shape is assumed to be of Gaussian type. The presented and treated curves are raw data without smoothing for noise reduction.

We note in some cases some negative absorption peaks which are located around 1100 cm^{-1} and which can be associated with a loss of phosphate entities concomitant with the adsorption of BSA. We note that this phenomenon is pH and surface dependent since it occurs only for BSA adsorption at pH 7.0 and 10.0 on the surface of CaP.nT-TiO₂ on the surface of Sr.CaP.nT-TiO₂ (Sr 30%). This concurrent disappearance of phosphate ions and adsorption of BSA indicates a process of molecule-surface interaction with ions exchange, deprotonated carboxyl groups of the BSA can substitute PO₄³⁻ or HPO₄²⁻ ions, which are weakly bound to the surface of the CaP deposit.

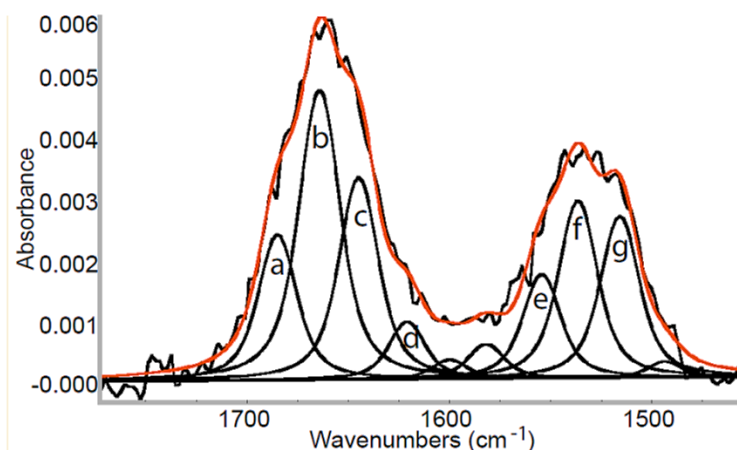


Fig.4.16. Spectral decomposition of amide I band and amide II band for BSA adsorption on CaP.nT-TiO₂. (Fit peak parameters constraints: Voigt profile: $\nu_0 \pm 2 \text{ cm}^{-1}$, peak width $\approx 11 \text{ cm}^{-1} \pm 2 \text{ cm}^{-1}$) (a) β -sheet at 1680 cm^{-1} , (b) α -helix at 1656 cm^{-1} , (c) Random at 1643 cm^{-1} (d) β -sheet at 1627 cm^{-1} , (e) β -sheet at 1564 cm^{-1} (f) α -helix at 1540 cm^{-1} (g) β -sheet and random at 1520 cm^{-1} (a, b, c, d peaks for amide I band, e, f, g peaks for amide II band)

In order to investigate BSA secondary structure we realized (Fig.4.16) a decomposition of amide I and amide II band for BSA adsorption on different surfaces (Peak Voigt profile: $\nu_0 \pm 2 \text{ cm}^{-1}$, peak width $\approx 11 \text{ cm}^{-1} \pm 2 \text{ cm}^{-1}$) that showed the different components of each amide band. To evaluate the R parameter we investigate the rapport of the peak area b/f (peak helix α in amide I to peak helix α in amide II).

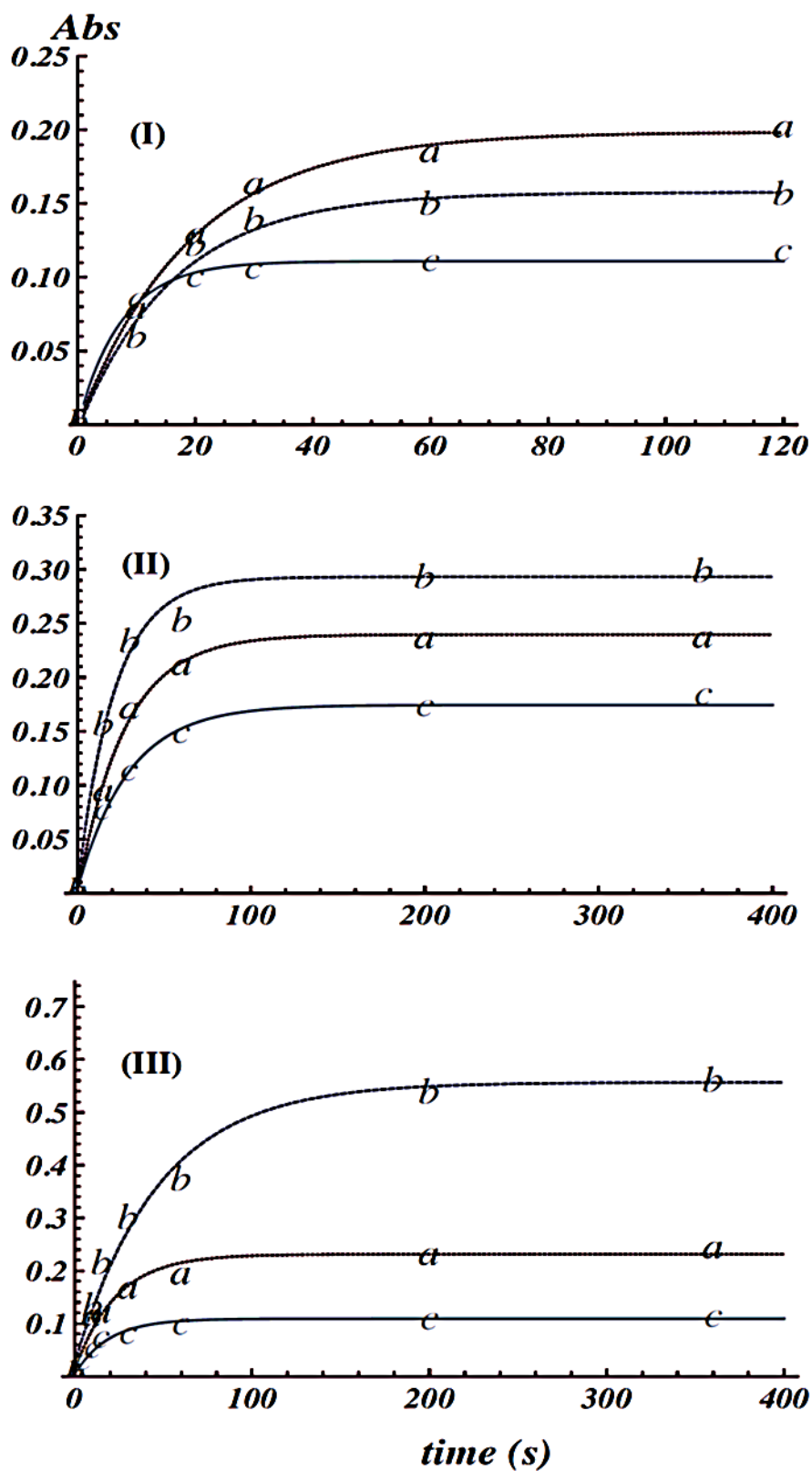


Fig.4.17. Evolution of Amide I band (total area) as a function of time on (I) nT-TiO₂, (II) CaP.nT-TiO₂ and (III) Sr.CaP.nT-TiO₂. For (a), pH = 7.0, (b), pH = 4.5, (c) pH = 10.

(Fig.4.17) shows the evolution of Amide I band (total area) as a function of time on the different surfaces for the different pH values. We always notice a higher value of adsorption intensity, regardless of the nature of the surface, for pH 4.5 and 7.0 compared to basic pH 10.0. For nT-TiO₂ surface we note higher adsorption intensity at pH 7 (Fig.4.17 (I. a)) as compared to pH 4 and pH 10 (Fig.4.17 (I. b & c)) whereas for CaP.nT-TiO₂ (Fig.4.17 (II)) and Sr.CaP.nT-TiO₂ (Fig.4.17 (III)) surfaces, the highest adsorption intensity was observed at acidic pH value (4.5) (Fig.4.17 (I.b and III.b)). In addition, we note that the saturation occurs faster on non-coated surface as compared to coated ones.

However, the highest adsorption intensity was observed for Sr.CaP.nT-TiO₂ and in all cases we note that saturation is obtained very quickly (few minutes).

Actually, similar results were obtained in similar conditions by Zeng et al [227] who indicated the increase of BSA adsorption according to time particularly at the first several minutes. At about 5 min, the amounts of BSA adsorbed on all surfaces were close to the saturation values [227]. All curves have a similar appearance with a monotonous variation of the intensity following an exponential law; $I = I_{\max}(1 - \exp^{-\frac{t}{\tau}})$. This type of evolution is characteristic for the formation of a single molecular layer (no simultaneous multi-layer growth or layer by layer growth) and indicates that once adsorbed on the surface, the protein layer presents to the aqueous solution an inactive surface for molecular interactions toward other proteins in the solution. Information obtained from (Fig.4.17) are summarized in (Table.4.3).

	nT-TiO ₂			CaP.nT-TiO ₂			Sr.CaP.nT-TiO ₂		
	4.5	7.0	10.0	4.5	7.0	10.0	4.5	7.0	10.0
I_{max} A_I	0.15	0.20	0.11	0.30	0.23	0.16	0.58	0.22	0.13
β	0.010	0.010	0.016	0.011	0.010	0.006	0.014	0.010	0.006

Table.4.3. Summary of I max (for Amide I band) and β values

Concerning the β parameter, which is related to the adsorption rate for very low coverage rates, and from the experimental low followed by BSA adsorbed amount onto the surfaces, we can estimate the initial adsorption speed $\beta = V_0 = \left(\frac{dI}{dt}\right)_0$

observing that β is proportional to the number of adsorbed molecules per second. From table (Table.4.3) we can observe that β value is the highest for basic pH onto non coated surfaces nT-TiO₂ as compared to other pH values whereas it's the lowest in basic pH for coated surfaces CaP.nT-TiO₂ and Sr.CaP.nT-TiO₂.

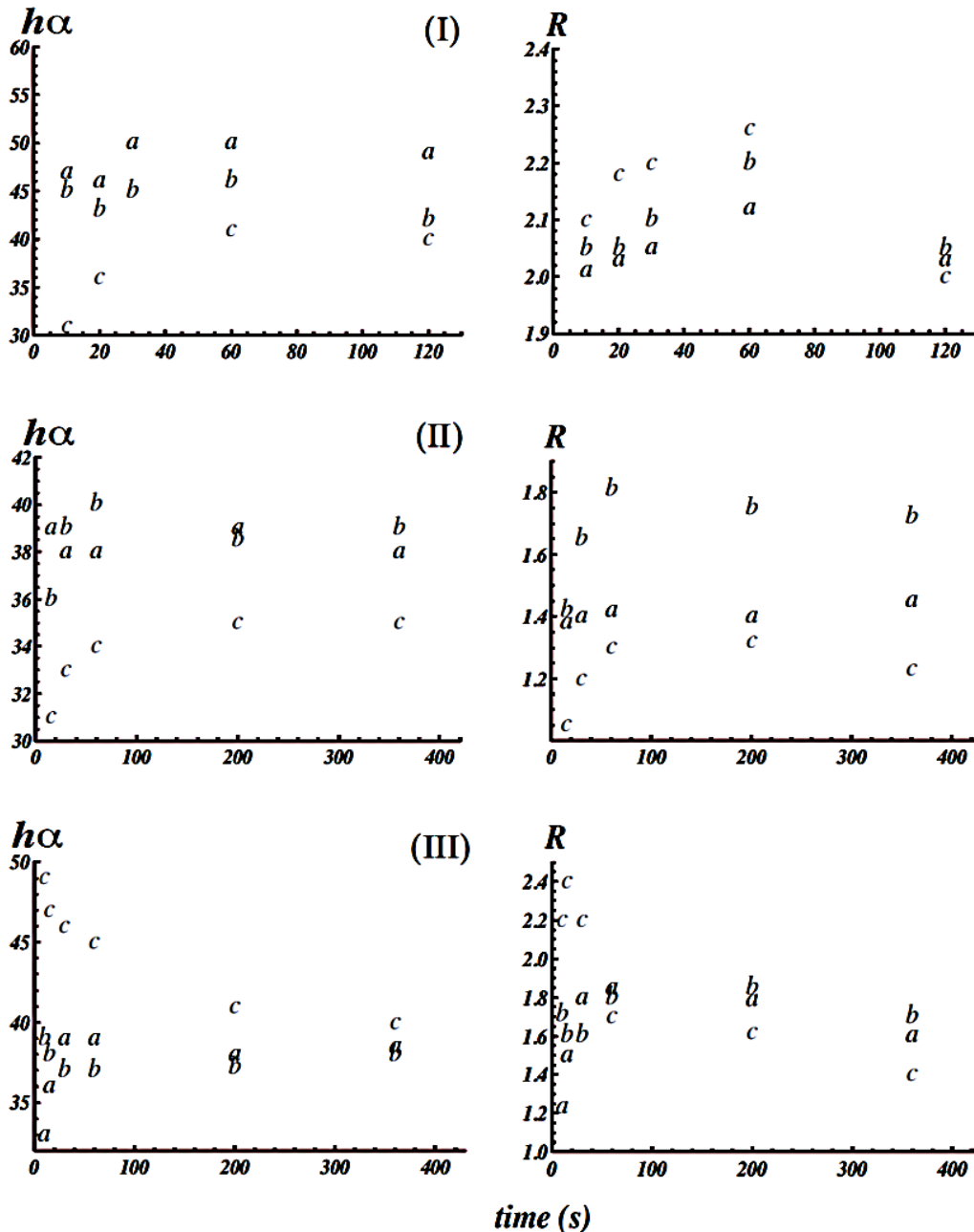


Fig.4.18 (Left) Evolution of α -helix % in Amide I band as a function of time on (I) nT-TiO₂, (II) CaP.nT-TiO₂ and (III) Sr.CaP.nT-TiO₂. For (a), pH = 7.0, (b), pH = 4.5, (c) pH = 10. **(Right)** Evolution of R ($I_{AI,ha} / I_{AII,ha}$) as a function of time on (I) nT-TiO₂, (II) CaP.nT-TiO₂ and (III) Sr.CaP.nT-TiO₂. For (a), pH = 4.5, (b), pH = 7.0, (c) pH = 10.

To make the interpretation of such developments clearer, we calculated the proportion of helices α (**%h α**) in the mass of the amide I band (component at 1650 cm^{-1}) and reported their evolution according to the deposition time. While the **R** parameter gives us information on the tertiary structure and/or about the orientation of the molecule with respect to the surface, **%h α** parameter is linked to secondary structure modifications [245, 246]. (Fig.4.18, left) represents the evolution of α -helix % in Amide I band as a function of time on the different surfaces at different pH values. (Fig.4.18, right) represents the evolution of R ($I_{AI,h\alpha}/I_{AII,h\alpha}$) as a function of time on the three studied surfaces for the different pH values.

First of all, we remark that the pH dependency of $\%h\alpha = f(t)$, depends on the surface properties. Curves shown in (Fig.4.18 (I.c, II.c)) have a similar pH dependency for the two nt-TiO₂ and CaP.nt-TiO₂ basic surfaces, where $\%h\alpha$ increases with deposition time. This evolution is quite different on the Sr.CaP.nt-TiO₂ surface where $\%h\alpha$ decreases with deposition time (coverage rate θ). (Fig.4.18 (III.c)).

We observe that $\%h\alpha$ stays relatively stable as a function of coverage rate θ at acidic and neutral pH values. For nT-TiO₂ (Fig.4.18 (I.a, I.b)) ($\%h\alpha \approx 47\%$), for CaP.nt-TiO₂ (Fig.4.18 (II.a, II.b)) ($\%h\alpha \approx 38\%$), and for Sr.CaP.nt-TiO₂ (Fig.4.18 (III.a, III.b)) ($\%h\alpha \approx 37\%$). Note that $\%h\alpha$ is higher for non-coated surfaces as compared to coated ones.

For basic pH we can observe a variation of $\%h\alpha$ depending on the adsorbing surface, for nT-TiO₂(Fig.4.18 (I.c)) we observed that $\%h\alpha$ starts with a value about 30% for low coverage rates and increased as a function of time to reach 37% for high coverage rates. For CaP.nT-TiO₂ surface (Fig.4.18 (II.c)) $\%h\alpha \approx 34\%$, whereas for Sr.CaP.nT-TiO₂ (Fig.4.18 (III.c)) we observe a diminution of $\%h\alpha$ as a function of time or coverage rate as it starts with a value of about 50% for low coverage rate and ends with value about 40% for high coverage rate which suggest a conformational changes of BSA secondary structure as a function of time/ coverage rate θ .

Concerning the R parameter; we have to remember that for the BSA N-form ($R \approx 2.3$ for end on adsorption geometry and $R \approx 3.0$ for flat adsorption geometry). From (Fig.4.18 right) we can note that for nT-TiO₂ surface for all pH studied values, R we

relatively stable about 2.10 ± 0.1 (Fig.4.18.I). While for CaP.nT-TiO₂, R was remarkably lower; $R \approx 1.4$ for pH 7 (Fig.4.18 (II.a)) $R \approx 1.8$ for pH 4.5 (Fig.4.18 (II.b)) and $R \approx 1.3$ for pH 10 (Fig.4.18 (II.c)). R values for CaP.nT-TiO₂ were lower than 2.3 (the value which corresponds to end on adsorption geometry for the BSA N-form) indicating that BSA is expanded on the surface with conformational changes of its tertiary structure as a function of time/ coverage rate θ .

For Sr.CaP.nT-TiO₂ surface, we remark a relatively stable value of $R \approx 1.6$ for acidic and neutral pH values (Fig.4.18 (III.a, III.b)) whereas we observe a decrease of R value for basic pH as a function of coverage rate θ (Fig.4.18 (III.c)) where R value decreases rapidly from 2.4 for low coverage rate to a value around 1.6 indicating that for Sr.CaP.nT-TiO₂ surface at basic pH, BSA adsorbed first as N-form with end on adsorption geometry and then a conformational changes occur as a function of time and the BSA expands onto the surface.

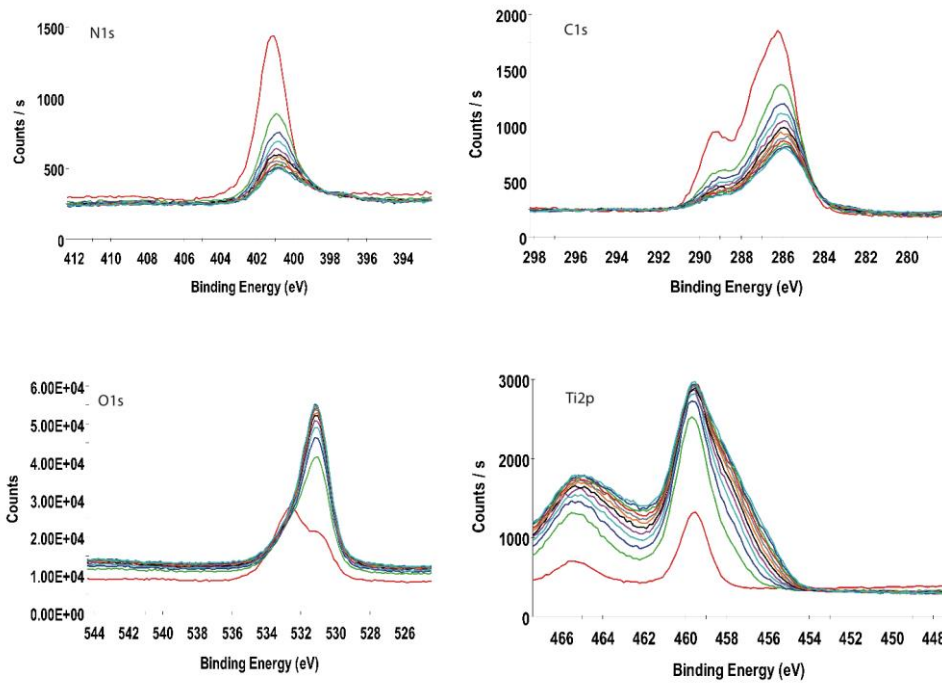


Fig.4.19. Evolution of the N1s, C1s, O1s and Ti2p XPS spectra with sputtering time in the case of BSA adsorbed onto nt-TiO₂

To investigate the localization of the adsorbed BSA on the functionalized surfaces, we have realized an XPS depth profiling in the same conditions as for the case of phosphate adsorption. XPS present characteristic peaks of adsorbed protein (C, O, N, S) and we look at the N_{1s} , O_{1s} and C_{1s} with sputtering time. The evolution of these spectra is presented in (Fig. 4.19).

We can observe that the N_{1s} signal characteristic of the protein strongly decrease with sputtering time meaning that the BSA is mainly adsorbed on the tube edges, as it was the case for the CaP deposit, confirming the inertness of tube walls.

Attempting to explain the evolution of $\%h\alpha$ and I_{max} with the chemical nature of the surface and the pH of the solution, we have to remember that the surface and the BSA have local charges that depend on the pH of aqueous medium where the adsorption occurs. For BSA, the ionization of different groups gives a global charge of +20e, -20e and -60e, respectively for pH 4.5, 7.0, and 10.0. Note that each of the charges of side groups of amino acids is associated with a counter-ion, which results in the existence of a dipole rather than a locally isolated charge. This distribution of the dipole on the molecular surface is of course related to the secondary and tertiary structure of the BSA.

Concerning the state of charge of the surfaces studied in our work, if we assume a PZC ≈ 3.0 for nT-TiO₂, the surface charge is generally negative for all pH studied in our work. In the case of the two others basic surfaces, they are globally negatively charged. The net ionic charge is due to the preferential dissolution-adsorption mechanisms of lattice ions. The surface charge of CaP compounds has been studied by measuring the zeta potential [247] and a PZC value around 10.5 is generally observed.

An apatite surface at acidic pH is less negative than at higher pH, and the surface charge is mainly determined by H⁺, Ca²⁺ and H₂PO₄⁻ ions. At higher basic pH, more negatively charged phosphate ions are present.

Comparing the evolutions of $\%h\alpha$ and I_{max} for adsorptions done onto nt-TiO₂ surfaces, we observe a constant value at pH 7.0 and pH 4.5, while an increase of $\%h\alpha$ with coverage for pH=10. For the nT-TiO₂ surface, the net charge is negative and we

expect a strong electrostatic interaction between the BSA and the TiO₂ nanotubes in all cases.

The R value is just lower than 2.3 indicating that the BSA is mostly adsorbed as N-form with an end on geometry onto the surface. Nevertheless, the increase of %h α with coverage rate at basic pH 10, indicates that molecular conformation changes and secondary structure modifications arise when the adsorbed proteins get closer from each other in the surface layer. For low coverage rate θ , higher amount of helix- α denatures as compared to high coverage rate θ .

Two assumptions can be then suggested; the first one concerns a structural modification of the secondary structure with coverage, adsorbed proteins getting from a flatter configuration with a large proportion of helices α transformed to random coils at low coverage to a more stable globular shape with a higher proportion helices α at high coverage. These structural modifications can be induced by stronger intermolecular forces than the molecule-substrate interactions.

The second explanation could be that at low coverage, BSA is more strongly adsorbed in a flatter configuration, leading to a decrease of the active adsorbing surface with increasing BSA coverage. Thus, due to steric hindrance, BSA molecules cannot lie flat on the surface and should be weakly adsorbed in a more globular form containing a higher helices α proportion at high coverage. At saturation, the BSA should then be adsorbed with both denatured conformation flattered and more globular N-form molecules, giving rise to a statistical value for %h α around 40% that is lower than the value of 60% for the native BSA.

For pH 7.0 and 4.5, the nT-TiO₂ surface is negative while BSA has a low global charge. Concerning the adsorption in a neutral solution, the BSA is weakly negatively charged. This means that it is the charge distribution on the protein surface that drives the BSA-surface interactions rather than the global protein charge (globally repulsive). This can be understood assuming a great adaptability for the protein shape (soft protein). On the other hand, the %h α evolution is remarkably different, as it remains constant with deposition time.

When the adsorption is realized in a basic solution onto the nT-TiO₂ surface, the BSA global charge is around -60 e and the molecule-substrate interaction should be less favourable. We observe *I_{max}* value lower than in the previous case (0.11 compared to 0.15 and 0.20). In that case, the %*hα* increases as a function of coverage rate, these observations about *I_{max}* and %*hα* evolution agree with a model where a part of the surface is occupied with flatter absorbed BSA at basic pH 10 (less BSA is absorbed at saturation coverage)

For CaP.nT-TiO₂ surface, photoemission allowed us to estimate a formula of the type Ca₄(HPO₄)₃OH₂, which indicates that at pH= 4.5, the surface is composed of H₂PO₄⁻ groups. Based on the structure of this compound, we can estimate a density of 4.5 ions/ nm² for both Ca²⁺ and OH⁻ and 3.4 ions/nm² for the phosphate ions. In the case of surfaces modified with Sr we had Ca_{1-x}Sr_x(HPO₄) type, the same type of phosphate groups is expected, but with a greater surface density. In this case similar to brushite-like composition, a surface density of 6.3 ions/nm² for both Ca²⁺ and phosphate can be estimated. We can assume that the greater *I_{max}* for the adsorption onto Sr.CaP.nT-TiO₂ results from the greater H₂PO₄⁻ groups surface density and thus to stronger interactions between the positively charged BSA and the surface as the coating have the same localisation on the tube edges.

The evolution of %*hα* for CaP.nT-TiO₂ and Sr.CaP.nT-TiO₂ surfaces suggests a similar behaviour of BSA adsorption structure during the adsorption on these two surfaces at pH 4.5 and pH 7.0. For these two surfaces, at neutral pH, the pH of the solution is close to the pKa of H₂PO₄⁻/HPO₄²⁻ couple and we can estimate that the surface is composed of an equal surface density of groups H₂PO₄⁻ and HPO₄²⁻. For both surfaces, CaP.nT-TiO₂ and Sr.CaP.nT-TiO₂, the parameter %*hα* is about (38%) a value which is slightly lower than in the case of non-coated surface nT-TiO₂. In this case, both R and %*hα* indicate a stronger interaction between BSA and coated surfaces.

The most interesting feature is the influence of Sr incorporation on R and %*hα* evolution as a function of coverage rate θ at pH=10.0. When Sr is incorporated with CaP coating, both R and %*hα* decrease with time (coverage rate) indicating that BSA

conformation changes and denaturation increase as a function of coverage rate θ , while it's the contrary for both pH=7.0 and pH= 4.5.

This evolution reveals that at low coverage rate (or at first steps of the adsorption), BSA molecule interacts weakly with Sr.CaP.nT-TiO₂ surface (both R and %h α values are high) on the contrary to what happens on nT-TiO₂ or CaP.nT-TiO₂. This can be correlated with the high total negative charge of BSA at pH 10 where strong repulsive electrostatic interactions occur between the molecule and the surface. This corresponds to a slower initial speed of adsorption (0.006 as compared to 0.014 for pH 4.5).

The diminution of %h α and R with coverage rate/ time implies that some dynamic processes must be taken in consideration; a. Surface chemical modification consecutive to BSA molecule previously adsorbed or b. Evolution of the adsorption geometry as a function of time where protein adapts its shape to surface reactive sites distribution to minimize the adsorption energy. We can note that in this case, phosphate ions are not released during the adsorption process (Fig.4.15) with no strong negative adsorption band around 1100cm⁻¹ correlated with the appearance of the amide bands of BSA.

Concerning the initial adsorption speeds, we remark that on CaP coating, it's always higher for adsorption process held at pH 4.5 in agreement with stronger global electrostatic interactions between BSA positively charged and negatively charged surfaces.

CONCLUSION

Dental implants are invasive medical prosthetic devices that integrate with the bone through a process called osseointegration. The term "osseointegration" is synonymous to a physical and biological contact between the surface of an implant and the surrounding bone. These interactions should persist in unfavorable mechanical and bacteriological conditions over time.

Historically, titanium is considered to be a material of choice for the majority of dental and orthopedic implants because of its biocompatibility and good mechanical properties. Clinical osseointegration is not synonymous to total bone-implant interactivity. Moreover, there are immediate and mediate failures in the current implantology. The effects of surface properties on the osseointegration of implants were investigated in many studies which reported that the osteoblasts proliferation and differentiation and proteins interactions are influenced by both the surface morphology and chemistry.

Nanostructuring is a promising technique that aims to create surfaces with a controlled topography and chemistry. Such morphologies allow to modulate cell behavior and to control the proteins-surface interactions. In addition to surface topography, its chemical composition is also essential to protein adsorption and cell adhesion.

The objective of this thesis is to create new nanostructured titanium surfaces functionalized with bioactive coatings and to study their physico-chemical properties to develop better models of dental implants in order to promote the process of osseointegration.

In this work, we have realized a double functionalization of titanium surface by topographical (nanotubes formation) and chemical (deposition of functional coatings) modifications. X-ray photoelectron spectroscopy (XPS) and Infrared Reflection-Absorption Spectroscopy (IRRAS) were used in order to study the interfacial chemistry and to characterize the adsorbed species onto the Ti nanostructured

surfaces. The scanning electron microscopy (SEM) is also used to characterize the topography of surfaces.

We started with the nanostructuring of TiO₂ surface using the anodizing method to create TiO₂ nanotubes aligned perpendicularly to the surface. The anodized surface presents amorphous TiO₂ nanotubes aligned in a compact structure perpendicularly to the surface with an average diameter of about 35nm. The formation of thin nanostructured film of TiO₂ was visualized by SEM and confirmed by XPS and IRRAS spectroscopy.

We have first evaluated the ability of such nanotubes to adsorb small molecules such as phosphate ions. We also tested the influence of the alkaline pretreatment on TiO₂ nanostructured surfaces reactivity on phosphate adsorption. From the analysis of IRRAS spectra of the studied samples, we found that PO₄³⁻ is adsorbed by nanotubes (nT-TiO₂) in the form of two types of complexes. NaOH pretreatment of TiO₂ nanotubes resulted in the growth of a sodium titanate layer on the edges of (nT- TiO₂). IRRAS spectra of the samples pretreated with NaOH, after adsorption of phosphate, presented a new adsorbed species associated with a tri-coordinated surface complex, confirming that alkaline pretreatment induced a stronger molecular adsorption.

We have then evaluated the growth of CaP and Sr doped CaP (CaPSr) onto nT-TiO₂ surfaces by pulsed electrodeposition at room temperature. Strontium was used as an ionic substituent to optimize bone formation. The topography and the chemistry of the coating are evaluated according to the time of deposition by SEM, XPS and IRRAS. SEM images of the samples coated with CaP and CaPSr showed that they were grown on the outer edges of TiO₂ nanotubes and that these edges were the most reactive sites of the nanostructured surface as they act as anchoring point of the coating. The surface coverage by the deposits increases as a function of time and the CaP nanoparticles anchored to the edges of the nanotubes aggregate and eventually cover the entire surface of the material. From the XPS spectra, we deduced that for the non-doped CaP coating, the concentration ratio between calcium and phosphorus is about [Ca]/[P]=1.30. The peak deconvolution of O_{1s} and P_{2p} indicated a compound rich of OH. In the case of a disordered amorphous compound (Amorphous Calcium Phosphate ACP) developed in an alkaline medium with a calcium deficiency, a group

of ACP compositions may be represented by the following formulas: $\text{Ca}_{9-y}(\text{PO}_4)_{6-x}(\text{HPO}_4)_x(\text{OH})_{2-x}$. Quantification by photoemission suggests a compound of $\text{Ca}_4(\text{HPO}_4)_3(\text{OH})_2$. Under the same conditions of the electrodeposition of CaPSr, we found that $[\text{Ca}]/[\text{P}] \approx 1.0$. In this case we have a compound of $\text{Ca}_{1-x}\text{Sr}_x\text{HPO}_4$. It was also noted that $[\text{O}]/[\text{P}] > 4.0$ which means that the coatings are strongly hydrated. XPS and IRRAS spectra of Sr doped CaP coatings have clearly showed that addition of Sr in the CaP layer promotes a non-apatitic compound $\text{Ca}_{1-x}\text{Sr}_x\text{HPO}_4$ which is similar to DCPD (Dicalcium phosphate dihydrate) or DCPA (Dicalcium Phosphate Anhydrous) while the undoped CaP coating resembled to a composition of amorphous apatite (ACP). It has been reported that non-apatitic compounds are more soluble in organic media than those of apatite. Thus, strontium addition has the double advantage of supporting cellular activities and obtaining an inorganic phase with a better bio-performance than apatite compounds when used for dental implants.

In the last part of this thesis, we studied the adsorption properties of the functionalized surfaces with regards to interactions with BSA. BSA adsorption was performed on blank nanotubes (nT-TiO₂), nanotubes coated with CaP (CaP.nT-TiO₂) and nanotubes coated with Sr doped CaP (Sr.CaP.nT-TiO₂) in order to evaluate the influence of the chemical nature of the surface on protein adsorption process. Furthermore, we have evaluated the role of the pH of the solution in the adsorption of the protein (acid~4.5, neutral~7.0, and basic~10.0). In order to achieve a qualitative study of BSA adsorption onto the different surfaces, we have deconvoluted the IRRAS spectra as a function of the quantity of the BSA adsorbed by the surface (Amide I band). We have also investigated the rapport of adsorption bands Amide I and Amide II which can be related to the structural modification and/ or adsorption geometry. We have found that BSA adsorption depends strongly on the physico-chemical characteristics of both surface and solution.

The observations obtained in this work can be used to design a functionalization of implant surface in order to favor the cellular adhesion and colonization. The evaluation of protein adsorption and its conformation as well as the protein-protein interactions may offer an opportunity to understand its interactions with adhering cells during the first steps of cellular colonization.

As prospects, this work should be followed by biological tests of the functionalized surfaces and test of the coating adhesion. Moreover a study of the release kinetics of bioactive ions (Sr) would be very useful to control the healing period. Actually, such surface functionalization can be applied on other alloys such as TiZr. Furthermore, other agents / drugs (anti-inflammatory, growth factors) can be incorporated to create hybrid implants (inorganic-organic).

REFERENCES

- [1] A.D. Pye, D.E.A. Lockhart, M.P. Dawson, C.A. Murray, A.J. Smith. A review of dental implants and infection”, *Journal of Hospital Infection*, Nr.72, pp.104-110, 2009.
- [2] P-I. Brånemark. Vital microscopy of bone marrow in rabbit. *Scand J Clin Lab Invest* 1959; Suppl 38.
- [3] P-I. Brånemark, U. Breine, R. Adell, B.O. Hansson, J. Lindstrom and A. Ohman. Intra-osseous anchorage of dental prostheses. Experimental studies. *Scand J Plast Reconstr Surg* 11: 81-100. 1969.
- [4] P-I. Brånemark, B.O. Hansson, R. Adell, et al. Osseointegrated implants in the treatment of the edentulous jaw. Experience from a 10-year period. *Scand J Plast Reconstr Surg* 1977; 16:1- 32.
- [4] R. Adell, B. Eriksson, U. Lekholm, P-I. Brånemark and T. Jemt. Long-term follow-up study of osseointegrated implants in the treatment of totally edentulous jaws. *The International Journal of Oral & Maxillofacial Implants*, vol. 5, no. 4, pp. 347–359, 1990
- [5] J.L. Rosenlicht. Immediate implant placement and immediate provisionalization: Steps for integration. *Implantology* 2003 , Mahwah, NJ , 2003 , Montage Media Corp , pp 46-52.
- [6] G.E. Romanos. Present status of immediate loading of oral implants, *J Oral Implantol* 30:189 - 197, 2004.
- [7] C.N. Elias C.N. Factors Affecting the Success of Dental Implants, *Implant Dentistry -A Rapidly Evolving Practice*, Prof. Ilser Turkyilmaz (Ed.), ISBN: 978-953-307-658-4. (2011)
- [8] E.P. Solomon, R.R. Schmidt, P.J. Adragna. *Human anatomy & physiology* ed.2nd 1990 (Sunders College Publishing, Philadelphia) ISBN 0-03-011914-6.
- [9] D.A. Somayajula. *Biocompatibility Of Osteoblast Cells On Titanium Implants*, thesis may 2008.
- [10] A. Atala, R. Lanza, J.A. Thomson, R.M. Nerem. *Principles of Regenerative Medicine*; Elsevier: Burlington, MA, USA, 2008; Volume 1448.
- [11] A.Peterson-Ford. PhD apetersonford@collin.edu Chapter 6 Bones and Skeletal Tissue, *The human body* 2012

- [12] C.H. Turner, T. Wang, D.B. Burr (2001). Shear Strength and Fatigue Properties of Human Cortical Bone Determined from Pure Shear Tests. *Calcified Tissue International* 69 (6): 373–378.
- [13] C. Rey. "Calcium phosphate biomaterials and bone mineral. Differences in composition, structure and properties." *Biomaterials* 11 (1990): 13-15
- [14] C.N. Elias, J.H.C. Lima, R. Valiev, and M.A Meyers. Biomedical Applications of Titanium and its Alloys www.tms.org/jom.html JOM • March 2008
- [15] R.E. Krebs. (2006). *The History and Use of Our Earth's Chemical Elements: A Reference Guide* (2nd edition). Westport, CT: Greenwood Press. ISBN 0-313-33438-2.
- [16] R.Z. Valiev, R.K. Islamgaliev, and I.V. Alexandrov. Bulk Nanostructured Materials from Severe Plastic Deformation. *Prog. Mater. Sci.*, 45 (2000), p. 103.
- [17] J. Emsley (2001). "Titanium". *Nature's Building Blocks: An A-Z Guide to the Elements*. Oxford, England, UK: Oxford University Press. ISBN 0-19-850340-7.
- [18] T. Albrektsson, H.A. Hansson and B. Ivarsson. (1985). Interface analysis of titanium and zirconium bone implants. *Biomaterials*, Vol.6, No.2, pp. 97-101, ISSN 0142-9612
- [19] X. Liu, P.K. Chub, C. Ding. Surface modification of titanium, titanium alloys, and related materials for biomedical applications. *Materials Science and Engineering R* 47(2004)49–121.
- [20] P. Stathopoulos, G. Theodossiades, C. Mourouzis, A. Evangelou. Effect of titanium maxillofacial implants and osteosynthesis materials on platelet function. *Br J Oral Maxillofac Surg*. 2011 Oct;49 (7):538-41.
- [21] P-I. Brånemark (1983). Osseointegration and its experimental background. *The Journal of Prosthetic Dentistry* 50 (3): 399-410 .
- [22] T. Albrektsson, G.A. Zarb. Current interpretations of the osseointegrated response: Clinical significance. *Int J Prosthodont* 1993;6:95-105.
- [23] D.A. Puleo, A. Nanci. Understanding and controlling the bone-implant interface. *Biomaterials* 1999, 20:2311-2321.
- [24] O.E. Pohler. Unalloyed titanium for implants in bone surgery. *Injury* 2000,31 (Suppl 4):7-13.
- [25] L.F. Cooper (2003). Cellular interactions at cp Ti implants. In, *Bio-implant interface. Improving biomaterials and tissue reactions*. Jan Eirik Ellingsen and S. Petter Lyngstadaas. CRC Press 2003. pp.165-181

- [26] G.C. Menezes, C.N. Elias, M. Attias, F.C. Silva-Filho. (2003). Osteoblast Adhesion onto Titanium Dental Implants. *Acta Microscopica*. Vol.12, pp.13-19, ISSN 1728-5917.
- [27] J.F. Osborn. (1979). Biomaterials and their application to implantation. *SSO Schweizerische Monatsschrift für Zahnheilkunde* Vol.89, No.11, pp. 1138-1139, ISSN 0036-7702.
- [28] H.J. Haugen, M. Monjo, M. Rubert, A. Verket, S.P. Lyngstadaas, J.E. Ellingsen, H.J. Ronald, J.C. Wohlfahrt (2013). Porous ceramic titanium dioxide scaffolds promote bone formation in rabbit peri-implant cortical defect model, *Acta Biomaterialia* , Volume 9, Issue 2, February 2013, Pages 5390–5399
- [29] S. Anil, P.S. Anand, H. Alghamdi and J.A. Jansen (2011). Dental Implant Surface Enhancement and Osseointegration, *Implant Dentistry - A Rapidly Evolving Practice*, Prof. Ilser Turkyilmaz (Ed.), ISBN: 978-953-307-658-4, InTech.
- [30] T. Albrektsson, P-T.Brånemark, H.A. Hansson and J. Lindström (1981). Osseointegrated titanium implants. *Acta Orthopaedica Scandinavica*, 52, pp.155–179, ISSN 0001-6470.
- [31] T. Albrektsson, P-I. Brånemark, H.A. Hansson and U. Jonsson. Ultrastructural analysis of the interface zone of titanium and gold implants, in *Clinical Applications of Biomaterials* (Eds Lee AJC, Albrektsson T and Brånemark P.-I.), John Wiley, New York, USA, 1982. pp 167-177 Plenk. H. Pflüger, G. and Bohler. ISBN 0-86715-129-3.
- [32] J.E. Davies. (2003). Understanding peri-implant endosseous healing. *Journal of Dental Education* Vol.67, No.8, pp. 932-949, ISSN 0022-0337
- [33] D. Chappard, E. Aguado, G. Huré, F; Grizon and M.F. Basle (1999). The early remodeling phases around titanium implants: a histomorphometric assessment of bone quality in a 3- and 6-month study in sheep. *The International Journal of Oral and Maxillofacial Implants*, Vol.14, No.2, pp. 189-196, ISSN 0882-2786.
- [34] J.P. Fiorellini, G. Martuscelli and H.P. Weber. (1998) Longitudinal studies of implant systems. *Periodontology* 2000 17: 125-131.
- [35] M. Esposito, J.M. Hirsch, U. Lekholm and P. Thomsen (1998) Biological factors contributing to failures of osseointegrated oral implants. (I).Success criteria and epidemiology. *European Journal of Oral Sciences* 106:527-551.
- [36] E.T. Ashley, L.L. Covington, B.G. Bishop, L.G. Breault. Ailing and failing endosseous dental implants: a literature review. *J Contemp Dent Pract*. 2003 15;4(2):35-50.PMID:12761588.

- [37] L. Levin , D. Schwartz-Arad. The effect of cigarette smoking on dental implants and related surgery. *Implant Dent.* 2005;14 (4):357-61.
- [38] R. Adell, U. Lekholm, B. Rockler and P-I. Brånemark. (1981) A15-year study of osseointegrated implants in the treatment of the edentulous jaw. *International Journal of Oral Surgery* 10: 387-416.
- [39] T. Albrektsson, G. Zarb, P. Worthington, A.R. Eriksson. The long term efficacy of currently used dental implants: a review and proposed criteria of success. *Int J Oral Maxillofac Implants.* 1986;1:11-25.
- [40] Y. Oshida (2000). Requirements for successful biofunctional implants. *International Symposium on Advanced Biomaterials.* p.5.
- [41] G. Mendonça, D.B. Mendonça, F.J. Aragão, L.F. Cooper. (2010) The combination of micron and nanotopography by H(2)SO(4)/H(2)O(2) treatment and its effects on osteoblast-specific gene expression of hMSCs. *Journal of Biomedical Materials Research Part A*, 9411691791549-3296
- [42] K.C. Dee, D.A. Puleo, R. Bizios (2002). *An Introduction To Tissue-Biomaterial Interactions.* John Wiley&Sons, ISBN 9780471253945, New Jersey, US.
- [43] C.N. Elias and L. Meirelles (2010) Improving osseointegration of dental implants. *Expert review of medical devices*, 7, 241-256.
- [44] A.M.C. Barradas, H.Yuan, C.A. Blitterswijk van and P. Habibovic. *Osteoinductive Biomaterials: Current Knowledge Of Properties, Experimental Models And Biological Mechanism* , *European cells and materials*, vol 21, 2011
- [45] A. Wennerberg, T. Albrektsson. (2009) Effects of titanium surface topography on boneintegration: a systematic review. *Clinical oral implants research*, 20 Suppl 4, 172-184.
- [46] G. Mendonça, D.B. Mendonça, F.J. Aragão, L.F. Cooper, (Advancing dental implant surface technology – From micronto nanotopography *Biomaterials* 29 (2008) 3822–3835).
- [47] K. Conner, R. Sabatini, B. Mealey, V. Takacks, M. Mills, D. Cochran. Guided bone regeneration around titanium plasma-sprayed, acid-etched and hydroxyapatite-coated implants in the canine model. *J Periodontol* 2003;74:658–68.
- [48] A. Wennerberg and T. Albrektsson (2010) On implant surfaces: a review of current knowledge and opinions. *The International journal of oral & maxillofacial implants*, 25,63-74.

- [49] A. Wennerberg and T. Albrektsson (2000) Suggested guidelines for the topographic evaluation of implant surfaces. *The International journal of oral & maxillofacial implants*, 15, 331-344.
- [50] G. Zhao, O. Zinger, Z. Schwartz, M. Wieland, D. Landolt and B. Doyan (2006) Osteoblastlike cells are sensitive to submicron-scale surface structure. *Clinical oral implants research*, 17, 258-264.
- [51] A. Wennerberg and T. Albrektsson and B. Andersson (1996) Bone tissue response to commercially pure titanium implants blasted with fine and coarse particles of aluminum oxide. *The International journal of oral & maxillofacial implants*, 11, 38-45.
- [52] M.M. Shalabi, A. Gortemaker, M.A. Van't Hof, J.A. Jansen, N.H. Creugers (2006) Implant surface roughness and bone healing: a systematic review. *Journal of dental research*, 85, 496-500.
- [53] A. Wennerberg and T. Albrektsson. The impact of oral implants—past and future, 1966–2042. *J Can Dent Assoc* 2005;71:327.
- [54] D.M. Ehrenfest, P.G. Coelho, B.S. Kang, Y.T. Sul and T. Albrektsson (2010) Classification of osseointegrated implant surfaces: materials, chemistry and topography. *Trends in biotechnology*, 28, 198-206.
- [55] M.J. Dalby, A. Andar, A. Nag, S. Affrossman, R. Tare, S. McFarlane, R.O. Oreffo (2008) Genomic expression of mesenchymal stem cells to altered nanoscale topographies. *Journal of the Royal Society, Interface / the Royal Society*, 5, 1055-1065.
- [56] K. Kubo, N. Tsukimura, F. Iwasa et al., Cellular behavior on TiO₂ nanonodular structures in a micro-to-nanoscale hierarchy model. *Biomaterials*, vol. 30, no. 29, pp. 5319–5329, 2009.
- [57] X. Zhu, J. Chen, L. Scheideler, T. Altebaeumer, J. Geis-Gerstorfer, D. Kern. Cellular reactions of osteoblasts to micron- and submicron-scale porous structures of titanium surfaces. *Cells Tissues Organs*. 2004;178:13–22. 49.
- [58] S. Oh, K.S. Brammer, Y.S. Li et al. Stem cell fate dictated solely by altered nanotube dimension. *Proc Natl Acad Sci U S A*. 2009;106:2130–5.
- [59] G. Colon, B.C. Ward, Webster TJ. Increased osteoblast and decreased *Staphylococcus epidermidis* functions on nanophase ZnO and TiO₂. *J Biomed Mater Res A*. 2006;78:595–604.
- [60] J.E. Davies. Bone bonding at natural and biomaterial surfaces. *Biomaterials* 2007;28:5058–67.

- [61] X. Zou, X. Li, Z.H. Qu, Q. Zhao, Y. Shi, Y. Chen, M. Tade, S. Liu. Photocatalytic degradation of gaseous toluene over TiO₂-SiO₂ composite nanotubes synthesized by sol-gel with template technique *Materials Research Bulletin* Volume 47, Issue 2, February 2012, Pages 279–284
- [62] M-P. Ginebra, C. Canal, M. Espanol, D. Pastorino, E.B. Montufar. Calcium phosphate cements as drug delivery materials *Advanced Drug Delivery Reviews* 64 (2012) 1090–1110
- [63] M. Altind, CaP Coating Of Porous Sintered Ti6al4v Powder Compacts Using Biomimetic And Sol-Gel Methods ,August 2006.
- [64] S.V. Dorozhkin, Nanodimensional and Nanocrystalline Calcium Orthophosphates *American Journal of Biomedical Engineering* 2012,2(3): 48-97.
- [65] M. Vallet-Regi, J.M. González-Calbet. Calcium phosphates as substitution of bone tissues. *Progr. Solid State Chem.* 2004, 32, 1-31.
- [66] F.C.M. Driessens, M.G. Boltong, J.A. Planell, O. Bermudez, M.P. Ginebra, E. Fernandez. A new apatitic calcium phosphate bone cement: preliminary results. *Bioceramics* 6: 469–473; 1993.
- [67] F. Theiss, D. Apelt, B. Brand, A. Kutter, K. Zlinszky, M. Bohner et al., Biocompatibility and resorption of a brushite calcium phosphate cement, *Biomaterials* 26 (2005) 4383–4394.
- [68] R.Z. LeGeros, *Calcium Phosphates in Oral Biology and Medicine*, Karger, Basel, 1991.
- [69] I. Khairoun, M. Boltong, F. Driessens, J. Planell, Effect of calcium carbonate on clinical compliance of apatitic calcium phosphate bone cement, *J. Biomed. Mater. Res.* 38 (1997) 356–360.
- [70] W. Singhatanadgit, Biological responses to new advanced surface modifications of Endosseous medical implants, *Bone and Tissue Regeneration Insights*, 2, 1-11 (2009).
- [71] J.Y. Park and J.E. Davies (2000) Red blood cell and platelet interactions with titanium implant surfaces. *Clinical oral implants research*, 12, 530-539.
- [72] G. Orsini, B. Assenza, A. Scarano, M. Piattelli and A. Piattelli (2000) Surface analysis of machined versus sandblasted and acid-etched titanium implants. *The International journal of oral & maxillofacial implants*, 15, 779-784.

- [73] K. Yokoyama, T. Ichikawa, H. Murakami, Y. Miyamoto, K. Asaoka. Fracture mechanisms of retrieved titanium screw thread in dental implants. *Biomaterials* 2002;23:2459–65.
- [74] G. Juodzbaly, M. Sapragoniene, A. Wennerberg. New Acid Etched Titanium Dental Implant Surface, *Stomatoloija, Baltic Dental and Maxillofacial Journal*, 5:101-105, 2003
- [75] C. Galli, S. Guizzardi, G. Passeri, D. Martini, A. Tinti G. Mauro and G.M. Macaluso (2005) Comparison of human mandibular osteoblasts grown on two commercially available titanium implant surfaces. *Journal of periodontology*, 76, 364-372.
- [76] T. Albrektsson, A. Wennerberg. Oral implant surfaces: Part 1-review focusing on topographic and chemical properties of different surfaces and in vivo responses to them. *Int J Prosthodont* 2004;17(5):536-43.
- [77] K. Hyeongil, C. Seong-Ho, R. Jae-Jun, K. Seung-Yong, P. Ju-Han and L. In-Seop, The biocompatibility of SLA-treated titanium implants, *Biomed. Mater.*3(2008) 025011 (6pp) .
- [78] D. van Steenberghe, G. De Mars, M. Quirynen, R. Jacobs and I. Naert (2000). A prospective split-mouth comparative study of two screw-shaped self-tapping pure titanium implant systems. *Clinical oral implants research*, 11, 202-209.
- [79] A. Wennerberg, T. Albrektsson, B. Albrektsson, J.J. Krol. Histomorphometric and removal torque study of screw-shaped titanium implants with three different surface topographies. *Clin Oral Implant Res* 1996;6:24–30.
- [80] Y.T. Sul, C. Johansson, Y. Jeong, K. Roser, A. Wennerberg, T. Albrektsson. Oxidized implants and their influence on the bone response. *J Mater Sci Mater Med* 2001;12:1025–31.
- [81] Y.T. Sul, C. Johansson, A. Wennerberg, L.R. Cho, B.S. Chang, T. Albrektsson. Optimum surface properties of oxidized implants for reinforcement of osseointegration: surface chemistry, oxide thickness, porosity, roughness, and crystal structure. *Int J Oral Maxillofac Implants* 2005;20:349–59.
- [82] M. Jungner, P. Lundqvist, S. Lundgren. Oxidized titanium implants (Nobel Biocare TiUnite) compared with turned titanium implants (Nobel Biocare mark III) with respect to implant failure in a group of consecutive patients treated with early functional loading and two-stage protocol. *Clin Oral Implants Res* 2005;16:308–12.
- [83] D. Buser, R. Schenk, S. Steinemann, J. Fiorellini, C. Fox, H. Stich. Influence of surface characteristics on bone integration of titanium implants. A histomorphometric study in miniature pigs. *J Biomed Mater Res* 1991;25:889–902.

- [84] R.M. Urban, J.J. Jacobs, M.J. Tomlinson, J. Gavrilovic, J. Black, M. Peoch. Dissemination of wear particles to the liver, spleen and abdominal lymph nodes of patients with hip or knee replacement. *J Bone Jt Surg Am* 2000;82:457–77.
- [85] P. Ducheyne, J.M. Cuckler. (1992) Bioactive ceramic prosthetic coatings. *Clinical orthopaedics and related research*, 102-114.
- [86] F. Barrere, C.M. van der Valk, G. Meijer, R.A. Dalmeijer, K. de Groot, P. Layrolle. Osteointegration of biomimetic apatite coating applied onto dense and porous metal implants in femurs of goats. *J Biomed Mater Res* 2003;67:655–65.
- [87] M.H. Prado da Silva, G.A. Soares, C.N. Elias, J.H.C. Lima, H. Schechtman, I.R. Gibson. Best Surface Analysis of Titanium Dental Implants with Different Topographies *Mat. Res.* vol.3 n.3 São Carlos July 2000.
- [88] L. Le Guehenec, E. Goyenvalle, M.A. Lopez-Heredia, P. Weiss, Y. Amouriq, and P. Layrolle. Histomorphometric analysis of the osseointegration of four different implant surfaces in the femoral epiphyses of rabbits. *Clinical Oral Implants Research*, vol. 19, no. 11, pp. 1103–1110, 2008.
- [89] L. Gan, J. Wang, A. Tache, N. Valiquette, D. Deporter and R. Pilliar (2004) Calcium phosphate sol-gel-derived thin films on porous-surfaced implants for enhanced osteoconductivity. Part II: Short-term in vivo studies. *Biomaterials*, 25, 5313-5321.
- [90] C.M. Cotell, D.B. Chrisey, K.S. Grabowski, J.A. Sprague, C.R. Gossett. Pulsed laser deposition of hydroxylapatite thin films on Ti-6Al-4V. *J. Appl. Biomater.* **1992**, 3, 87–93.187.
- [91] C. Hallgren, H. Reimers, D. Chakarov, J. Gold and A. Wennerberg (2003) An in vivo study of bone response to implants topographically modified by laser micromachining. *Biomaterials*, 24, 701-710.
- [92] J.L. Ong, K. Bessho, R. Cavin, D.L. Carnes. (2002) Bone response to radio frequency sputtered calcium phosphate implants and titanium implants in vivo. *Journal of biomedical materials research*, 59, 184-190
- [93] S. Vercaigne, J.G. Wolke, I. Naert, J.A. Jansen. (2000a) A histological evaluation of TiO₂- gritblasted and Ca-P magnetron sputter coated implants placed into the trabecular bone of the goat: Part 2. *Clinical oral implants research*, 11, 314-324.
- [94] B. Al-Nawas, W. Wagner, K.A. Grotz. (2006) Insertion torque and resonance frequency analysis of dental implant systems in an animal model with loaded implants. *The International journal of oral & maxillofacial implants*, 21, 726-732

- [95] P.G. Coelho, R. Granato, C.H. Marin, E.A. Bonfante, M.N. Janal, M. Suzuki. Biomechanical and bone histomorphologic evaluation of four surfaces on plateau root form implants: An experimental study in dogs Volume 109, Issue 5, May 2010, Pages e39–e45.
- [96] S. Radin, P. Ducheyne. Plasma spraying induced changes of calcium phosphate ceramic characteristics and the effect on in vitro stability. *Mater Med* 1992;3:33–42.
- [97] S. Wheeler. Eight-year clinical retrospective study of titanium plasma-sprayed and hydroxyapatite-coated cylinder implants. *Int J Oral Maxillofac Implants* 1996;11:340–50.
- [98] D. Tinsley, C. Watson, J. Russell. A comparison of hydroxyapatite coated implant retained fixed and removable mandibular prostheses over 4 to 6 years. *Clin Oral Implant Res* 2001;12:159–66.
- [99] L. Le Guehennec, A. Soueidan, P. Layrolle, Y. Amouriq. Surface treatments of titanium dental implants for rapid osseointegration dental materials 23 (2007) 844–854
- [100] B. Yang, M. Uchida, H.M. Kim, X. Zhang, T. Kokubo. Preparation of bioactive titanium metal via anodic oxidation treatment. *Biomaterials* 2004;25:1003–10.
- [101] J. Wang, J. de Boer, K. de Groot. Preparation and characterization of electrodeposited calcium phosphate/chitosan coating on Ti6Al4V plates. *J Dent Res* 2004;83:296–301.
- [102] F. Barrere, M. Snel, C. Van Blitterswijk, K. de Groot, P. Layrolle. Nano-scale study of the nucleation and growth of calcium phosphate coating on titanium implants. *Biomaterials* 2004;25:2901–10;
- [103] S. Leeuwenburgh, P. Layrolle, F. Barrere, J. de Bruijn, J. Schoonman, C.A. van Blitterswijk et al. Osteoclastic resorption of biomimetic calcium phosphate coatings in vitro. *J Biomed Mater Res* 2001;56:208–15.
- [104] C. Costa de Almeida, L.A.S. Marcelo Pinto, C.A. Muller, J.H.C. Lima, G. de Almeida Soares. In Vivo Characterization of Titanium Implants Coated with Synthetic Hydroxyapatite by Electrophoresis, *Braz. Dent. J.* vol.16 no.1 Ribeirão Preto Jan./Apr. 2005.
- [105] S.J. Meraw, C.M. Reeve, P.C. Wollan. Use of alendronate in peri-implant defect regeneration. *J Periodontol* 1999;70:151–8.
- [106] J. Beuvelot, D. Portet, G. Lecollinet et al. In vitro kinetic study of growth and mineralization of osteoblast-like cells (Saos-2) on titanium surface coated with a RGD functionalized bisphosphonate. *J Biomed Mater Res B Appl Biomater.* 2009.

- [107] M. Stigter, J. Bezemer de GK, P. Layrolle. Incorporation of different antibiotics into carbonated hydroxyapatite coatings on titanium implants, release and antibiotic efficacy. *J Control Release*. 2004;99:127–37.
- [108] A.R. El Ghannam, P. Ducheyne, M. Risbud et al. Model surfaces engineered with nanoscale roughness and RGD tripeptides promote osteoblast activity. *J Biomed Mater Res A*. 2004;68:615–27.
- [109] A. Lasserre and P.K. Bajpai. Ceramic drug-delivery devices. *Crit Rev Ther Drug Carrier Syst* 1998;15:1-56.
- [110] C.R. Brundle, C.A. Evans, J.S. Wilson(1992). *Encyclopedia of materials characterization. Surfaces, Interfaces, Thin Films*, Stoneham, USA , Butterworth-Heinemann & Manning publication; 1992.
- [111] J. Lausmaa. (1996) Surface spectroscopic characterization of titanium implant materials. *Journal of Electron Spectroscopy and Related Phenomena*,(81), 1996.
- [112] Q. Chen, G.H. Du, S. Zhang, L.M. Peng (2002b). The structure of trititanate nanotubes. *Acta Cryst., B*, 58 (4), 587-593.
- [113] T. RadetiÉ. (2011) *Fundamentals of Scanning Electron Microscopy and Energy Dispersive X-ray Analysis in SEM and TEM* University of Belgrade Faculty of Technology and Metallurgy, Beograd, Serbia, NFMC Spring School on Electron Microscopy, April 2011
- [114] S. Bragadeeswaran, S.T. Balasubramanian, S.M. Raffi and S. Rani Sophia (2010). Scanning electron microscopy elemental studies of primary film. *World Applied Sciences Journal*. Vol.10, No.2, pp.169-172
- [115] J.F. Moulder, P.E. Sobol, W.F. Stickle, (1995) *Handbook of X-ray photoelectron spectroscopy : a reference book of standard spectra for identification and interpretation of XPS data*. Eden Prairie, Minn.: Physical Electronics Inc.; 1995
- [116] D. Briggs and J.T. Grant, (2003) Eds. *Surface Analysis by Auger and X-ray Photoelectron Spectroscopy*, IM Publications, Chichester, 2003 ISBN: 1-901019-04-7.
- [117] D. Briggs and M.P. Seah. *Practical Surface Analysis. Volume 1 – Auger and X-ray Photoelectron Spectroscopy* , Second Edition, John Wiley and Sons, Chichester, 1990.
- [118] L. Qian , Z-L. Du, S-Y. Yang and Z-S Jin. (2005) Jin, "Raman study of titania nanotube by soft chemical process," *Journal of Molecular Structure*, vol. 749, pp. 103-107, 2005.

- [119] P.R. Griffiths and J.A. de Haseth, Fourier Transform Infrared Spectrometry, Wiley, New York, 1986.
- [120] K. Nakamoto. (1997) Infrared and Raman spectra of inorganic and coordination compounds, 5th. edition, Part A, Wiley, 1997.
- [121] R. Mendelsohn, G. Mao, and C.R. Flach, Infrared Reflection-Absorption Spectroscopy: Principles and Applications to Lipid-Protein Interaction in Langmuir Films, *Biochim Biophys Acta*. 2010 April; 1798(4): 788–800.
- [121] C.D. Wagner, D. eds. Briggs and M.P. Seah. (1990) *Practical Surface Analysis*", Vol.1, 2nd Edition, Published by J. Wiley and Sons in 1990.
- [122] D.A. Long. Raman Spectroscopy, McGraw-Hill, New York (1977).
- [123] D. Gong, C.A. Grimes, O.K. Varghese, W. Hu, R.S. Singh, Z. Chen, E.C. Dickey. (2001) Titanium oxide nanotube arrays prepared by anodic oxidation, *J. Mater. Res.* 16, 3331-3334.
- [124] G.K. Mor, O.K. Varghese, M. Paulose, N. Mukherjee, C.A. Grimes. (2003) Fabrication of tapered, conical-shaped titania nanotubes, *J. Mater. Research* 18, 2588-2593.
- [125] G.K. Mor, K. Shankar, M. Paulose, O.K. Varghese, C.A. Grimes. (2005) Enhanced photocleavage of water using titania nanotube arrays *Nano Letters* 5(1), 191–195
- [126] G.K. Mor, M.A. Carvalho, O.K. Varghese, M.V. Pishko, C.A. Grimes. (2004) A room-temperature TiO₂-nanotube hydrogen sensor able to self-clean photoactively from environmental contamination *J. Mater. Res.*, 19, 628-634.
- [127] K. Shankar, G.K. Mor, H.E. Prakasam, O.K. Varghese and C.A. Grimes. (2007) Self-Assembled Hybrid Polymer-TiO₂ Nanotube Array Heterojunction Solar Cells. *Langmuir* 23, no. 24 (2007): 12445-9.
- [128] K.S. Brammer, S. Oh, C.J. Frandsen and S. Jin (2011). Biomaterials and Biotechnology Schemes Utilizing TiO₂ Nanotube Arrays, *Biomaterials Science and Engineering*, Prof. Rosario Pignatello (Ed.), ISBN: 978-953-307-609-6, InTech
- [129] G.K. Mor, O.K. Varghese, M. Paulose, K. Shankar, C.A. Grimes. (2006) A review on highly ordered, vertically oriented TiO₂ nanotube arrays: Fabrication, material properties, and solar energy applications. *Solar Energy Materials & Solar Cells* 90 (2006) 2011–2075
- [130] K. Yasuda and P. Schmuki, "Control of morphology and composition of self-organized zirconium titanate nanotubes formed

in (NH₄)₂SO₄/NH₄F electrolytes,” *Electrochimica Acta*, vol. 52, no. 12, pp. 4053–4061, 2007

[131] P. Roy, S. Berger, P. Schmuki. (2011) TiO₂ nanotubes: Synthesis and applications, *Angew. Chem. Int. Ed.*, 50 (2011) 2904-2939

[132] L.V. Taveira, J.M. Macak, K. Sirotka, L.F.P. Dick and P. Schmuki. (2005) Initiation and Growth of Self-Organized TiO₂ Nanotubes Anodically Formed in NH₄F/(NH₄)₂SO₄- Electrolytes, *J. Electrochem. Soc.* 152 (2005) B405.

[133] H. Ishizawa, M. Fujino, M. Ogino. Mechanical and histological investigation of hydrothermally treated and untreated anodic titanium oxide films containing Ca and P. *J Biomed Mater Res.* 1995;29:1459-68.

[134] Y.T. Sul, B.S. Kang, C. Johansson, H.S. Um, C.J. Park, T. Albrektsson. The roles of surface chemistry and topography in the strength and rate of osseointegration of titanium implants in bone. *J Biomed Mater Res A.* 2009;89:942-50.

[135] K. Othmer *Encyclopedia of Chemical Technology*, 3rd ed.; Wiley- Interscience: New York, 1978; Vol. 4, p 26.

[136] J. Sundgren, E. Bodo, P. Lundstro, I. J. *Colloid Interface Sci.* 1986, 110, 9.

[137] J. Hall, J. Lausmaa. Properties of a new porous oxide surface on titanium implants. *Appl Osseointegration Res.* 2001;1:5-8

[138] O.M. Omar, M.E. Lenneras, F. Suska, L. Emanuelsson, J.M. Hall, A. Palmquist et al. The correlation between gene expression of proinflammatory markers and bone formation during osseointegration with titanium implants. *Biomaterials.* 2011;32:374-86.

[139] D. Krupa , J. Baszkiewicz, J.A. Kozubowski, A. Barcz, J.W. Sobczak, A. Bilinski et al. Effect of phosphorus-ion implantation on the corrosion resistance and biocompatibility of titanium. *Biomaterials.* 2002;23:3329-40.

[140] F. Washington. *Electron Microscopy Sciences*, Catalog #21190 Sodium Phosphate Monobasic.

[141] D.E.C. Corbridge. (1960). "The crystal structure of sodium triphosphate, Na₅P₃O₁₀, phase I". *Acta Crystallographica* 13: 263.

[142] Y.T. Sul, C.B. Johansson, Y. Jeong, T. Albrektsson. The electrochemical oxide growth behaviour on titanium in acid and alkaline electrolytes. *Med Eng Phys.* 2001;23:329-46.

- [143] H.M. Kim, H. Kaneko, M. Kawashita, T. Kokubo, T. Nakamura. (2004) Mechanisms of apatite formation on anodically oxidized titanium metal in simulated body fluid. *Key Engineering Materials* 2004; 254-256: 741-4.
- [144] G. Herzberg. (1945), *Molecular Spectra and Molecular Structure. II. Infrared and Raman Spectra of Polyatomic Molecules* D Van Nostrand Co., Inc., New York.
- [145] A. C. S. Samia , J. A. Schlueter , J. S. Jiang , S.D. Bader , Ch-J. Qin , and X-M. Lin. Effect of Ligand–Metal Interactions on the Growth of Transition-Metal and Alloy Nanoparticles *Chem. Mater.*, 2006, 18 (22), pp 5203–5212.
- [146] A.K. Lynn, W. Bonfield. (2005) A novel method for the simultaneous, titrant-free control of pH and calcium phosphate mass yield. *Acc Chem Res* 38:202–207
- [147] M. I. Tejedor-Tejedor , M. A. Anderson , The protonation of phosphate on the surface of goethite as studied by CIR-FTIR and electrophoretic mobility. *Langmuir*, 1990, 6 (3), pp 602–611
- [148] A. Michelmore, P. Jenkins, J. Ralston. (2003), 'The interaction of linear polyphosphates with zincite surfaces', *International Journal of Mineral Processing*, 68, 1-16, 2003.
- [149] A. Michelmore, W.Gong, P. Jenkins, J. Ralston The interaction of linear polyphosphates with titanium dioxide surfaces *Physical Chemistry Chemical Physics* 2 (13), 2985-2992.
- [150] P. Persson, N. Nilsson, S. Sjöberg. Structure and Bonding of Orthophosphate Ions at the Iron Oxide-Aqueous Interface. *J Colloid Interface Sci.* 1996 Jan15;177(1):263-275.
- [151] P. A. Connor and A. J. McQuillan, Phosphate Adsorption onto TiO₂ from Aqueous Solutions: An in Situ Internal Reflection Infrared Spectroscopic Study, *Langmuir* 1999, 15, 2916-2921
- [152] K. Yamashita , N. Oiwawa , T. Umegaki. Acceleration and deceleration of bone-like crystal growth on ceramic hydroxyapatite by electric poling. *Chem Mater* 1996;8:2697–700.
- [153] P. Calvert, S. Mann. (1997) The negative side of crystal growth. *Nature*, 386, 127–128.
- [154] X. X. Wang, W. Yan, S. Hayakawa, K. Tsuru, A. Osaka (2001). A comparative study of in vitro apatite deposition on heat-, H₂O(2)-, and NaOH-treated titanium. *J Biomed Mater Res.* 2001 Feb;54(2):172-8.

- [155] H.M. Kim , F. Miyaji , T. Kokubo , T. Nakamura . (1996) Preparation of bioactive Ti and its alloys via simple chemical surface treatment. *J Biomed Mater Res.* 1996 Nov;32(3):409-17.
- [156] T. Ohtsuka, N. Nomura. The dependence of the optical property of Ti anodic oxide film on its growth rate by ellipsometry. *Corros Sci.* 1997;39:1253-63.
- [157] T. Kokubo, “Bioceramics and Their Clinical Applications,” CRC Press, USA, 2008.
- [158] K.J . Raj, R. Shanmugam, R. Mahalakshmi, B. Viswanathan , (2010) XPS and IR spectral studies on the structure of phosphate and sulphate modified titania – A combined DFT and experimental study *Indian Journal of Chemistry* 49A, 2010 Page 9-17.
- [159] Y. Arai and D.L. Sparks. ATR–FTIR Spectroscopic Investigation on Phosphate Adsorption Mechanisms at the Ferrihydrite–Water Interface, *Journal of Colloid and Interface Science* 241, 317–326 (2001)
- [160] B. León, J.A. Jansen, *Thin Calcium Phosphate Coatings for Medical Implants*, Springer Science Business Media, LLC , New York, 2009. Pages 215-263. ISBN: 978-0-387-77718-4 2009
- [161] S.V. Dorozhkin. (2008) Calcium orthophosphate cements for biomedical application. *J. Mater. Sci.* 2008,43, 3028-3057
- [162] H. Schliephake, R. Gruber, M. Dard, R. Wenz, S. Scholz. Repair of calvarial defects in rats by prefabricated hydroxyapatite cement implants. *J. Biomed. Mater. Res. A* 2004, 69, 382–390.
- [163] M. Bohner, U. Gbureck. Thermal reactions of brushite cements. *J. Biomed. Mater. Res. B.* 2008,84, 375–385.
- [164] U. Gbureck, S. Dembski, R. Thull, J.E. Barralet. Factors influencing calcium phosphate cement shelf-life. *Biomaterials* 2005, 26, 3691–3697.
- [165] L.Wang and G.H. Nancollas. Calcium Orthophosphates: Crystallization and Dissolution, *Chem Rev.* 2008 November ; 108(11): 4628–4669
- [166] S. Kannan, S. Pina, J.M.F. Ferreira. Formation of strontium-stabilized alpha-tricalcium phosphate from calcium-deficient apatite. *J. Amer. Ceram. Soc.* 2006, 89, 3277–3280.
- [167] M.H. Alkhraisat, F.T. Marino, C.R. Rodriguez, L.B. Jerez, E.L. Cabarcos. Combined effect of strontium and pyrophosphate on the properties of brushite cements. *Acta Biomater.* 2008, 4,664–670.

- [168] P.J. Marie, P. Ammann, G. Boivin, C. Rey. Mechanisms of action and therapeutic potential of strontium in bone. *Calcif Tissue Int* 2001;69:121–9.
- [169] E. Bonnelye, A. Chabadel, F. Saltel, P. Jurdic, Dual effect of strontium ranelate: stimulation of osteoblast differentiation and inhibition of osteoclast formation and resorption in vitro, *Bone* 42 (2008) 129–138.
- [170] R. Baron, Y. Tsouderos. In vitro effects of S12911-2 on osteoclast function and bone marrow macrophage differentiation. *Eur J Pharmacol* 2002;450:11–7.
- [171] P.J. Marie, M.T. Garba, M. Hott, L.Miravet. Effect of low doses of stable strontium on bone metabolism in rats, *Miner. Electrolyte Metab.* 11 (1985) 5–13
- [172] S.C. Skoryna. Effects of oral supplementation with stable strontium. *Can Med Assoc J* 1981;125:703–712.
- [173] D.L. Kendler. (2006) Strontium ranelate data on vertebral and non vertebral fracture efficacy and safety: mechanism of action. *Curr Osteoporos Rep* 2006; 4: 34-9.
- [174] M.H. Salimi, J.C. Heughebaert, G.H. Nancollas. Crystal growth of calcium phosphates in the presence of magnesium ions. *Langmuir* 1985, 1, 119–122.
- [175] F. Barrere, C.A. van Blitterswijk, K. de Groot, P. Layrolle, P. Nucleation of biomimetic Ca-Pcoatings on Ti6Al4V from a SBF× 5 solution: influence of magnesium. *Biomaterials* 2002, 23,2211–2220
- [176] J-H. Park, Y-K. Lee, K-M. Kim. Bioactive calcium phosphate coating prepared on H₂O₂ -treated titanium substrate by electrodeposition ,*Surface & Coatings Technology* 195 (2005) 252– 257
- [177] R.Z. LeGeros. Properties of osteoconductive biomaterials: calcium phosphates, *Clinical Orthopaedics and Related Research*, no. 395, pp. 81–98, 2002
- [178] S.V. Dorozhkin (2012) Calcium orthophosphate coatings, films and layers ,*Kudrinskaja sq. 1-155, Moscow, 123242, Russia Progress in Biomaterials* 2012, 1:1.
- [179] A. Kar. K.S. Raj, M. Misra Electrodeposition of hydroxyapatite onto nanotubular TiO₂ for implant applications *Surface & Coatings Technology* 201 (2006) 3723–3731
- [180] M. Shir Khanzadeh. (1998) Direct formation of nanophase hydroxyapatite on cathodically polarized electrodes. *J Mater Sci Mater Med* 9:67-72.
- [181] W. Paul, C.P. Sharma. Development of porous spherical hydroxyapatite granules: application towards protein delivery. *Journal of Materials Science: Materials in Medicine*, 1999;10:383-388.

- [182] D. Farlay, G. Panczer, C. Rey, P.D. Delmas, G. Boivin. Mineral maturity and crystallinity index are distinct characteristics of bone mineral. *J Bone Miner Metab.* 2010 Jul;28(4):433-45.
- [183] M. Shirkhazadeh. Electrochemical preparation of bioactive calcium phosphate coatings on porous substrates by the periodic pulse technique. *J Mater Sci Lett* 1993;12:16–19.
- [184] S.J. Gadaleta, A. Cericke, A.L. Boskey, R. Mendelsohn. Two-Dimensional Infrared Correlation Spectroscopy of Synthetic and Biological Apatites *Biospectroscopy*, Vol. 2,353-364 (1996) © 1996 John Wiley & Sons.
- [185] F.S. Casciani, R.A. Condrate. Sr Proceedings - International Congress on Phosphorus Compounds 2nd (1980) 175.
- [186] K. Suguna, C. Sekar. Role of Strontium on the Crystallization of Calcium Hydrogen Phosphate Dihydrate, *J. Miner. Mater. Charac. Eng.* 10 (2011) 625
- [187] J.Y. Mevellec, S. Quillard, P. Deniard, O. Mekmene, F. Gaucheron, J.M. Bouler, J.P. Buisson. Polarized infrared reflectance spectra of brushite (CaHPO₄·2H₂O) crystal investigation of the phosphate stretching modes. *Spectrochim Acta A Mol Biomol Spectrosc.* 2013 Jul;111:7-13.
- [188] J. Xu. Vibrational Spectroscopic Investigations of Calcium Phosphates and Dental Materials, October 1996, McGill University, Montreal-Quebec, Canada
- [189] L. Muller, E. Conforto, D. Caillard, F.A. Muller. Biomimetic apatite coatings—Carbonate substitution and preferred growth orientation. *Biomol. Eng.* 2007, 24, 462–466.
- [190] S. Ntais, V. Dracopoulos, A. Siokou. TiCl₄(THF)₂ impregnation on a flat SiO_x/Si(1 0 0) and on polycrystalline Au foil: Determination of surface species using XPS. *J. Mol. Catal. A Chem* 2004, 220, 199–205.
- [191] J. Kunze, L. Muller, J.M. Macaka, P. Greilb, P. Schmuki, F.A. Muller, Time-dependent growth of biomimetic apatite on anodic TiO₂ nanotubes; *Electrochimica Acta*, Volume 53, Issue 23, 1 October 2008, Pages 6995–7003.
- [192] B.L. Hongbo, C.T. Campbell, D. J. Graham and B. D. Ratner Surface Characterization of Hydroxyapatite and Related Calcium Phosphates by XPS and TOF-SIMS *Anal. Chem.* 2000, 72, 2886-2894.
- [193] A. M. Stranick, M. J. Root. Influence of strontium on monofluorophosphate uptake by hydroxyapatite XPS characterization of the hydroxyapatite surface, *Colloids and Surfaces* Volume 55, 1991, Pages 137–147.

- [194] K. Nakamoto. Infrared and Raman Spectra of Inorganic and Coordination Compounds. Wiley, New York, 1997. (USE BOTH 151)
- [195] S. V. Dorozhkin and M. Epple Biological and Medical Significance of Calcium Phosphates *Angew. Chem. Int. Ed.* 2002, 41, 3130} 3146.
- [196] C. Combes and C. Rey. (2010) Amorphous calcium phosphates: synthesis, properties and uses in biomaterials. *Acta Biomaterialia*, vol. 6 (n° 9). pp. 3362-3378. ISSN 1742-7061.
- [197] J. Christoffersen, M.R. Christoffersen, W. Kibaczyc, F.A. Andersen. A contribution to the understanding of the formation of calcium phosphates. *J Cryst Growth* 1989;94:767–77.
- [198] J.C. Heughebaert, G. Montel. Conversion of amorphous tricalcium phosphate into apatitic tricalcium phosphate. *Calcif Tissue Int* 1982;34:S103–8.
- [199] S. Gomesa, J-M. Nedeleca, E. Jallot, C. Bonhomme, F. Babonneau, Y. Filinchuk, D. Sheptyakovh and G. Renaudina. Etude structurale des substitutions ioniques dans les BCP (Phosphates Calciques Biphases) MATERIAUX 2010 – 18-22 octobre 2010 – Nantes, France.
- [200] S.Pina and J.M.F. Ferreira Brushite-Forming Mg-, Zn- and Sr-Substituted Bone Cements for Clinical Applications *Materials* 2010, 3, 519-535; doi:10.3390/ma3010519
- [201] Ch. C. Chusuei and D. Wayne Goodman *Anal. Chem* 71 (1999) 149-153
- [202] J. Christoffersen, M.R. Christoffersen, N. Kolthoff, O. Barenholdt. Effects of strontium ions on growth and dissolution of hydroxyapatite and on bone mineral detection. *Bone* 1997; 20: 47-54.
- [203] S.V. Dorozhkin. Calcium Orthophosphates in Nature, Biology and Medicine *Materials* 2009, 2, 399-498; doi:10.3390/ma2020399
- [204] M. Bohner, F. Theiss, D. Apelt, W. Hirsiger, R. Houriet, G. Rizzoli (2003) Compositional changes of a Dicalcium phosphate dihydrate cement after implantation in sheep. *Biomaterials* 24: 3463-3474
- [205] F. Tamimi, B. Kumarasami, C. Doillon, U. Gbureck, D.L. Nihouannen, E.L. Cabarcos, J.E. Barralet. Brushite-collagen composites for bone regeneration. *Acta Biomaterialia*. 2008, 4,1315–1321.
- [206] S. Pina, S.I. Vieira, P. Rego, P.M.C. Torres, O.A.B. Da Cruz E Silva, E.F. Da Cruz E Silva, and J.M.F. Ferreira. Biological Responses Of Brushite-Forming Zn-

And Znsr-Substituted B-Tricalcium Phosphate Bone Cements Eur Cell Mater. 2010 Sep 7;20:162-77.

[207] H.B. Wen, F.Z. Cui, Q.L. Feng, H.D. Li, X.D. Zhu (1995) Microstructural investigation of the early external callus after diaphyseal fractures of human long-bone. J Struct Biol 114: 115-122.

[208] D.R. Villareal, A. Sogal, J.L. Ong, The Journal of Oral Implantology 24 (2) (1998) 67.

[209] B.S. Park, S.J. Heo, C.S. Kim, J.E. Oh, J.M. Kim, G. Lee, W.H. Park, C.P. Chung, B.M. Min. (2005). Effects of adhesion molecules on the behavior of osteoblast-like cells and normal human fibroblasts on different titanium surfaces. Journal of Biomedical Materials Research Part A, Vol.74, No.4, pp. 640-651.

[210] Y. Wang, L. Lu, Y. Zheng, X. Chen (2006). "Improvement in hydrophilicity of PHBV films by plasma treatment". J. Biomed. Mater. Res. A76 (3): 589–595

[211] B. Kasemo, J. Gold, Adv. Dent. Res. 13 (1999) 8.

[212] B. Kasemo , Biological surface science , Surface Science 500 (2002) 656–677

[213] P. Laffargue, P. Fialdes, P. Frayssinet, M. Rtaimate, H. F. Hildebrand and X. Marchandise, "Adsorption and Release of Insulin-Like Growth Factor-I on Porous Tricalcium Phosphate Implant," Journal of Biomedical Materials Research, Vol. 49, No. 3, 2000, pp. 415-421

[214] Y. Liu, J. P. Li, E. B. Hunziker and K. de Groot, "Incorporation of Growth Factors into Medical Devices via Biomimetic Coatings," Philosophical Transactions of the Royal Society a-Mathematical Physical and Engineering Sciences, Vol. 364, No. 1838, 2006, pp. 233-248.

[215] T. Y. Liu, S. Y. Chen, D. M. Liu and S. C. Liou, "On the Study of BSA-Loaded Calcium-Deficient Hydroxyapatite Nano-Carriers for Controlled Drug Delivery," Journal of Control Release, Vol. 107, No. 1, 2005, pp. 112-121.

[216] E. Wernike, W. Hofstetter, Y. Liu, G. Wu, H.J. Sebald, D. Wismeijer, E.B. Hunziker, K.A. Siebenrock, F.M. Klenke. Long-Term Cell-Mediated Protein Release From Calcium Phosphate Ceramics . J Biomed Mater Res A. 2009 Feb 4.

[217] M. Yamaguchi, A. Igarashi, H. Misawa, Y. Tsurusaki. (2003) Enhancement of albumin expression in bone tissues with healing rat fractures. J cell biochem. 89(2): 356-363.

- [218] H.B. Wen, J.R. De Wijn, C.A. Van Blitterwijk, K. De Groot. Incorporation of bovine serum albumin in calcium phosphate coating on titanium. *J Biomed Mater Res*1999;46:245–52.
- [219] K. Ishida, M. Yamaguchi. Role of albumin in osteoblastic cells: Enhancement of cell proliferation and suppression of alkaline phosphatase activity (2004) *Inter. j. mol. med.*14(6): 1077-1081
- [220] M.T. Bernards, Ch. Qin, S. Jiang. (2008) MC3T3-E1 cell adhesion to hydroxyapatite with adsorbed bone sialoprotein, bone osteopontin, and bovine serum albumin. *Colloid. surf. b-biointerfaces.* 64:236-247.
- [221] W. Gallagher, FTIR Analysis of Protein Structure, http://download.bion.com.cn/upload/201110/10233820_7954.pdf
- [222] C. Dewey, Introduction to Protein Structure Prediction BMI/CS 776. www.biostat.wisc.edu/bmi776/
- [223] J.J. Ramsden. Experimental Methods for Investigating Protein Adsorption-Kinetics at Surfaces. *Quarterly Reviews of Biophysics* 1994; 27: 41-105
- [224] T. Peters Jr., All about Albumin, Biochemistry, Genetics, and Medical Applications, Academic Press, San Diego, 1996.
- [225] L. Lartundo-Rojas, Influence de l'adsorption de protein (BSA) sur le comportement electrochimique et la composition de surface d'un alliage Fe-17Cr en solution aqueuse. Thesis, école doctorale 388, University of Paris VI, France ,2007
- [226] D.T.H. Wassell, R.C. Hall, G. Embery. 1995 Adsorption of bovine serum albumin onto hydroxyapatite. *Biomaterials* 16, 697–702.
- [227] H. Zeng, K.K. Chittur, W.R. Lacefield. Analysis of bovine serum albumin adsorption on calcium phosphate and titanium surfaces. *Biomaterials* 1999;20:377–84.
- [228] H-J. Butt, K. Graf, M. Kappl. (2006). *Physics and chemistry of interfaces.* Germany: Wiley-VCH. pp. 45, 55, 56, 76–82. ISBN 978-3-527-40629-6.
- [229] B. Feng, J. Chen, X. Zhang. 2002 Interaction of calcium and phosphate in apatite coating on titanium with serum albumin. *Biomaterials* 23, 2499–250 .
- [230] J. Clayden, S. Warren, et al. (2000) "Organic Chemistry" Oxford University Press pp. 182–184
- [231] M. Kosmulski ,surface charging and points of zero charge,. CRC Press, Taylor and Francis Group. Vol 145. 2009

- [232] D.V. Bavykin , E.V. Milsom , F. Marken , D.H. Kim , D.H. Marsh , D.J. Riley , F.C. Walsh , K.H. El-Abiary , A.A. Lapkin. A novel cation-binding TiO₂ nanotube substrate for electro- and bioelectro-catalysis: *Electrochemistry Communications* 7 (2005) (1050–1058).
- [233] M. Kosmulski, "Chemical Properties of Material Surfaces", Marcel Dekker Inc., 2001
- [234] W. Norde. Protein adsorption at solid surfaces: A thermodynamic approach, *Pure & Appl. Chem.*, Vol. 66, No. 3, pp. 491–496, 1994
- [235] G. Daculsi. 1998 Biphasic calcium phosphate concept applied to artificial bone, implant coating and injectable bone substitute. *Biomaterials* 19, 1473–1478.
- [236] E. Fujii, M. Ohkubo, K. Tsuru, S. Hayakawa, A. Osaka, K. Kawabata, C. Bonhomme, F. Babonneau. 2006 Selective protein adsorption property and characterization of nano-crystalline zinc-containing hydroxyapatite. *Acta Biomater.* 2, 69–74.
- [237] S. Dasgupta, A. Bandyopadhyay, S. Bose. Zn and Mg Doped Hydroxyapatite Nanoparticles for Controlled Release of Protein, *Langmuir*. 2010 April 6; 26(7): 4958–4964.
- [238] A. Bouhekka. Thesis : Adsorption of BSA protein on Silicon , Germanium and Titanium Dioxide investigated by In situ ATR-IR spectroscopy, Université d'Oran , Faculté de sciences, Département de Physique, Algérie 2013.
- [239] S. Krimm, J. Bandekar. Vibrational spectroscopy and conformation of peptides, polypeptides, and proteins. *Adv Protein Chem* 1986, 38: 181–364
- [240] K. Fu, K. Griebenow, L. Hsieh, A.M. Klibanov, R. Lang. FTIR characterization of the secondary structure of proteins encapsulated within PLGA microspheres. *Journal of Controlled Release*, 1999, 58, 357–366
- [241] P. Garidel, H. Schott. Fourier-Transform Midinfrared Spectroscopy for Analysis and Screening of Liquid Protein Formulations: Part 1, Understanding Infrared Spectroscopy of Proteins. *BioProcess International* 4(5) 2006: 40–46)
- [242] K. J. Rothschild, R. Sanches, T. L. Hsiao and N. A. Clark. A spectroscopic study of rhodopsin alpha-helix orientation. *Biophys. J.*, 1981, 31, 53–64.
- [243] F. I. Gallardo and J. Lauren. Webb Tethering Hydrophobic Peptides to Functionalized Self-Assembled Monolayers on Gold through Two Chemical Linkers Using the Huisgen Cycloaddition, *Langmuir*, 2010, 26 (24), pp 18959–18966)

[244] X.D. Zhu, H.S. Fan, Y.M. Xiao, D.X. Li, H.J. Zhang, T. Luxbacher, X.D. Zhang. 2009 Effect of surface structure on protein adsorption to biphasic calcium-phosphate ceramics in vitro and in vivo. *Acta Biomater.* 5, 1311–1318

[245] B. J. M. Harmsen and W. J. M. Braam. On the conformation of BSA after alkaline or thermal denaturation. *Int. J. Protein Research* (1969), 1, 225-233

[246] H. Wu, Y. Fan, J. Sheng and S. Fang Sui. Induction of changes in the secondary structure of globular proteins by hydrophobic surface. *Eur. Biophys J.* (1993), 22, 201-205.

[247] “Surface Chemical Characteristics and Adsorption Properties of Apatite,” P. Somasundaran, Y. H. C. Wang, *Adsorption on and Surface Chemistry of Hydroxyapatite*, D.N. Misra Ed., Plenum Press: New York, pp. 129 (1984).

Functionalization of titanium surface for dental implants design

Abstract: The objective of this thesis is to create new nanostructured surfaces with bioactive coatings and to study their physicochemical properties in order to develop better dental implants designs and promote their osseointegration. This functionalization was performed in two steps; starting by the nanostructuring of TiO₂ surface by anodisation to create reactive sites on the edges of titanium nanotubes which acts as points of "attachment" to bioactive coatings. The second step was the surface chemical modification by coating the nanostructured surface with bioactive coatings of calcium phosphate (CaP) and strontium doped calcium phosphate (Sr.CaP). This coating was performed by pulsed electrodeposition. The physicochemical characterization by XPS, SEM and IR showed that doping with Sr promotes a non-apatitic compound similar to DCPD or DCPA (Dicalcium Phosphate Dihydrate or Anhydrous), while undoped CaP coating looks like an amorphous apatite-like compound ACP. The addition of strontium has the double advantage of optimizing the cellular multiplication and of giving an inorganic phase with bio-performance better than apatitic compounds. We also evaluated the adsorption proprieties of these functionalized surfaces by investigating the adsorption of proteins (BSA). This adsorption was performed onto blank nanotubes, nanotubes coated with CaP and Sr doped CaP and evaluated according to deposition time and to the pH value of the solution that affect both protein and surface charge. The kinetic and structural evaluation reveals different adsorption geometries according to pH and adsorption time and also according to the chemical nature of surface. Such results of protein adsorption and conformation may form a database to understand and control protein activities and reactions with living body when used for dental implants system.

Keywords: Titanium dental implants, Nanotubes, Physicochemical functionalization, Calcium phosphate coating, Protein adsorption, XPS, SEM, IRRAS.

Fonctionnalisation de la surface du titane pour les implants dentaires

Résumé: L'objectif de cette thèse est de créer de nouvelles surfaces nanostructurées avec des revêtements bioactifs et d'étudier leurs propriétés physico-chimiques afin de développer de meilleurs modèles d'implants dentaires et d'optimiser leur ostéointégration. Cette fonctionnalisation a été réalisée en deux étapes ; on a commencé par la nanostructuration de la surface de TiO₂ par anodisation pour créer des sites réactifs sur les bords extérieurs des nanotubes qui agissent comme des points d'ancrage du revêtement bioactif et améliorent le verrouillage mécanique entre le revêtement et le substrat. Ensuite, la modification chimique est réalisée par revêtement de la surface nanostructurée avec des revêtements bioactifs de phosphate de calcium (CaP) et phosphate de calcium dopé par strontium (Sr.CaP). Ce revêtement a été réalisé par électrodeposition pulsée. La caractérisation physico-chimique par MEB, XPS et IR a montré que le dopage avec Sr favorise un composé non-apatitique similaire à DCPD ou DCPA (Dicalcium Phosphate Dihydrate ou Anhydrous), tandis que le revêtement de CaP non-dopé ressemble à un composé d'apatite amorphe ACP. L'addition de strontium s'offre le double avantage de favoriser les mécanismes de la croissance cellulaire et d'obtenir une phase inorganique avec de bio-performances meilleurs que les composés apatitiques. Nous avons également évalué les propriétés d'adsorption de ces surfaces fonctionnalisées en étudiant l'adsorption des protéines (BSA). Cette adsorption a été réalisée sur nanotubes fonctionnalisés vierges, nanotubes enrobés avec CAP et CAP dopé Sr et elle a été évalués selon le temps de déposition et la valeur du pH de la solution qui affecte la charge de la protéine et de la surface. L'évaluation cinétique et structurelle révèle différentes géométries d'adsorption en fonction du pH, du temps d'adsorption et aussi en fonction de la nature chimique de la surface. Ces résultats de l'adsorption et conformation de protéine forment une base de données pour comprendre et contrôler ses activités et réactions avec le vivant lorsqu'elle est utilisée dans le system des implants dentaires.

Mots-clés: Implants dentaires en titane, nanotubes, fonctionnalisation physico-chimique, revêtement de phosphate de calcium, adsorption des protéines, XPS, MEB, IRRAS.